Diss. ETH No. 19912

IDENTIFICATION AND FORECASTS OF FINANCIAL BUBBLES

A dissertation submitted to

ETH ZÜRICH

for the degree of Doctor of Sciences

presented by

WANFENG YAN
(闫晚丰)

Dipl. - Ing. ETH Zürich
B.Sc. Peking University
born on October 18th, 1984
citizen of China

accepted on the recommendation of

Prof. Dr. Didier Sornette, examiner
Prof. Dr. Paul Embrechts, co-examiner
Prof. Dr. Thorsten Hens, co-examiner

2011

Acknowledgements

I would like to express my sincerest gratitude to my supervisor Prof. Dr. Didier Sornette for his excellent guidance. He opened the wonderful undiscovered science world to me and led me on the road to dig out the fantastic treasure in this world. I am deeply grateful to Dr. Ryan Woodard, who has been taking care of me in every tiny aspect in the past three years. With his guidance and help, I am making progress rapidly to be a mature researcher and a complete person. I am also grateful to Prof. Dr. Wei-Xing Zhou and Reda Rebib for their hard work and useful advices. Part of the research written in this thesis is the joint work with them. My special thanks go to my family and Rujun Jia for their love and support. I would like to thank Prof. Dr. Thorsten Hens and Prof. Dr. Paul Embrechts for their acceptance to be my doctoral co-examiners and the guidance on this thesis, and Prof. Dr. Antoine Bommier for his acceptance to be the assessor of the doctoral examination. My sincere thanks also go to Heidi Demuth for all her kind help during my doctoral studies. I would like to express my deep thanks to Andreas Hüsler and Heidi Demuth for their excellent work on the German abstract of this thesis. Finally, I thank the members of Chair of Entrepreneurial Risks: Prof. Dr. Alexander Saichev, Prof Dr. Yannick Malevergne, Prof. Dr. Vyacheslav Yukalov, Prof. Dr. Taisei Kaizoji, Prof. Dr. Jeffrey Satinover, Shengsui Hu, Moritz Hetzer, Qunzhi Zhang, Dr. Vladimir Filimonov, Dr. Peter Cauwels, Georges Harras, Andreas Hüsler, Dr. Thomas Maillart, Dr. Riley Crane, Dr. Hilary Woodard, Maroussia Favre, Susanne von der Becke, Dr. Monika Gisler, Dr. Ching-Yi Tsai, Ryohei Hisano, Meng Li, Dr. Zhi-Qiang Jiang, Dr. Li Lin, Xiao-Hui Ni, Dr. Maxim Fedorovsky, Stanislav Gora, Amine Issami, et cetera.

Abstract

Financial bubbles are well known for their dramatic dynamics and consequences that affect much of the world's population. Consequently, much research has aimed at understanding, identifying and forecasting bubbles and, in particular, the related, subsequent crashes. However, researchers still cannot come to an agreement on the definition and the causes of financial bubbles, let alone to correctly identify and forecast them in advance.

The Johansen-Ledoit-Sornette (JLS) model is a framework to understand bubbles and crashes from rational expectations. The model states that bubbles are not characterized by exponential increase of price but rather by faster-than-exponential growth of price, which is due to imitation and herding behavior of noise traders creating a positive feedback mechanism during the bubble regime. Over longer than the past decade, the predictability of the JLS model in detecting bubbles and crashes has been confirmed both ex-post and ex-ante in various kinds of markets.

This thesis contributes to the current research on financial bubbles and the JLS model by four aspects:

(i) Documentation of previous research on financial bubbles and the JLS model with detailed clarifications to questions and criticisms on the JLS model. This offers a synthesis of the existing state-of-the-art and best-practice advices in order to catalyze useful future developments of research on bubbles.

(ii) Development of the generalized JLS models to estimate the fundamental value of a stock and market risk diversification during a bubble. The first extension solved the problem that the fundamental value of an asset is generally not directly observable, poorly constrained to calculate and not distinguishable from an exponentially growing bubble price. While the second extension provides the information about the concentration of stock gains in a market over time. This new information is very helpful to understand the risk diversification and to explain the investors' behavior during the bubble generation.

(iii) The standard JLS model has been extended to identify negative bubbles and subsequent possible large market rebounds. By introducing a pattern recognition method from the field of earthquake prediction, the systematic predictability of the

JLS model in detecting crashes and rebounds has been confirmed in many major global indices over a long period.

(iv) The JLS model has been used to make ex-post prediction of the 2008 financial crash through analysis of the US repurchase agreements market size. This enhances our understanding of the development of financial instabilities by providing the first quantitative study of a leverage variable which complements other pieces of evidence in equities, real estates and commodities.

Zusammenfassung

Turbulenzen an den Märkten und Finanzblasen betreffen alle. Konsequenterweise wird grosser Aufwand betrieben um Finanzblasen zu identifizieren, zu verstehen und insbesondere deren Platzen vorherzusagen. Trotzdem ist es der wissenschaftlichen Forschung bis heute nicht gelungen, Finanzblasen (und deren Platzen) zuverlässig vorherzusagen. Stattdessen melden sich im Nachhinein immer wieder Koryphäen und Experten, um die Tatsache zu vermelden, dass eine Finanzblase offensichtlich war.

Das Johansen-Ledoit-Sornette (JLS) Modell ist ein Framework zum Verstehen von Finanzblasen und deren Platzen aus der Sicht eines rationalen Investors. In diesem Modell werden Blasen nicht als exponentielles Preiswachstum, sondern aufgrund von Imitations- und Herdenverhalten von "Noise Tradern" und mit positivem Feedback als "schneller-als-exponentielles" Preiswachstum beschrieben. Das JLS-Modell hat sich sowohl bei ex-ante, wie auch bei ex-post Analysen für verschiedene Marktumfeldern in den letzten Jahrzehnten als zuverlässig erwiesen.

Die vorliegende Arbeit trägt in vier Aspekten zum besseren Verständnis von Marktblasen und des JLS-Modells bei:

(i) Dokumentation über bisher vorhandene Forschungsresultate über Marktblasen und das JLS-Modells, inklusive einer detaillierten Diskussion und einer Klarstellung zu Fragen und Kritik am JLS-Modell. Des Weiteren werden neue Entwicklungen rund um das JLS-Modell sowie dessen praktische Anwendung diskutiert.

(ii) Verallgemeinerungen des JLS-Modells zur Berechnung des Fundamentalwertes von Aktien und Marktrisiken während Finanzblasen. Eine erste Erweiterung löst das Problem, dass der Fundamentalwert einer Aktie üblicherweise nicht direkt beobachtbar und nicht unterscheidbar von einem exponentiell wachsendem Preis ist. Eine zweite Erweiterung untersucht die Konzentration von Aktienpreisgewinnen im Verlauf der Zeit. Diese Erweiterung ist hilfreich für das Verständnis der Risikodiversifikation und erklärt das Investorenverhalten bei der Bildung einer Finanzblase.

(iii) Erweiterung des Standard-JLS-Modell zur Identifikation von "negativen" Finanzblasen und der damit verbundenen Trendwende. Durch die Benutzung von Mustererkennungsmethoden aus der Erdbebenforschung kann die Fähigkeit des JLS-

Modells, systematisch Finanzblasen und Trendveränderungen in Marktindexes über lange Zeiträume vorherzusagen, bewiesen werden.

(iv) Analyse der Marktgrösse der US Rückkauf Vereinbarungen mittels JLS-Modell zur ex-post Voraussage der Finanzmarktkrise von 2008. Dadurch wird das Verständnis für die Bildung von Instabilitäten an den Finanzmärkten verbessert, da erstmals die Fremdfinanzierung von Institutionen berücksichtigt wird und damit vorhandene Studien über Aktienmärkte, Immobilien und Rohstoffe ergänzt werden.

Contents

1

Introduction

Financial bubbles are of extreme importance in modern society. Their formation and dramatic bursts are usually considered to have great impact on most people all over the world. Take the recent real estate bubble and the subsequent subprime crisis as examples: Up to 2009, it led to more than four trillion global cumulative losses of financial institutions [1], over six million job losses in the US [2] and the destruction is still ongoing.

However, as the president of the Federal Reserve Bank of New York, William C. Dudley stated in 2010[3]: "... what I am proposing is that we try—try to identify bubbles in real time, try to develop tools to address those bubbles, try to use those tools when appropriate to limit the size of those bubbles and, therefore, try to limit the damage when those bubbles burst ..." it is still very difficult in identifying, understanding bubbles, and more importantly, trying to forecast and possibly avoid them in advance. In this thesis, I will start the discussion on financial bubbles by addressing the most fundamental questions which still remain unsolved: (i) What are bubbles? (ii) What are the causes of bubbles? and (iii) How to diagnose bubbles ex-ante?

1.1   What are bubbles?

Financial bubbles can be generally defined as transient upward acceleration of prices above fundamental value [4, 5, 6, 7]. However, identifying unambiguously the presence of a bubble remains an unsolved problem in standard econometric and financial economic approaches [8, 9], due to the fact that the fundamental value is in general poorly constrained and it is not possible to distinguish between exponentially growing fundamental price and exponentially growing bubble price. Therefore, a more precise definition of bubbles is required for the purpose to detect them.

An investigation into some famous historical bubbles would give some more perceptual knowledge of financial bubbles, and subsequently, crucial insights of their definition.

The tulip mania

Perhaps the first famous bubble in economy history is the tulip mania that struck Republic of Netherlands in 1630s. The country was experiencing a great prosperity in the sixteenth and seventeenth century, during which the tulip was introduced to Europe from the Ottoman Empire. The flower rapidly became a coveted luxury item and a status symbol because of it beauty and profusion of varieties. A huge number of the speculators started trading tulip, and consequently, the price of the tulip bulbs raised to an unbelievable high level. For example, the bulb of "Viceroy" cost between 3000 and 4200 florins, while as a comparison, a skilled craftsman at the time earned about 300 florins a year [10]. In February 1637, the tulip market suddenly collapsed [11].

The South Sea bubble

The South Sea bubble in 1720 was a great economic bubble leaded by speculation of stock in the South Sea Company. During the War of the Spanish Succession, a large amount of the British government debt was issued, and the government wanted to cut off the interest rate of the debt to relieve its financial pressure. At the same time, the stock of South Sea company was very popular because it was granted a monopoly to trade in Spain's South American colonies as part of a treaty during the War of Spanish Succession. The company would like to hedge its risk by buying the
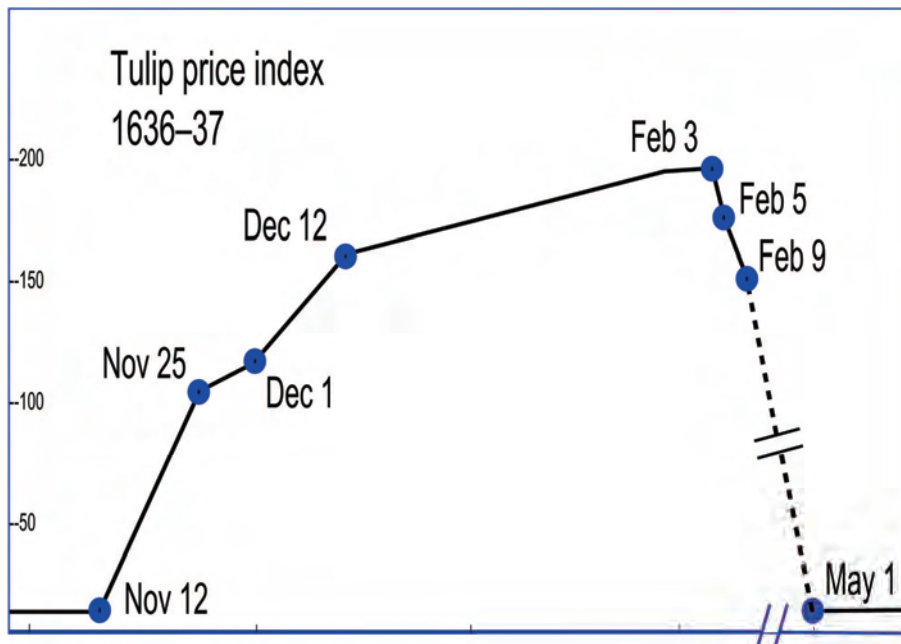
Figure 1.1: A standardized price index for tulip bulb contracts, created by Earl Thompson [11]. From February to May, the tulip market collapsed abruptly.

debts with its highly evaluated stocks and get stable income from the government. Under this circumstance, the South Sea Scheme was activated exactly the same as our discussion above. This scheme was considered to be a win-win trading. As a consequence, the public started to buy the stocks of South Sea company and the illegal actions from the company (fraud, lending money to the buyers to enable their purchase of the stocks, etc.) escalated the irrational behavior. As Fig. 1.2 shows, the share price had risen from the time the scheme was proposed: from £128 in January to £1,000 in early August, followed by a dramatic fall down to about 100 pounds within several months. Hundreds of people lost a huge amount of money, including Sir Issac Newton. When he was asked about the continuance of the rising of South Sea stock, he answered: "I can calculate the movement of the stars, but not the madness of men" [12].

The late 1920s bubble and the great depression

The sharp rise and subsequent crash of stock prices in late 1920s is perhaps the most striking episode in the history of American financial markets [13]. Before the crash, hundreds of thousands of Americans invested heavily in the stock market in the belief
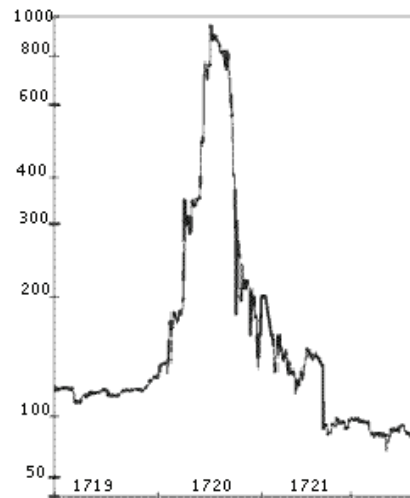
Figure 1.2: Share price of South Sea company around the bubble. Source: Wikipedia
(`zh.wikipedia.org/zh/File:South-sea-bubble-chart.png`)

that the development of utility would lead to a "new" economy, and a significant
number of them were borrowing money to buy more stocks. The rising share prices
encouraged more people to invest, which created a positive feedback loop. A massive
bubble was generated by such kind of speculation. The bubble began to deflate, and
October 24, 1929 , which became known as "Black Thursday", marked the beginning
of the "Great Crash". This crash is one of the most devastating stock market crashes
in the history of the United States. It triggered the 12-year Great Depression that
affected all Western industrialized countries [14] and that did not end in the United
States until the onset of American mobilization for World War II at the end of 1941.

These famous historical bubbles offer some qualitative ideas on the reasons for
the absence of a quantitative definition: the term "bubble" refers to a situation
in which excessive public expectations of future price increases cause prices to be
temporarily elevated [15]. Take the dot-com bubble as an example, in the late
twentieth century, investors thought that better business models, network effects,
first-to-scale advantages, and real options effect could be considered as rational
reasons for the high prices of internet companies [16]. Based on this consideration,
the stock prices of information technology companies were temporarily elevated
in the late 1990s and finally crashed in 2000. The former U.S. Federal Reserve
chairman Alan Greenspan addressed this situation precisely [17]: "Is it possible that

there is something fundamentally new about this current period that would warrant such complacency? Yes, it is possible. Markets may have become more efficient, competition is more global, and information technology has doubtless enhanced the stability of business operations. But, regrettably, history is strewn with visions of such new eras that, in the end, have proven to be a mirage. In short, history counsels caution."

1.2   What are the causes of bubbles?

What are the causes of bubbles? Many theories have been developed to answer this question.

Financial bubbles can be generated by irrationality of the investors. According to [4], the rise in the stock market depended on "the vested interest in euphoria that leads men and women, individuals and institutions to believe that all will be better, that they are meant to be richer and to dismiss as intellectually deficient what is in conflict with that conviction." This eagerness to buy stocks was then fueled by an expansion of credit in the form of brokers' loans that encouraged investors to become dangerously leveraged. In this respect, Shiller [18] argues that the stock price increase was driven by irrational euphoria among individual investors, fed by an emphatic media, which maximized TV ratings and catered to investor demand for pseudo-news.

Recent theories also show that bubbles can be generated even if there is no irrational investors, because of (i) heterogeneous beliefs of investors together with a limitation on arbitrage, (ii) positive feedback trading by "noise traders", (iii) synchronization failures among rational traders.

Many researches [19, 20, 21, 22, 23, 24, 25] show that the combined effects of heterogeneous beliefs and short-sales constraints may cause large movements in asset. In this kind of models, the asset prices are determined at equilibrium to the extent that they reflect the heterogeneous beliefs about payoffs. But short sales restrictions force the pessimistic investors out of the market, leaving only optimistic investors and thus inflated asset price levels. However, when short sales restrictions no longer bind investors, then prices fall back down.

In another class of models, the role of "noise traders" in fostering positive feedback trading has been emphasized. These "noise" positive feedback traders buy securities when prices rise and sell when prices fall. Due to this positive feedback mechanism, the deviation between the market price and the fundamental value has been amplified [26, 27, 28, 29]. The empirical evidence on this theory are mainly from the studies on momentum trading strategies. Stocks which performed poorly in the past will perform better in a long-term perspective (over the next three to five years) than stocks which performed well in the past [30]. In contrast, at intermediate horizon (three to twelve months), the stocks which performed well previously will still perform better [31, 32].

Another mechanism preventing the growth of bubbles has been argued to be the failure of synchronization of rational traders [33]. In this model, rational investors decide to ride the bubble to make profit on it, which has been confirmed by empirical studies on hedge funds (ideal rational investors) during the dot-com bubble [34]. They know that the market will eventually collapse when a sufficient number of rational traders will sell out. However, the dispersion of their opinions on market timing and the consequent uncertainty of the synchronization of their sell-off are delaying this coming collapse, allowing the bubble to grow.

Here we only presented a brief summary on causes of bubbles. The detailed survey on the existing bubble theories and main causes of bubbles can be found in [35, 36].

1.3 The Johansen-Ledoit-Sornette model as a tool to diagnose bubbles ex-ante?

The former Federal Reserve chairman Alan Greenspan said that "...we recognized that, despite our suspicions, it was very difficult to definitively identify a bubble until after the fact—that is, when its bursting confirmed its existence." [37] at a symposium sponsored by the Federal Reserve Bank of Kansas City, Jackson Hole, Wyoming in August 2002.

This statement also reflects the current situation in bubbles research. None of the theories mention above can diagnose bubbles ex-ante. This may be due to

the fact that all these theories cannot distinguish between exponentially growing fundamental price and exponentially growing bubble price and cannot give a price dynamics which leads to a crash.

To diagnose bubbles ex-ante, Sornette and his collaborators have proposed a theoretical model, which is known as the Johansen-Ledoit-Sornette (JLS) model. The JLS model describes the price dynamics during a bubble regime (identification) by analyzing the cumulative human behaviors in a new perspective (causes). It also has the ability to predict the most probable crash time after a bubble ex-ante (forecasts).

In the JLS model, bubbles are actually not characterized by exponential prices (sometimes referred to as "explosive"), but rather by faster-than-exponential growth of price (that should therefore be referred to as "super-explosive"). The reason for such faster-than-exponential regimes is that imitation and herding behavior of noise traders and of boundedly rational agents create positive feedback in the valuation of assets, resulting in price processes that exhibit a finite-time singularity at some future time t_c. See [38] for a general theory of finite-time singularities in ordinary differential equations, [39] for a classification and [40, 41, 42] for applications. This critical time t_c is interpreted as the end of the bubble, which is often but not necessarily the time when a crash occurs [43]. Thus, the main difference with standard bubble models is that the underlying price process is considered to be intrinsically transient due to positive feedback mechanisms that create an unsustainable regime. Furthermore, the tension and competition between the value investors and the noise traders may create deviations around the finite-time singular growth in the form of oscillations that are periodic in the logarithm of the time to t_c. Log-periodic oscillations appear to our clocks as peaks and valleys with progressively greater frequencies that eventually reach a point of no return, where the unsustainable growth has the highest probability of ending in a violent crash or gentle deflation of the bubble. Log-periodic oscillations are associated with the symmetry of discrete scale invariance, a partial breaking of the symmetry of continuous scale invariance, and occurs in complex systems characterized by a hierarchy of scales. The detailed theory on discrete scale invariance can be found in [44] and references therein.

The theory will be extended in Chapter 2 and relevant ongoing experiments will be introduced to show that financial bubbles can be diagnosed ex-ante.

1.4   Contribution of this thesis

This thesis builds on and contributes to the research on the Johansen-Ledoit-Sornette (JLS) model to identify and forecast financial bubbles in four aspects:

1.4.1   Introduction and clarifications to questions and criticisms on the JLS model

Background of the JLS model

During an endogenous bubble regime, the price of an asset follows a log-periodic power law. We introduce the background of the JLS model in Sec. 2.1. The log-periodic power law behavior in the JLS model can be interpreted by four steps: the long time scale fermentation, imitation and herding among humans, positive feedback among traders leads to power law growth in asset price and the competition between different types of traders lead to log-periodic oscillations.

Derivation of the JLS model

The JLS model is an extension of the rational expectation bubble model of [45]. In this model, a crash is seen as an event potentially terminating the run-up of a bubble. A financial bubble is modeled as a regime of accelerating (super-exponential power law) growth punctuated by short-lived corrections organized according to the symmetry of discrete scale invariance [44]. The super-exponential power law is argued to result from positive feedback resulting from noise trader decisions that tend to enhance deviations from fundamental valuation in an accelerating spiral. We will give the derivation in Sec. 2.2.

Fit procedure

In Sec. 2.3, we briefly introduce the standard fit procedure of the JLS model. This procedure is a combination of the heuristic search for the initial estimates and the refine process to minimize the residuals between the model and the data. We normally use the taboo algorithm as the heuristic search method and the Levenberg-Marquardt as the refine procedure.

Clarifications to questions and criticisms on the JLS model

Having been developed for more than one decade, the JLS model has been studied, analyzed, used and criticized by several researchers. Much of this discussion is helpful for advancing the research. However, several serious misconceptions seem to be present within this collective conversation both on theoretical and empirical aspects. Several of these problems appear to stem from the fast evolution of the literature on the JLS model and related works. In the hope of removing possible misunderstanding and of catalyzing useful future developments, in Sec. 2.4, we summarize these common questions and criticisms concerning the JLS model and offer a synthesis of the existing state-of-the-art and best-practice advices.

1.4.2 The generalized JLS models

Generalize the JLS model by introducing new factors in order to detect the important but unknown market features during the bubble regime. With the knowledge of these keynote factors, one can understand the bubble mechanisms more deeply and take actions based on these new findings to regulate the market. Two types of the generalized JLS model will be presented in this thesis.

The generalized JLS models by inferring fundamental value and crash nonlinearity from bubble calibration

Identifying unambiguously the presence of a bubble in an asset price remains an unsolved problem in standard econometric and financial economic approaches. A large part of the problem is that the fundamental value of an asset is, in general, not directly observable and it is poorly constrained to calculate. Further, it is not possible to distinguish between an exponentially growing fundamental price and an exponentially growing bubble price.

In Sec. 3.1, we present a series of the generalized JLS models by inferring the fundamental value of an asset price and a crash nonlinearity from a bubble calibration. In addition to forecasting the time of the end of a bubble, the new models can also estimate the fundamental value and the crash nonlinearity, meaning that identifying the presence of a bubble is enabled by these models. In addition, the crash nonlinearity obtained in the new models presents a new approach to possibly identify the dynamics of a crash after a bubble.

We test the models using data from three historical bubbles ending in crashes from different markets. They are: the Hong Kong Hang Seng index 1997 crash, the S&P 500 index 1987 crash (black Monday) and the Shanghai Composite index 2009 crash. All results suggest that the new models perform very well in describing bubbles, forecasting their ending times and estimating fundamental value and the crash nonlinearity.

The performance of the new models is tested under both the Gaussian residual assumption and the non-Gaussian residual assumption. Under the Gaussian residual assumption, nested hypotheses with the Wilks statistics are used and the p-values suggest that models with more parameters are necessary. Under non-Gaussian residual assumption, we use a bootstrap method to get type I and II errors of the hypotheses. All tests confirm that the generalized JLS models provide useful improvements over the standard JLS model.

The generalized JLS model by considering the diversification risk of the stock market

We present an extension of the JLS model in Sec. 3.2 to include an additional pricing factor called the "Zipf factor", which describes the diversification risk of the stock market portfolio. Keeping all the dynamical characteristics of a bubble described in the JLS model, the new model provides additional information about the concentration of stock gains over time. This allows us to understand better the risk diversification and to explain the investors' behavior during the bubble generation.

We apply this new model to two famous Chinese stock bubbles, from August 2006 to October 2007 (Bubble 1) and from October 2008 to August 2009 (Bubble 2). The Zipf factor is found highly significant for Bubble 1, corresponding to the fact that valuation gains were more concentrated on the large firms of the Shanghai index. It is likely that the widespread acknowledgement of the 80-20 rule in the Chinese media and discussion forums led many investors to discount the risk of a lack of diversification, therefore enhancing the role of the Zipf factor. For Bubble 2, the Zipf factor is found marginally relevant, suggesting a larger weight of market gains on small firms. We interpret this result as the consequence of the response of the Chinese economy to the very large stimulus provided by the Chinese government

in the aftermath of the 2008 financial crisis.

1.4.3 Systematic diagnosis and prediction of rebounds and crashes in financial markets

We will develop a new method which can diagnose and predict rebounds and crashes in financial markets systematically by introducing a pattern recognition method into the JLS framework of bubble calibration.

Diagnosis and prediction of rebounds in financial markets

In Sec. 4.1, we introduce the concept of "negative bubbles" as the mirror (but not necessarily exactly symmetric) image of standard financial bubbles, in which positive feedback mechanisms may lead to transient accelerating price falls. To model these negative bubbles, we adapt the JLS model of rational expectation bubbles with a hazard rate describing the collective buying pressure of noise traders. The price fall occurring during a transient negative bubble can be interpreted as an effective random down payment that rational agents accept to pay in the hope of profiting from the expected occurrence of a possible rally. We validate the model by showing that it has significant predictive power in identifying the times of major market rebounds. This result is obtained by using a general pattern recognition method that combines the information obtained at multiple times from a dynamical calibration of the JLS model. Error diagrams, Bayesian inference and trading strategies suggest that one can extract genuine information and obtain real skill from the calibration of negative bubbles with the JLS model. We conclude that negative bubbles are in general predictably associated with large rebounds or rallies, which are the mirror images of the crashes terminating standard bubbles.

Detection of Crashes and Rebounds in Major Equity Markets

In Sec. 4.2 we extend the method in Sec. 4.1 to systematic ex-post forecasts and detections of market crashes and rebounds from ten major global equity markets. We show quantitatively that our developed alarm performs much better than chance in forecasting market crashes and rebounds. We use the derived signal to develop elementary trading strategies that produce statistically better performances than a simple buy and hold strategy.

1.4.4 Ex-post case study on the US repurchase agreements market by using the JLS model to detect the leverage bubble

Leverage is strongly related to liquidity in a market and lack of liquidity is considered a cause and/or consequence of the recent financial crisis. A repurchase agreement is a financial instrument where a security is sold simultaneously with an agreement to buy it back at a later date. Repurchase agreements (repos) market size is a very important element in calculating the overall leverage in a financial market. Therefore, studying the behavior of repos market size can help to understand a process that can contribute to the birth of a financial crisis. In Chapter 5, we hypothesize that herding behavior among large investors led to massive over-leveraging through the use of repos, resulting in a bubble (built up over the previous years) and subsequent crash in this market in early 2008. We use the JLS model of rational expectation bubbles and behavioral finance to study the dynamics of the repo market that led to the crash. As we know that the JLS model qualifies a bubble by the presence of log-periodic power law (LPPL) behavior in the price dynamics. We show that there was significant LPPL behavior in the market before the crash in 2008 and that the predicted range of times predicted by the model for the end of the bubble is consistent with the observations.

2

The Johansen-Ledoit-Sornette Model

Bubbles and crashes in financial markets are of global significance because of their effects on the lives and livelihoods of a majority of the world's population. In spite of this, the science to correctly identify bubbles in advance of their associated crashes produces fewer successful results than that used to treat baldness, choose 'quality' videos to watch or find a date on the internet. Instead, pundits and experts alike line up after the fact to claim that a particular bubble was obvious in hindsight.

Under this circumstance, the Johansen-Ledoit-Sornette (JLS) model [46, 47, 48, 5] has been developed to describe the dynamics of financial bubbles and crashes. The model states that bubbles are not characterized by exponential increase of price but rather by faster-than-exponential growth of price. This phenomenon is generated by behaviors of investors and traders that create positive feedback in the valuation of assets and unsustainable growth, leading to a finite-time singularity at some future time t_c. From a technical view point, the positive feedback mechanisms include (i) option hedging, (ii) insurance portfolio strategies, (iii) market makers bid-ask spread in response to past volatility, (iv) learning of business networks and human capital build-up, (v) procyclical financing of firms by banks (boom versus contracting times), (vi) trend following investment strategies, (vii) asymmetric information on hedging strategies (viii) the interplay of mark-to-market accounting and regulatory capital requirements. From a behavior view point, positive feedbacks emerge as a result of the propensity of humans to imitate, their social gregariousness and the resulting herding. This critical time t_c of the model is interpreted as the end of the

bubble, which is often but not necessarily the time when a crash occurs in the actual system. During this growth phase, the tension and competition between the value investors and the noise traders create deviations around the power law growth in the form of oscillations that are periodic in the logarithm of the time to t_c. Combining these two effects, this model succinctly describes the price during a bubble phase as log-periodic power law (LPPL).

Over longer than the past decade, the JLS model has been used widely to detect bubbles and crashes ex-ante (i.e., with advanced documented notice in real time) in various kinds of markets such as the 2006-2008 oil bubble [49], the Chinese index bubble in 2009 [50], the real estate market in Las Vegas [51], the U.K. and U.S. real estate bubbles [52, 53], the Nikkei index anti-bubble in 1990-1998 [54] and the S&P 500 index anti-bubble in 2000-2003 [55]. Other recent ex-post studies include the Dow Jones Industrial Average historical bubbles [56], the corporate bond spreads [57], the Polish stock market bubble [58], the western stock markets [59], the Brazilian real (R$) - US dollar (USD) exchange rate [60], the 2000-2010 world major stock indices [61], the South African stock market bubble [62] and the US repurchase agreements market [63]. Moreover, new experiments in ex-ante bubble detection and forecast has been launched since November 2009 in the Financial Crisis Observatory at ETH Zurich [64, 65, 66].

In this chapter, we present the JLS model to advance the science of understanding why, how and when bubbles form so that they can be identified *before* they spectacularly crash and spread misfortune to those who knowingly or unknowingly had bet on a long position. We will also give a detailed derivation of the JLS model to show that the JLS model is an extension of the rational expectation bubble model and present the fit procedure of the JLS model. We finally discuss the questions and criticisms on the JLS model and give a clarification.

2.1   Background of the JLS Model

The basis for the JLS approach contradicts the accepted wisdom of the Efficient Market Hypothesis, which claims that large deviations from fundamental prices (i.e., bubbles and crashes) only exist when a new piece of information drops (exoge-

nously) onto an unsuspecting market on a very short time scale. Instead, we claim that bubbles are the result of endogenous market dynamics over a much longer time scale—weeks, months and years. Because of the long build-up of these effects, bubbles can be identified by particular dynamical signatures predicted by our theoretical framework.

Among the well-documented history of financial bubbles and crashes over the past 400 years, through countless significantly different countries and kings, empires and economies, regulations and reform, there has been one consistent ingredient in all booms and busts: humans. Only human behavior has survived all attempts at preventing repeats in the wake of disastrous crashes. Much of the dynamics of the long time scales mentioned above is due to humans acting like humans: those without the knowledge imitate one another in the absence of a clearly better alternative and take refuge in the comfort of the crowd (herding) while those with the knowledge refute the masses and claim these noise traders are wrong.

We hypothesize that the signatures of this characteristic human behavior can be quantitatively identified. The imitation and herding behavior creates positive feedback in the valuation of an asset, resulting in a greater-than-exponential (power law) growth of the price time series. The tension and competition between the learned experts and the noise traders creates decorations on this power law growth comprising oscillations that are periodic in the logarithm of time. Log-periodic oscillations appear to our clocks as peaks and valleys with progressively smaller amplitudes and greater frequencies that eventually reach a point of no return, where the unsustainable growth has the highest probability of ending in a violent crash or gentle deflation of the bubble.

The JLS model has thus been developed as a flexible tool to detect bubbles. This model combines (i) the economic theory of rational expectation bubbles, (ii) behavioral finance on imitation and herding of investors and traders and (iii) the mathematical and statistical physics of bifurcations and phase transitions. The JLS model considers the faster-than-exponential (power law with finite-time singularity) increase in asset prices decorated by accelerating oscillations as the main diagnostic of bubbles. It embodies a positive feedback loop of higher return anticipations competing with negative feedback spirals of crash expectations.

2.1.1 Long time scale fermentation of bubbles

In sharp contrast to the Efficient Market Hypothesis (EMH) that crashes result from novel negative information incorporated in prices at short time scales, we build on the radically different hypothesis summarized by Sornette [5], that the underlying causes of the crash should be found in the preceding year(s). We define a bubble as a market regime in which the price accelerates "super-exponentially". The term "super-exponential" means that the growth rate of the price grows itself. A constant price growth rate (also called return) leads to an exponential growth, the normal average trajectory of most economic and financial time series. When the growth rate grows itself, the price accelerate hyperbolically. This growth of the growth rate is interpreted as being due to progressively increasing build-up of market cooperation between investors. As the bubble matures, its approaches a critical point, at which an instability can be triggered in the form of a crash, or more generally a change of regime. This critical point can also be called a phase transition, a bifurcation, a catastrophe or a tipping point. According to this "critical" point of view, the specific manner by which prices collapse is not the most important problem: a crash occurs because the market has entered an unstable phase and any small disturbance or process may reveal the existence of the instability. Think of a ruler held up vertically on your finger: this very unstable position will lead eventually to its collapse as a result of a small (or an absence of adequate) motion of your hand or due to any tiny whiff of air. The collapse is fundamentally due to the unstable position; the instantaneous cause of the collapse is secondary. In the same vein, the growth of the sensitivity and the growing instability of the market close to such a critical point might explain why attempts to unravel the proximal origin of the crash have been so diverse. Essentially, anything would work once the system is ripe.

What is the origin of the maturing instability? A follow-up hypothesis underlying this proposal is that, in some regimes, there are significant behavioral effects underlying price formation leading to the concept of "bubble risks". This idea is probably best exemplified in the context of financial bubble, where, fueled by initially well-founded economic fundamentals, investors develop a self-fulfilling enthusiasm by an imitative process or crowd behavior that leads to the building of castles in the air, to paraphrase Malkiel [67].

Our previous research suggests that the ideal economic view, that stock markets are both efficient and unpredictable, may be not fully correct. We propose that, to understand stock markets, one needs to consider the impact of positive feedbacks via possible technical as well as behavioral mechanisms such as imitation and herding, leading to self-organized cooperation and the development of possible endogenous instabilities. We thus propose to explore the consequences of the concept that most of the crashes have fundamentally an endogenous, or internal, origin and that exogenous, or external, shocks only serve as triggering factors. As a consequence, the origin of crashes is probably much more subtle than often thought, as it is constructed progressively by the market as a whole, as a self-organizing process. In this sense, the true cause of a crash could be termed a systemic instability.

2.1.2   Imitation and herding among humans as the cause of bubbles

Humans are perhaps the most social mammals and they shape their environment to their personal and social needs. This statement is based on a growing body of research at the frontier between new disciplines called neuroeconomics, evolutionary psychology, cognitive science and behavioral finance ([68, 69, 70]). This body of evidence emphasizes the very human nature of humans with its biases and limitations, opposed to the previously prevailing view of rational economic agents optimizing their decisions based on unlimited access to information and to computation resources.

We hypothesize that financial bubbles are footprints of perhaps the most robust trait of humans and the most visible imprint in our social affairs: imitation and herding (see Sornette [5] and references therein). Imitation has been documented in psychology and in neurosciences as one of the most evolved cognitive processes, requiring a developed cortex and sophisticated processing abilities. In short, we learn our basics and how to adapt mostly by imitation all through our life. It seems that imitation has evolved as an evolutionary advantageous trait, and may even have promoted the development of our anomalously large brain (compared with other mammals), according to the so-called "social brain hypothesis" advanced by R. Dunbar [71]. It is actually "rational" to imitate when lacking sufficient time, energy and information to make a decision based only on private information and processing, that is, most of the time. Imitation, in obvious or subtle forms, is a

pervasive activity of humans. In the modern business, economic and financial worlds, the tendency for humans to imitate leads in its strongest form to herding and to crowd effects. Imitation is a prevalent form in marketing with the development of fashion and brands. Cooperative herding and imitation lead to positive feedbacks, that is, an action leads to consequences which themselves reinforce the action and so on, leading to virtuous or vicious circles.

The methodology that we have developed consists in using a series of mathematical and computational formulations of these ideas, which capture the hypotheses that (1) bubbles can be the result of positive feedbacks and (2) the dynamical signature of bubbles derives from the interplay between fundamental value investment and more technical analysis. The former can be embodied in nonlinear extensions of the standard financial Black-Scholes model of log-price variations [72, 73, 74, 75]. The later requires more significant extensions to account for the competition between (i) inertia separating analysis from decisions, (ii) positive momentum feedbacks and (iii) negative value investment feedbacks [73].

2.1.3 Positive feedback among traders leads to power law growth in asset price

The idea of positive feedback has led us to propose that one of the hallmarks of a financial bubble is the faster-than-exponential growth of the price of the asset under consideration, as already mentioned. It is convenient to model this accelerated growth by a power law with a so-called finite-time singularity [42]. This feature is nicely illustrated by the price trajectory of the Hong Kong Hang Seng index from 1970 to 2000, as shown in Fig. 2.1. The Hong Kong financial market is repeatedly rated as providing one of the most pro-economic, pro-entrepreneurship and free market-friendly environments in the world, and thus provides a textbook example of the behavior of weakly regulated liquid and striving financial markets. In Fig. 2.1, the logarithm of the price $p(t)$ is plotted as a function of time (in linear scale), so that an upward trending straight line qualifies as exponential growth with a constant growth rate: the straight solid line corresponds indeed to an approximately constant growth rate of the Hang Seng index equal to 13.8% per year.

The most striking feature of Fig. 2.1 is not this average behavior but instead the obvious fact that the real market is never following and abiding to a constant growth

rate. One can observe a succession of price run-ups characterized by growth rates ... growing themselves: this is reflected visually in Fig. 2.1 by transient regimes characterized by strong upward curvature of the price trajectory. Such an upward curvature in a linear-log plot is a first visual diagnostic of a faster than exponential growth (which of course needs to be confirmed by rigorous statistical testing). Such a price trajectory can be approximated by a characteristic transient finite-time singular power law of the form

$$\log p(t) = A + B(t_c - t)^m \tag{2.1}$$

where $B < 0$, $0 < m < 1$ and t_c is the theoretical critical time corresponding to the end of the transient run-up (end of the bubble). Such transient faster-than-exponential growth of $p(t)$ is our definition of a bubble. It has the major advantage of avoiding the conundrum of distinguishing between exponentially growing fundamental price and exponentially growing bubble price, which is a problem permeating most of the previous statistical tests developed to identify bubbles [9, 8]. The conditions $B < 0$ and $0 < m < 1$ ensure the super-exponential acceleration of the price, together with the condition that the price remains finite even at t_c. Stronger singularities can appear for $m < 0$.

To see that faster-than-exponential growth is naturally related to positive feedback, let us consider the following simple presentation. Consider a population of animals of size x which grows with some constant rate k, i.e., $dx/dt = k\,x$. Then, growth is exponential in that $x(t) = x(0)\,e^{kt}$. On the other hand, positive feedback in growth dynamics arises if the growth rate k itself depends on the population size x in that the growth rate $k = k(x)$ increases with the population size. A particular simple example is the setting $k(x) \sim x^{m-1}$, where $m > 1$. Indeed, $m - 1$ can be regarded as a measure of the degree of cooperation within the population: the higher m is the larger is the degree of cooperation. In the case of no cooperation, growth dynamics is exponential. Positive multiplicative feedback generates growth which is faster than exponential. Indeed, due to growth dynamics given by $dx/dt = k\,x^m$, the size of the population growth exhibits a finite-time singularity at t_c. This singularity is attained according to $x(t) = x(0)[1 - \tau]^{\frac{1}{1-m}}$, $0 < \tau < 1$ where $\tau = \frac{t}{t_c}$. Note that when $m = 1$, no cooperation, growth is indeed exponential and when $m > 1$, growth dynamics is in fact faster than exponential. It is remarkable that a critical

time t_c emerges apparently out of nowhere. Actually, t_c is determined by the initial conditions and the structure of the growth equation. This emergence of t_c which depends on the initial conditions justifies its name in mathematical textbooks as a "movable singularity."
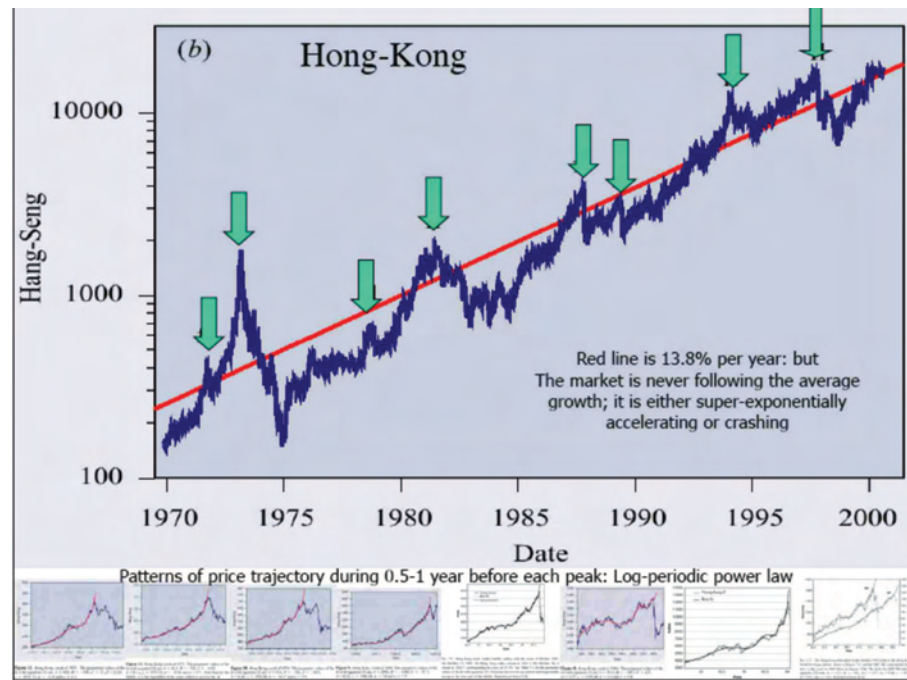
Figure 2.1: Trajectory of the Hong-Kong Hang Seng index from 1970 to 2000. The vertical log-scale together with the linear time scale allows one to qualify an exponential growth with constant growth rate as a straight line. This is indeed the long-term behavior of this market, as shown by the best linear fit represented by the solid straight line, corresponding to an average constant growth rate of 13.8% per year. The 8 arrows point to 8 local maxima that were followed by a drop of the index of more than 15% in less than three weeks (a possible definition of a crash). The 8 small panels at the bottom show the upward curvature of the log-price trajectory preceding each of these local maxima, which diagnose unsustainable bubble regimes, each of which culminates at its peak before crashing.

Many systems exhibit similar transient super-exponential growth regimes, which are described mathematically by power law growth with an ultimate finite-time singular behavior. An incomplete list of examples includes: planet formation in solar systems by runaway accretion of planetesimals, rupture and material failures, nucleation of earthquakes modeled with the slip-and-velocity, models of micro-organisms interacting through chemotaxis aggregating to form fruiting bodies, the Euler rotat-

ing disk, and so on. Such mathematical equations can actually provide an accurate description of the transient dynamics not too close to the mathematical singularity where new mechanisms come into play. The singularity at t_c mainly signals a change of regime. In the present context, t_c is the end of the bubble and the beginning of a new market phase, possibly a crash or a different regime.

Such an approach may be thought at first sight to be inadequate or too naive to capture the intrinsic stochastic nature of financial prices, whose null hypothesis is the geometric random walk model [67]. However, it is possible to generalize this simple deterministic model to incorporate nonlinear positive feedback on the stochastic Black-Scholes model, leading to the concept of stochastic finite-time singularities [72, 76, 77, 75, 78, 79]. Still much work needs to be done on this theoretical aspect.

Coming back to Fig. 2.1, one can also notice that each burst of super-exponential price growth is followed by a crash, here defined for the eight arrowed cases as a correction of more than 15% in less than 3 weeks. These examples suggest that the non-sustainable super-exponential price growths announced a "tipping point" followed by a price disruption, i.e., a crash. The Hong-Kong Hang Seng index shows that the average exponential growth of the index is punctuated by a succession of bubbles and crashes, which seem to be the norm rather than the exception.

2.1.4 Competition between different types of traders lead to log-periodic oscillations

More sophisticated models than Eq. (2.1) have been proposed to take into account the interplay between technical trading and herding (positive feedback) versus fundamental valuation investments (negative mean-reverting feedback). Accounting for the presence of inertia between information gathering and analysis on the one hand and investment implementation on the other hand [80], and taking additionally into account the coexistence of trend followers and value investing [73], the resulting price dynamics develop second-order oscillatory terms and boom-bust cycles. Value investing does not necessarily cause prices to track value. Trend following may cause short-term trend in prices but, together with value investing and inertia, also causes longer-term oscillations.

The simplest model generalizing Eq. (2.1) and including these ingredients is the so-called log-periodic power law (LPPL) model (see Sornette [5] and references

therein). Formally, some of the corresponding formulas can be obtained by considering that the exponent m is a complex number with an imaginary part, where the imaginary part expresses the existence of a preferred scaling ratio γ describing how the continuous scale invariance of the power law Eq. (2.1) is partially broken into a discrete scale invariance [44]. The LPPL structure may also reflect the discrete hierarchical organization of networks of traders, from the individual to trading floors, to branches, to banks, to currency blocks. More generally, it may reveal the ubiquitous hierarchical organization of social networks recently reported [81] to be associated with the social brain hypothesis [71].

Examples of calibrations of financial bubbles with one implementation of the LPPL model are the 8 super-exponential regimes discussed above in Fig. 2.1: the 8 small insets at the bottom of the figure show the LPPL calibration on the Hang Seng index. Preliminary tests [5] suggest that the LPPL model provides a good starting point to detect bubbles and forecast their most probable end. Rational expectation models of bubbles a la Blanchard and Watson implementing the LPPL model [48, 47] have shown that the end of the bubble is not necessarily accompanied by a crash, but it is indeed the time where a crash is the most probable. But crashes can occur before (with smaller probability) or not at all. That is, a bubble can land smoothly, approximately one-third of the time, according to preliminary investigations [43]. Therefore, only probabilistic forecasts can be developed. Probability forecasts are indeed valuable and commonly used in daily life, such as in weather forecast.

2.2   Derivation of the JLS Model and Bubble Conditions

The JLS model of financial bubbles and crashes is an extension of the rational expectation bubble model of [45]. As we discussed before, a crash in this model is seen as an event potentially terminating the run-up of a bubble. A financial bubble is modeled as a regime of accelerating (super-exponential power law) growth punctuated by short-lived corrections organized according the symmetry of discrete scale invariance [44]. The super-exponential power law is argued to result from positive feedback resulting from noise trader decisions that tend to enhance deviations from fundamental valuation in an accelerating spiral.

In the JLS model, the dynamics of stock markets is described as

$$\frac{dp}{p} = \mu(t)dt + \sigma(t)dW - \kappa dj \ , \tag{2.2}$$

where p is the stock market price, μ is the drift (or trend) and dW is the increment of a Wiener process (with zero mean and unit variance). The term dj represents a discontinuous jump such that $dj = 0$ before the crash and $dj = 1$ after the crash occurs. The loss amplitude associated with the occurrence of a crash is determined by the parameter κ. The assumption of the constant jump size is easily relaxed by considering a distribution of jump sizes, with the condition that its first moment exists. Then, the no-arbitrage condition is expressed similarly with κ replaced by its mean. Each successive crash corresponds to a jump of dj by one unit. The dynamics of the jumps is governed by a crash hazard rate $h(t)$. Since $h(t)dt$ is the probability that the crash occurs between t and $t + dt$ conditional on the fact that it has not yet happened, we have $E_t[dj] = 1 \times h(t)dt + 0 \times (1 - h(t)dt)$ and therefore

$$\mathrm{E}_t[dj] = h(t)dt \ . \tag{2.3}$$

Under the assumption of the JLS model, noise traders exhibit collective herding behaviors that may destabilize the market. The JLS model assumes that the aggregate effect of noise traders can be accounted for by the following dynamics of the crash hazard rate

$$h(t) = B'(t_c - t)^{m-1} + C'(t_c - t)^{m-1}\cos(\omega \ln(t_c - t) - \phi') \ . \tag{2.4}$$

The intuition behind this specification Eq. (2.4) has been presented at length in [46, 48, 47], among others, and further developed in [40] for the power law part and by [73, 81] for the second term in the right-hand-side of expression Eq. (2.4). In a nutshell, the power law behavior $\sim t_c - t)^{m-1}$ embodies the mechanism of positive feedback posited to be at the source of the bubbles. If the exponent $m < 1$, the crash hazard may diverge as t approaches a critical time t_c, corresponding to the end of the bubble. The cosine term in the r.h.s. of Eq. (2.4) takes into account the existence of a possible hierarchical cascade of panic acceleration punctuating the course of the bubble, resulting either from a preexisting hierarchy in noise trader sizes [82] and/or from the interplay between market price impact inertia and nonlinear fundamental value investing [73].

The no-arbitrage condition reads $E_t[dp] = 0$, where the expectation is performed with respect to the risk-neutral measure, and in the frame of the risk-free rate. This is the standard condition that the price process is a martingale. Taking the expectation of expression Eq. (2.2) under the filtration (or history) until time t reads

$$E_t[dp] = \mu(t)p(t)dt + \sigma(t)p(t)E_t[dW] - \kappa p(t)E_t[dj] . \qquad (2.5)$$

Since $E_t[dW] = 0$ and $E_t[dj] = h(t)dt$ (equation (3.19)), together with the no-arbitrage condition $E_t[dp] = 0$, this yields

$$\mu(t) = \kappa h(t) . \qquad (2.6)$$

This result (3.22) expresses that the return $\mu(t)$ is controlled by the risk of the crash quantified by its crash hazard rate $h(t)$.

Now, conditioned on the fact that no crash occurs, Eq. (2.2) is simply

$$\frac{dp}{p} = \mu(t)dt + \sigma(t)dW = \kappa h(t)dt + \sigma(t)dW . \qquad (2.7)$$

Its conditional expectation leads to

$$E_t\left[\frac{dp}{p}\right] = \kappa h(t)dt . \qquad (2.8)$$

Substituting with the expression Eq. (2.4) for $h(t)$ and integrating yields the so-called log-periodic power law equation:

$$\ln E[p(t)] = A + B(t_c - t)^m + C(t_c - t)^m \cos(\omega \ln(t_c - t) - \phi) \qquad (2.9)$$

where $B = -\kappa B'/m$ and $C = -\kappa C'/\sqrt{m^2 + \omega^2}$. Note that this expression Eq. (2.9) describes the average price dynamics only up to the end of the bubble. The JLS model does not specify what happens beyond t_c. This critical t_c is the termination of the bubble regime and the transition time to another regime. This regime could be a big crash or a change of the growth rate of the market. Merrill Lynch EMU (European Monetary Union) Corporates Non-Financial Index in 2009 [64] provides a vivid example of a change of regime characterized by a change of growth rate rather than by a crash or rebound.

For $m < 1$, the crash hazard rate accelerates up to t_c but its integral up to t which controls the total probability for a crash to occur up to t remains finite and less than 1 for all times $t \leq t_c$. It is this property that makes it rational for investors

to remain invested knowing that a bubble is developing and that a crash is looming. Indeed, there is still a finite probability that no crash will occur during the lifetime of the bubble. The excess return $\mu(t) = \kappa h(t)$ is the remuneration that investors require to remain invested in the bubbly asset, which is exposed to a crash risk. The condition that the price remains finite at all time, including t_c, imposes that $m > 0$.

Within the JLS framework, a bubble is qualified when the crash hazard rate accelerates. According to Eq. (2.4), this imposes $m < 1$ and $B' > 0$, hence $B < 0$ since $m > 0$ by the condition that the price remains finite. We thus have a first condition for a bubble to occur

$$0 < m < 1 \ . \tag{2.10}$$

By definition, the crash rate should be non-negative. This imposes [83]

$$b \equiv -Bm - |C|\sqrt{m^2 + \omega^2} \geq 0 \ . \tag{2.11}$$

2.3   The Standard Fitting Procedure

Among the seven parameters in the JLS model, three of them are the linear parameters (A, B and C). The other four (t_c, m, ω and ϕ) are nonlinear parameters.

In the standard fitting procedure, we first slave the linear parameters to the nonlinear ones [47]. The detailed equations and procedure is as follows. We rewrite Eq. (2.9) as:

$$\mathrm{E}[\ln p(t)] = A + Bf(t) + Cg(t) := RHS(t) \ . \tag{2.12}$$

We have also defined

$$f(t) = (t_c - t)^m, \tag{2.13}$$

$$g(t) = (t_c - t)^m \cos(\omega \ln(t_c - t) - \phi) \ . \tag{2.14}$$

The minimization of the sum of the squared residuals should satisfy

$$\frac{\partial \Sigma_t [\ln p(t) - RHS(t)]^2}{\partial \theta} = 0, \quad \forall \ \theta \in \{A, B, C\}. \tag{2.15}$$

The linear parameters A, B and C are determined as the solutions of the linear

system of four equations:

$$\sum_{t=t_1}^{t_2} \begin{pmatrix} 1 & f(t) & g(t) \\ f(t) & f^2(t) & f(t)g(t) \\ g(t) & f(t)g(t) & g^2(t) \end{pmatrix} \begin{pmatrix} A \\ B \\ C \end{pmatrix} = \sum_{t=t_1}^{t_2} \begin{pmatrix} \ln p(t) \\ f(t)\ln p(t) \\ g(t)\ln p(t) \end{pmatrix}, \qquad (2.16)$$

where $[t_1, t_2]$ is the fitting interval of the time series. t_1 is the starting time and t_2 is the ending time of the price time being fitted by expression Eq. (2.9) or equivalently Eq. (2.12). This provides three analytical expressions for the three linear parameters as a function of the remaining nonlinear parameters t_c, m, ω, ϕ. The resulting cost function (sum of square residuals) becomes function of just the four nonlinear parameters t_c, m, ω, ϕ. This achieves a very substantial gain in stability and efficiency as the search space is reduced to the 4 dimensional parameter space (t_c, m, ω, ϕ). A heuristic search implementing the taboo algorithm [84] is used to find initial estimates of the parameters which are then passed to a Levenberg-Marquardt algorithm [85, 86] to minimize the residuals (the sum of the squares of the differences) between the model and the data.

The bounds of the search space are normally selected as:

$$t_c \in [t_2, t_2 + 0.375(t_2 - t_1)] \qquad (2.17)$$

$$m \in [10^{-5}, 1 - 10^{-5}] \qquad (2.18)$$

$$\omega \in [0.01, 40] \qquad (2.19)$$

$$\phi \in [0, 2\pi - 10^{-5}] \qquad (2.20)$$

We choose these bounds because m has to be between 0 and 1 according to the discussion before; the log-angular frequency ω should be greater than 0. The upper bound 40 is large enough to catch high-frequency oscillations (though we later discard fits with $\omega > 20$); the phase ϕ should be between 0 and 2π; The predicted critical time t_c should be after the end t_2 of the fitted time series. Finally, the upper bound of the critical time t_c should not be too far away from the end of the time series since predictive capacity degrades far beyond t_2. Jiang et al. [50] have found empirically that a reasonable choice is to take the maximum horizon of predictability to extent to about one-third of the size of the fitted time window.

2.4 Clarifications to Questions and Criticisms on the JLS Model

Having been developed for more than one decade, the JLS model has been studied, used and criticized by many researchers including Feigenbaum [87], Chang and Feigenbaum [88, 89], van Bothmer and Meister [83], Fry [90], and Fantazzini and Geraskin [91]. The most recent papers addressing the pros and cons of past works on the JLS model are written by Bree and his collaborators [92, 93]. Many ideas in these last two papers are correct, pointing out that some of the earlier works had some inconsistencies. However, there are some serious misunderstandings present of both the theoretical and empirical parts of the model. Therefore, it is necessary to address and clarify the misconceptions that some researchers seem to hold concerning this model and to provide an updated, concise reference on the JLS model.

In this section, we first discusses the questions about the theory of the JLS model in Sec. 2.4.1. The questions on fitting methods of the model are commented in Sec. 2.4.2. Issues on probabilistic forecast will be addressed in Sec. 2.4.3.

2.4.1 Discussions on theory of the JLS model

We discuss three issues related to the derivation and the proper parameter ranges.

Why m should be between 0 and 1?

We claim that the parameter m in the JLS model should be between 0 and 1. This point has been discussed in the Sec. 2.2. However, Bree and Joseph asked why m cannot be greater than 1 in [92]. Therefore, we would like to give a detailed answer as follows:

1. For $m < 1$, the crash hazard rate accelerates up to t_c but its integral up to t, which controls the total probability for a crash to occur up to t, remains finite and less than 1 for all times $t \leq t_c$. It is this property that makes rational for investors to remain invested knowing that a bubble is developing and that a crash is looming. Indeed, there is still a finite probability that no crash will occur during the lifetime of the bubble. The excess return $\mu(t) = \kappa h(t)$ is the remuneration that investors require to remain invested in the bubbly asset, which is exposed to a crash risk. The crash hazard may diverge as t approaches a critical time t_c, corresponding to

the end of the bubble.

2. Within the JLS framework, a bubble exists when the crash hazard rate accelerates with time. According to Eq. (2.4), this imposes $m < 1$ and $B' > 0$. That is, $m \geq 1$ cannot lead to an accelerating hazard rate.

3. Finally, the condition that the price remains finite at all time, including t_c, imposes that $m > 0$.

Summarize the points above, we conclude that a proper range of m where the bubble occurs should be $0 < m < 1$.

Non-negative risk condition

van Bothmer and Meister derived a constraint on the variables of the JLS model [83] from the statement that the crash rate should be non-negative. It states that:

$$b := -Bm - |C|\sqrt{m^2 + \omega^2} \geq 0. \tag{2.21}$$

Most current research using the JLS model has taken this restriction into consideration. It is among the basic restrictive filters for identifying bubbles in a more modern framework. In [94, 95, 96, 97], b in Eq. (2.21) is even used as a key parameter for pattern recognition method to detect the market rebounds.

How can the price in the JLS model be decreasing during a bubble?

Bree and Joseph claim that "the mechanism proposed to lead to LPPL fluctuations as reported in [47] must be incorrect as it requires the price to be increasing throughout the bubble." Bree and Joseph are completely mistaken here. Sec. 2.2 presents the JLS model in a self-consistent way. The error of Bree and Joseph is that they do not realize that, even if not specified, the definition of the JLS model includes implicitly the stochastic term σdW as in expression Eq. (2.2). In expectations, this term disappears, hence it is not included in the description of the initial JLS paper. But, Bree and Joseph are wrong to conclude that the JLS model imposes that the price is always monotonously increasing. Note that the formulation is nothing but that of the rational expectation of [45], which follows exactly the same procedure, with a stochastic component which does not play a role in the specification of the crash hazard rate relationship to the μ term, but is present to ensure that the price can indeed decrease. As indicated at the Sec. 2.4.1, note that van Bothmer and Meister

showed that a certain condition between the parameters of the LPPL fit should hold in order for the crash hazard rate to remain positive at all times until the end of the bubble, *but* this condition is *not* that the price should be non-decreasing or always increasing!

Faster-than-exponential growth in the JLS model

One of the fundamental differences between the JLS model and standard models of financial bubbles is that the JLS model claims that the price follows a faster-than-exponential growth rate during the bubble. It is necessary to emphasize this statement as many researchers make mistakes here. For example, Bree and Joseph wrote "exponential growth is posited in the LPPL" in several places in [92].

Financial bubbles are generally defined as transient upward acceleration of prices above the fundamental value [4, 6, 7]. However, identifying unambiguously the presence of a bubble remains an unsolved problem in standard econometric and financial economic approaches [9, 8], due to (i) the fact that the fundamental value is in general poorly constrained and (ii) the difficulty in distinguishing between an exponentially growing fundamental price and exponentially growing bubble price. As we have already described, the JLS model defines a bubble in terms of faster-than-exponential growth [43]. Thus, the main difference with standard bubble models is that the underlying price process is considered to be intrinsically transient due to positive feedback mechanisms that create an unsustainable regime. See for instance [50] where this is made as clear as possible.

Which kind of bubbles can be detected by the JLS model?

In page 4 of [92], three claims are outlined. One of them states that: "Financial crashes are preceded by bubbles with fluctuations. Both the bubble and the crash can be captured by the JLS model when specific bounds are imposed on the critical parameters β and ω", where β is presented as m in this paper.

Here, we should stress that this above claim is not entirely correct because crashes can be endogenous or exogenous. The JLS model is suitable only for endogenous crashes! Or more precisely, the JLS model is for bubbles, not for crashes. Endogenous crashes are preceded by the bubbles that are generated by positive feedback mechanisms of which imitation and herding of the noise traders are probably the

dominant ones among the many positive feedback mechanisms inherent to financial system. In the abstract of the reference [43], Johansen and Sornette state: "Globally over all the markets analyzed, we identify 49 outliers (now referred more appropriately as "dragon-kings" [98]), of which 25 are classified as endogenous, 22 as exogenous and 2 as associated with the Japanese anti-bubble. Restricting to the world market indices, we find 31 outliers, of which 19 are endogenous, 10 are exogenous and 2 are associated with the Japanese anti-bubble." Although the endogenous outliers are more frequent than the exogenous ones, the exogenous outliers still constitute a quite large portion. Therefore, the JLS model cannot capture all of the crashes in the market. Only endogenous crashes which are preceded by the bubbles can be captured by the JLS model.

2.4.2 Fitting problems concerning the JLS Model

Extensions of the JLS model and their calibration

The form of the JLS model we obtained in Eq. (2.9) is called the first-order LPPL Landau JLS model. Extensions have been proposed, essentially amounting to choosing alternative forms of the crash hazard rate $h(t)$ that replace expression Eq. (2.4). Let us mention the so-called second-order and third-order LPPL Landau models [40, 54, 99, 55, 100], the Weierstrass-type LPPL model [101, 102], the JLS model extended with second-order and third-order harmonics [103, 104, 51, 62] and the JLS-factor model in which the LPPL bubble component is augmented by other financial risks factors [105, 106]. We should also mention that a non-parametric estimation of the log-periodic power law structure has been developed to complement the above parametric calibrations [107]. These extensions are warranted by the fact that the positive feedback mechanisms together with the presence of the symmetry of discrete scale invariance can be embodied in a general renormalization group equation [101], whose general solution is the Weierstrass-type LPPL model. Then, the first-order LPPL Landau JLS model can be considered to be just the first term in a general log-periodic Fourier series expansion of the general solution. Therefore, further away from the critical time t_c, corrections from the first-order expression can be expected to be relevant, depending on the context. In addition, nonlinear extensions to the renormalization group are embodied partially in the second-order and third-order LPPL Landau models, which extend the time domain over which

the model can be calibrated to the empirical data [82].

Let us mention that Sornette and Johansen [82] discussed the difference between the fitting results obtained using the first order and the second order LPPL Landau-type JLS models. They used daily prices of the S&P 500 index from 1980 to 1987. The results show that the fitting result of the second order form is much better than the first order form, as based on the measure of residual sum of squares. A standard Wilks test of nested hypotheses confirms the fact that the second-order form provides a statistically significant improvement over the first-order form (recall that the first-order LPPL Landau formula is recovered as a special case of the second-order LPPL Landau formula, hence the first model is nested within the second model). We reproduce the fitting results from [82] in Fig. 2.2 to give an intuition on the difference between the first order and second order LPPL Landau fits. One can observe that the first-order LPPL Landau formula accounts reasonably well for the data from mid-1985 to the peak in October 1987. In contrast, the second-order LPPL Landau formula provides a good fit all the way back to the beginning of 1980. This result helps explain why the results quoted by Bree et al. [93] for time windows of 834 trading days may be questionable.

Notwithstanding the improvement provided by the second-order LPPL Landau model for large time windows, it is sufficient in many cases to use the first-order version just to get a diagnostic of the presence of a bubble. This is true even when the time window is larger than 2-3 years. For instance, the first-order LPPL Landau model was implemented within a pattern recognition method [94, 95, 97] with time windows of up to 1500 days. The key to the reported performance in forecasting [94, 95, 97] is the combination of bubble diagnostics at multiple time scales, with common model parameters associated with robustness.

Selection of the start of the time window

A common question arising in fitting the JLS model is to decide which date t_1 should be selected as the beginning of the fitting time window. Bree and Joseph [92] are more consistent in defining bubbles to analyze and their exact beginnings than the papers of 1998-2000 they analyze, which date from a decade at least. This is a very good approach. However, we would like to note that more recent procedures are more systematic as shown for instance in [50, 95, 96, 108, 64, 91]. In these more
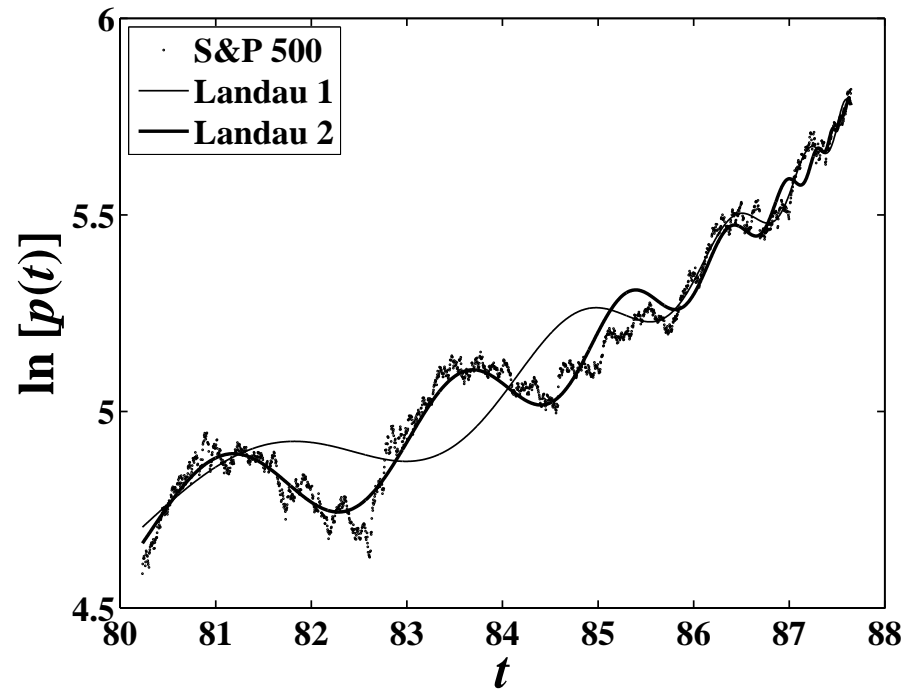
Figure 2.2: Time dependence of the logarithm of the New York stock exchange index S&P 500 from January 1980 to September 1987 and the best fits by the first and the second order LPPL Landau models. The crash of October 14, 1987 corresponds to 1987.78 decimal years. The thin line represents the best fit with the first-order LPPL Landau model on the interval from July 1985 to the end of September 1987 and is shown on the whole time span since January 1980. The thick line is the fit by the second-order LPPL Landau model from January 1980 to September 1987. (Reproduced from [82])

recent procedures, multiple t_1's are selected to make the prediction more statistically reliable. The key point here is that a single t_1 — corresponding to a single fit window — is unreliable and an ensemble of fits should be used.

Should real price or log-price be fitted?

As recalled by Bree and Joseph in [92], Sornette and Johansen [46] argued that log-price should be used when the amplitude of the expected crash is proportional to the price increase during the bubble. This is because Eq. (2.9) is derived from Eq. (2.2), which assumes that the changing price dp is proportional to the price p. Therefore, this statement is in accordance with Bree et al.'s definition of a crash (25% drop in price) in [92, 93]. Hence, it seems that the attempt by Bree et al. to compare the results of the fits when using the price (and not the log-price) is inconsistent.

One can also investigate the possibility that price changes may not be proportional to price. If this is the case, use of the real price is warranted according to the arguments put forward by Sornette and Johansen [46]. In practice, it is useful to try both fitting procedures with prices and log-prices and compare their relative merits. But one should be cautious because the fits using prices (and not log-prices) involve data values that may change over several orders of magnitude over the time window of interest. As a consequence, the standard least square fits is not suitable anymore. Instead, a normalized least square minimization is recommended so that each data point of the time series roughly contributes equally to the mean-square root diagnostic. This approach has been implemented recently in Ref. [108].

Sloppiness of the JLS models and search algorithm

Bree et al. [92, 93] claim that the concept of sloppiness and its consequence should be considered in fitting the JLS model to some empirical data with the Levenberg-Marquart algorithm. And they challenge the relevance of the obtained fits. It seems to us that this claim overlooks that the correct fitting procedure should include the combination of the Levenberg-Marquart algorithm [85] *and* a preliminary taboo search [84] or other meta-heuristics such as genetic algorithm and simulated annealing algorithm. This should occur together with the slaving of the linear parameters to the non-linear ones in order to reduce the effective number of parameters from 7 to 4 (and to 3 in the recently novel procedure of Filimonov and Sornette [109]). The

taboo search is a very good algorithm that provides a robust preliminary systematic exploration of the space of solutions, which prevents the Levenberg-Marquart algorithm later on to be stuck in special regions of the space of solutions. Also in a standard fitting procedure, the many results that may be obtained from the taboo search (i.e. results associated with different parts of the searching space) should be kept.

Taking into account the two points mentioned above, the quality of the fits with the JLS model is in general adequate [49, 50, 51, 62, 63, 108]. In contrast, it is obvious that fits using only the Levenberg-Marquart algorithm without a reasonably initial guess and sufficient preliminary exploration of the space of solutions will produce spurious results, with most of the parameters stuck at the boundary of the search space. A typical example of such fitting failure is shown in Ref.[93], where all the fitted m values are either very close to 0 or close to 1 and almost all the fitted t_c and ω values are very close to 0.

Reference [92] provides a sensitivity analysis of the root mean square error (RMSE), in which one parameter is scanned while the others remain fixed. The problem is that, because of the nonlinearity of expression Eq. (2.9), it is not obvious that the results of such a scan can be trusted. That is, if local minima in, say, ω are found while the other parameters are kept fixed, do the same minima appear when one or more of the other parameters are changed to different values? In other words, is the multi-dimensional parameter landscape around these minima smooth? The answer to this question is more important than showing the sensitivity of 2 dimensional subspaces, as in [92]. In practice, answering this question on the smoothness of the multi-dimensional parameter landscape is difficult. Filimonov and Sornette [109]) have documented that the standard slaving of three linear parameters (A, B and C in expression Eq. (2.9)) to the four remaining nonlinear parameters results into a quite corrugated fitness landscape that requires meta-heuristic (such as the taboo search). The meta-heuristic simultaneously changes all parameters to find acceptable minima as starting points for the Levenberg-Marquart algorithm. Yes, this approach does not guarantee finding *the* absolute minimum but it does provide *an ensemble of acceptable local minima*. This ensemble approach is more robust than searching in vain for a single global minimum.

Performance of the recommended fitting method on synthetic data

It is an essential building stone of any fitting procedure that it should be tested on synthetic data. Indeed, in any calibration exercise, one faces simultaneously two unknown: (i) the performance, reliability and robustness of the calibration procedure and (ii) the time series under study from which one hopes to extract meaningful information. How can one learn about an unknown dataset if one does not fully understand how the fitting method behaves on controlled well-known data sets? Early on, Johansen et al. [47, 48] set the stage by developing comparative tests on synthetic time series generated by the GARCH model. We also attract the attention to the fact that one of the most extensive set of synthetic tests concerning the possible existence of spurious log-periodicity is found in reference [110]. Zhou and Sornette [111] presented a systematic study of the confidence levels for log-periodicity only, using synthetic time series with many different types of noises, including noises whose amplitudes are distributed according to power law distributions with different exponents and long-memory modeled by fractional Brownian noises with various Hurst exponents spanning the full range from anti-persistent $(0 < H < 1/2)$ to persistent $(1/2 < H < 1)$.

We now show that the current fitting methods estimate the parameters of the JLS model within a reasonable range of uncertainty in the following. For this, a reference log-periodic power law (LPPL) time series of duration equal to 240 days is generated for a typical set of parameters, shown in Tab. 2.1. This series corresponds to a value of the critical time t_c equal to 300 (days). The choice of 240 days for the time window size is motivated by the typical length for the generation of bubbles found in various case studies in the literature.

The synthetic data is generated by combining the LPPL time series with noise. Two kinds of noise are considered: Gaussian noise and noise generated with a Student t distribution with four degrees of freedom (which exhibits a tail similar to that often reported in the literature for the distribution of financial returns). For both types of noise, the mean value is zero and the standard deviation is set to be 5% of the largest log-price among the 240 observations in the reference series. The standard deviation is chosen quite high in order to offer stringent test of the efficiency of the current fitting method. Synthetic samples obtained with both types

	Reference	Gaussian	Student's t
t_c	300	296.07 (20.44)	295.15 (20.81)
m	0.7	0.74 (0.15)	0.72 (0.18)
ω	10	9.75 (1.43)	9.71 (1.47)

Table 2.1: The parameter values used to generate the synthetic data are shown in the second column "Reference". The mean and standard (in format mean(std)) deviation values of the parameters obtained by fitting the JLS model to the synthetic LPPL time series decorated by the two types of noise discussed in the text are given in the last two columns. These numbers are estimated from 200 statistical realizations of the noise, and each realization is characterized by ten different best fits with the Levenberg-Marquart algorithm, leading to a total of 2000 estimated parameters. The other parameters used to generate the synthetic LPPL are $\phi = 1, A = 10, B = -0.1, C = 0.02$.

of noise along with the reference time series are shown in Fig. 2.3.

For each type of noise, 200 synthetic time series are generated. We fit each series with the JLS model Eq. (2.9) and keep the ten best fits for each one. Recall that our stochastic fit method produces multiple 'good' fits instead of the 'best' fit, which, in practice, is difficult, if not impossible, to find. In the new procedure developed by Filimonov and Sornette recently [109], the 'best' fit can be found in most cases that are qualified to be in a bubble regime. However, we still use the standard heuristic procedure in the present paper. This best ten selection results in 2000 sets of estimated parameters for each type of noise. The probability density functions of t_c, m and ω for the two types of noise are calculated by a non-parametric method (adaptive kernel technique). The results are shown is Fig. 2.4.

The mean and standard deviation of these parameters are shown in Tab. 2.1 alongside the original numbers used to generate the true LPPL function ($t_c = 300, m = 0.7, \omega = 10$) without noise. This test on synthetic data demonstrates that the fitting method combining the meta-heuristic Taboo search with the Levenberg-Marquart algorithm is satisfactory. We observe negligible biases, especially for the crucial critical time parameter t_c. The standard deviation for t_c of about 20 days is three times smaller than the 60 days separating the last observation (day 240) of the time series and the true critical time occurring at the 300-th day, showing that the calibration of a time series exhibiting LPPL structure, even with very large statistical noise, can provide significant skills in forecasting the critical time t_c.
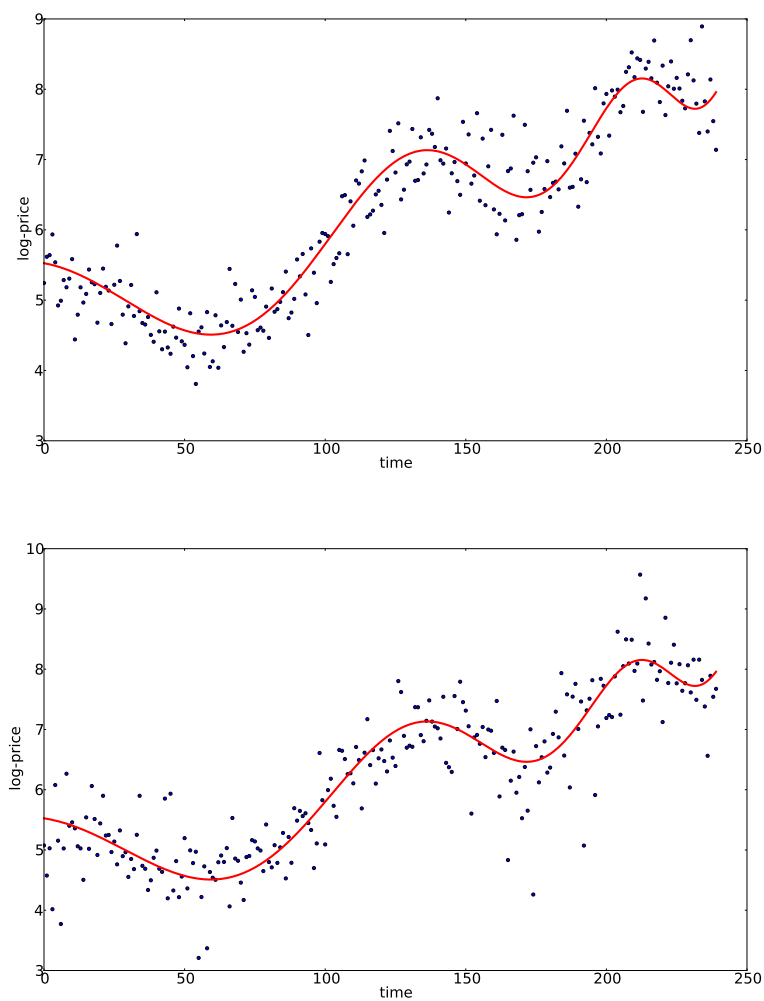
Figure 2.3: Synthetic data examples with zero mean and large standard deviation (5% of the largest log-price among 240 reference points). Upper panel: the synthetic data with Gaussian noise. Lower panel: the synthetic data with noise generated with a Student t distribution with four degrees of freedom. The red solid line shows the reference LPPL time series.
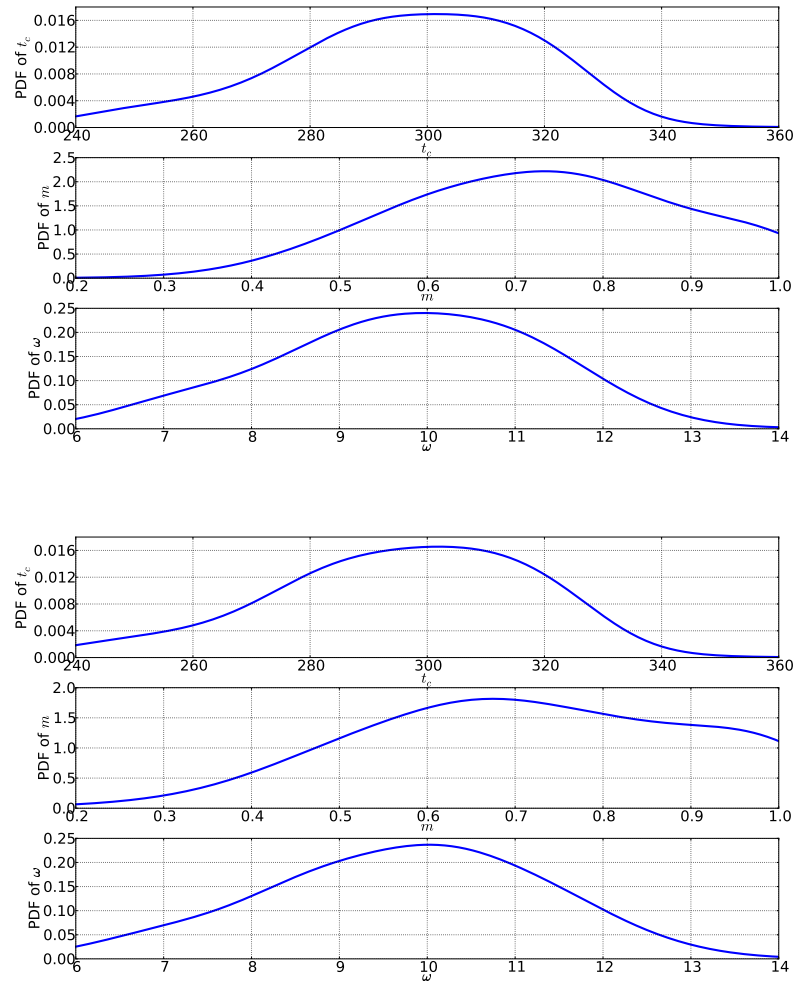
Figure 2.4: Probability density functions of t_c, m and ω obtained by a non-parametric kernel method applied to the parameter values determined by analyzing 200 synthetic time series, each of which being characterized by its ten best fits with the Levenberg-Marquart algorithm, leading to a total of 2000 estimated parameters.

2.4.3 Probabilistic forecast

From a practical risk management view point, one of the prizes obtained from the calibration of the JLS model to financial time series is the estimation of the most probable time of the end of the bubble t_c, which can take the form of a crash, but is more generally a smooth transition to a new market regime.

As we mentioned before, a distribution of t_c is obtained for a single bubble period, associated with the set of fitted time windows (see Sec. 2.4.2) and the recording of multiple locally optimal fits from the stochastic taboo search (see Sec. 2.4.2). Recall that the output of the meta-heuristic is used as the initial guess required by the Levenberg-Marquart algorithm. As demonstrated in the previous subsection, the estimation of the distribution of the most probable time t_c for the end of the bubble is generated by a reliable non-parametric method [112].

Bree et al. [93] make the interesting remark that the estimation of the probability density of t_c might be improved by augmenting the analysis of the original time series with that of many replicas. These replicas of the initial time series can be obtained for instance by using a LPPL function obtained for the first calibration on the original time series and adding to it noise generated by an AR(1) process. This methodology provides a measure of robustness of the whole estimation exercise. The choice of an AR(1) process for the noise is supported by the evidence provided in Refs. [78, 113] that the residuals of the calibration of the JLS model to a bubble price time series can be reasonably described by an AR(1) process. But, this is only one among several possibilities. Another one, which we have implemented in our group for quite some time and now use systematically, is to generate bootstraps in which the residuals of the first calibration on the original time series are used to seed as many synthetic time series as needed, using reshuffled blocks of residuals of different durations. For instance, reshuffling residuals in blocks of 25 days ensures that the dependence structure between the residuals is identical in the synthetic time series as in the original one up to a month time scale. Note that this bootstrap method does not assume Gaussian residuals in contrast with the AR(1) noise generation model. It captures also arguably better the dependence structure of the genuine residuals than the linear correlation embedded in the AR(1) model.

2.4.4   Conclusion

We have discussed the present theoretical status and some calibration issues concerning the JLS model of rational expectation bubbles with finite-time singular crash hazard rates. We have provided a guide to the advances that have punctuated the development of tests of the JLS model performed on a variety of financial markets during the last decade. We can say that the development of new versions and of methodological improvements have paralleled the occurrence of several major market crises, which have served as inspirations and catalyzers of the research. We believe that the field of financial bubble diagnostic is progressively maturing and we foresee a close future when it could become operational to help decision makers alleviate the consequences of excess leverage leading to severe market dysfunctions.

3

The Generalized JLS Models

The JLS model has been proved to be a very flexible and useful tool to detect financial bubbles and crashes. However, as the research on the financial bubbles goes deep and wide, more and more important information is required such as the fundamental value of the asset during the bubble regime, the diversification of the stock market and so on. Therefore, the standard JLS model is not enough to provide sufficient information anymore. A more powerful tool in identifying and forecasting the financial bubbles has to be developed. For this purpose, we present two types of the generalized JLS models in this chapter.

We first introduce the generalized JLS models with fundamental value of the stock and crash nonlinearity in Sec. 3.1. The new models can predict the critical time of the financial bubbles as the standard JLS model. In addition, the estimation of the fundamental value makes it possible to quantify the difference between the market price and the intrinsic value. This is essential for identifying the financial bubbles as the bubbles are generally defined as transient upward acceleration of price above the fundamental value. Furthermore, the standard JLS model just describes the dynamics of the price during the bubble generation. The price dynamics after the critical time is not specified in the standard JLS model. By introducing the crash nonlinearity, the new models present a new approach to possibly identify the dynamics of a crash after a bubble.

Then in Sec. 3.2, we discuss the generalized JLS model which can estimate the

diversification risk of the stock market. The Zipf factor is introduced in this model to describe the diversification risk. It is defined as proportional to the difference between the returns of the capitalization-weighted portfolio and the equal-weighted portfolio. By analyzing the value of the Zipf factor as well as the factor load, a new approach to understand the role of the diversification risk during a bubble regime is provided.

3.1   Inferring fundamental value of the stock and crash nonlinearity from bubble calibration

Financial bubbles are generally defined as transient upward accelerations of price above a fundamental value [4, 6, 5]. Fundamental value reflects the intrinsic value (and is sometimes called this) of the asset itself. It is ordinarily calculated by summing the future incomes generated by the asset, which are discounted to the present. However, as the future income flow is uncertain and not known in advance, and since the interest rates that should be used to discount future cash flows are bound to change in ways not yet known at the time of the calculation, the fundamental value of the asset is usually hard to estimate. In this sense, identifying unambiguously the presence of a bubble remains an unsolved problem in standard econometric and financial economic approaches [9, 8].

In this section, we generalize the standard JLS model by inferring fundamental value of the stock and crash nonlinearity from bubble calibration. The new models can not only detect the crash time but also estimate the fundamental value and the crash nonlinearity. This means that our new model has the ability to identify the presence of a bubble, thereby addressing the problem in the previous paragraph. With the estimated fundamental value, another famous unsolved problem becomes easier: distinguishing between an exponentially growing fundamental price and an exponentially growing bubble price. Furthermore, the new models can also detect the dynamics of crash after the bubble by specifying how the price evolves towards the fundamental value during the crash.

We test the models using data from three historical bubbles from different markets that ended in significant crashes. They are: the Hong Kong Hang Seng index

1997 crash, the S&P 500 index 1987 crash (black Monday) and the Shanghai Composite index 2009 crash. All results suggest that the new models perform very well in describing bubbles, forecasting their ending times and estimating fundamental value and the crash nonlinearity.

The performance of the new models is tested under both the Gaussian residual assumption and non-Gaussian residual assumption. Under the Gaussian residual assumption, nested hypotheses with the Wilks statistics are used and the p-values suggest that models with more parameters are necessary. Under non-Gaussian residual assumption, we use a bootstrap method to get type I and II errors of the hypotheses. All tests confirm that the generalized JLS models with fundamental value and crash nonlinearity provide useful improvements over the standard JLS model.

This section is constructed as follows. We introduce our new generalized JLS models in Sec. 3.1.1, then analyze three historical bubbles with the new models in Sec. 3.1.2. In Sec. 3.1.3, we compare the generalized models statistically to confirm that these new models provide useful improvements over the standard JLS model. We conclude in Sec. 3.1.4.

3.1.1 The generalized JLS models

In an effort to study the fundamental price, we modify and generalize the JLS model as follows. We now write the price dynamics of an asset as

$$dp = \mu(t)pdt + \sigma(t)pdW - \kappa(p - p_1)^\gamma dj, \tag{3.1}$$

where the first two items of the right hand side define the standard geometrical Brownian motion and the third term is the jump.

When the crash occurs at some time t^* (implying $\int_{t^*-}^{t^*+} dj = 1$), the price drops abruptly by an amplitude $\kappa(p(t^*) - p_1)^\gamma$.

The motivations and the interpretation of the three parameters p_1, κ and γ are as follows.

- For $\kappa = \gamma = 1$, the price drops from $p(t^{*-})$ to $p(t^{*+}) = p_1$, i.e., the price changes from its value just before the crash to a fixed well-defined valuation p_1. In the spirit of Fama's analysis of the 19 October 1987 crash [114], if one interprets the asset price after the crash as the "right" price, i.e., the price discovery towards rational equilibrium without mispricing, the crash is nothing

but an efficient assessment by investors of the "true" or fundamental value, once the panic has ended. Hence, p_1 can be interpreted as the fundamental price which is discovered during the crash dynamics.

- Then, κ can be thought of as a measure of market efficiency, that is, $1-\kappa$ is the relative inaccuracy of the discovery of the fundamental price by the market. If, say, $\kappa = 0.5$, this means that the price has dropped by only half of its bubble component, and remains over-valued compared with its fundamental component.

- When different from 1, the exponent γ can be interpreted as embodying a nonlinear (i) over-reaction for small variations and under-reaction for large deviations ($0 < \gamma < 1$) or (ii) under-reaction for small variations and over-reaction for large deviations ($\gamma > 1$) from the fundamental value.

Since p_1 is a fixed parameter, the generalized JLS model implies that we should measure the price dynamics in the frame moving with the fundamental price. In other words, p_1 is the fundamental price at the beginning t_1 of the time period over which the bubble develops. In order to compare in a consistent way the realized price to this fixed parameter, it is necessary to discount the asset price continuously by the rate of return of the fundamental price. If $p_{\text{obs}}(t)$ denotes the empirical price observed at time t, this means that the price $p(t)$ that enters in expression Eq. (3.1) is defined by

$$p(t) = p_{\text{obs}}(t) \prod_{s=t_1+1}^{t} \frac{1}{(1+r_f(s))^{\frac{1}{365}}} \,, \tag{3.2}$$

where $r_f(s)$ is the annualized growth (risk free) rate of the fundamental price. In our empirical analysis, we will take for $r_f(s)$ the annualized US 3-month treasury bill rate.

Applying the no-arbitrage condition $\mathrm{E}_t[dp] = 0$ to expression Eq. (3.1) leads to

$$\mu(t)p = \kappa(p - p_1)^\gamma h(t) \,. \tag{3.3}$$

Conditional on the absence of a crash, the dynamics of the expected price obeys the equation

$$dp = \mu(t)p\,dt = \kappa(p - p_1)^\gamma h(t)dt \,, \tag{3.4}$$

and the fundamental price must obey the condition $p_1 < \min p(t)$. For $\gamma = 1$, the solution of Eq. (3.4) generalizes the standard JLS equation into

$$\ln[p(t) - p_1] = \mathcal{F}_{LPPL}(t) , \tag{3.5}$$

where $\mathcal{F}_{LPPL}(t)$ is given by the standard JLS expression:

$$\mathcal{F}_{LPPL}(t) = A + B(t_c - t)^m + C(t_c - t)^m \cos(\omega \ln(t_c - t) - \phi) . \tag{3.6}$$

For $\gamma \in (0, 1)$, the solution is

$$(p - p_1)^{1-\gamma} = \mathcal{F}_{LPPL}(t) , \tag{3.7}$$

where again $\mathcal{F}_{LPPL}(t)$ is given by expression (3.6). We do not consider the case $\gamma > 1$ which would give an economically non-sensible behavior, namely the price diverges in finite time before the crash hazard rate itself diverges.

In summary, we shall consider four models M_0, M_1, M_2 and M_3, where some are nested in others. The goal will be to then apply statistical tests to the models to determine which are sufficient or not and which are necessary or not. In the following models, $\mathcal{F}_{LPPL}(t)$ below is given by expression (3.6).

0. The original JLS model M_0: $p_1 = 0, \gamma = 1$ (with $\kappa < 1$):

$$p_{M_0}(t) = \exp(\mathcal{F}_{LPPL}(t)) . \tag{3.8}$$

1. M_1: $p_1 \neq 0, \gamma = 1$:

$$p_{M_1}(t) = p_1 + \exp(\mathcal{F}_{LPPL}(t)) . \tag{3.9}$$

M_1 includes M_0 as a special case. In other words, M_0 is nested in M_1.

2. M_2: $p_1 = 0, \gamma \in (0, 1]$:

$$p_{M_2}(t) = \begin{cases} (\mathcal{F}_{LPPL}(t))^{\frac{1}{1-\gamma}} , & \gamma \in (0, 1) , \\ \exp(\mathcal{F}_{LPPL}(t)), & \gamma = 1 . \end{cases} \tag{3.10}$$

Since M_2 includes M_0 as a special case, M_0 is also nested in M_2.

3. M_3: $p_1 \neq 0, \gamma \in (0, 1]$:

$$p_{M_3}(t) = \begin{cases} p_1 + (\mathcal{F}_{LPPL}(t))^{\frac{1}{1-\gamma}} , & \gamma \in (0, 1) , \\ p_1 + \exp(\mathcal{F}_{LPPL}(t)), & \gamma = 1 . \end{cases} \tag{3.11}$$

M_3 includes all previous models, M_0, M_1 and M_2 as special cases, so that M_0, M_1 and M_2 are all nested in M_3.

3.1.2   Calibration and results on three historical bubbles

Calibration method of the models

Given an observed asset time series of prices $\{p_{\text{obs}}(t)\}$, we first transform it into a price time series of discounted prices $\{p(t)\}$ by using expression (3.2). We next determine the three parameters A, B and C in expression (3.6) for each model as a function of the other parameters, by solving analytically the system of three linear equations obtained by minimizing the square of deviations:

- $\ln[p(t)] - \mathcal{F}_{LPPL}(t)$ for M_0,

- $\ln[p(t) - p_1] - \mathcal{F}_{LPPL}(t)$ for M_1,

- $[p(t)]^{1-\gamma} - \mathcal{F}_{LPPL}(t)$ for M_2,

- $[p(t) - p_1]^{1-\gamma} - \mathcal{F}_{LPPL}(t)$ for M_3.

We then determine the other parameters for each model using a Taboo search (to find initial parameter estimates) coupled with a Levenberg-Macquardt algorithm. We constrain the values of plausible parameters as follows:

1. the fundamental price p_1 should be larger than $0.2p_{\min}$, where $p_{\min} := \text{Min}[p(t)]$ over the fitting time interval.

2. The fit parameters t_c, m, p_1 and γ should not be on the boundary of the search intervals. They should deviate from these boundaries by at least 1% in relative amplitude.

3. Among all the fits satisfying the above two conditions, the one with the smallest sum of normalized residuals is selected. The cost function we use here is the sum of squares of the relative discounted price differences

$$R(t) = \frac{p(t) - p_M(t)}{p_M(t)} \ , \tag{3.12}$$

   where $p_M(t)$ stands for one of the expressions Eq. (3.8–3.11).

The critical time t_c corresponding to the end of the bubble is searched in $[t_2, t_2 + 0.4(t_2 - t_1)]$, where the time window of analysis is $[t_1, t_2]$. The exponent m is constrained in $[10^{-5}, 1 - 10^{-5}]$. The log-angular frequency ω is searched in $[0.01, 40]$. The phase ϕ can take values in $[0, 2\pi - 10^{-5}]$. The fundamental price p_1 is in $[0.01, 0.99p_{\min}]$ and then restricted by condition (i) above.

Results

We calibrate models $M_0 - M_3$ to three well-documented bubbles, which ended in large crashes:

- Hong Kong Hang Seng index (HSI) ($t_1 =$ Feb. 1, 1995, $t_2 =$ March 13, 1997),

- S&P 500 index (GSPC) ($t_1 =$ Sept. 1, 1986, $t_2 =$ Aug. 26, 1987),

- Shanghai Composite index (SSEC) ($t_1 =$ Oct. 24, 2008, $t_2 =$ July 10, 2009.

The results are shown in Fig. 3.1–3.3 and the corresponding parameters are given in Tab. 3.1–3.3. Visually, all models seem to perform similarly, with the determined critical times t_c close to the true time of the crash. We note that the parameters p_1 and γ in M_1, M_2 and M_3 depart significantly from their reference values $p_1 = 0$ and $\gamma = 1$ characterizing model M_0.

Model M_0' corresponds to model M_0 with a slightly different cost-function. Instead of minimizing the sum of the squares of terms given by Eq. (3.12), for t going from t_1 to t_2, the parameters of M_0' are those of model M_0 obtained by minimizing the sum of the squares of the difference $\ln[p_{M_0}(t)] - \mathcal{F}_{LPPL}(t)$. Since $\ln y - \ln x = (y - x)/x + \mathcal{O}[(y - x)/x]^2$, the two methods should give similar results and the results summarized in Tab. 3.1–3.3 confirm this expectation.

Results of detailed statistical comparisons between the four models are shown below. Tab. 3.1–3.3 suggest that the five models perform almost equivalently in their ability to fit the price accelerations and to determine the time t_c of the peak of the bubbles. One can note a remarkable stability and consistency of the estimators for the two crucial parameters, the exponent m and the angular log-frequency ω. However, models M_1 and M_3 provide an interesting estimation of the size of the bubble, which appears stable with respect to these two specifications: at the beginning of the calibration interval, for the Hong Kong bubble, models M_1 and M_3
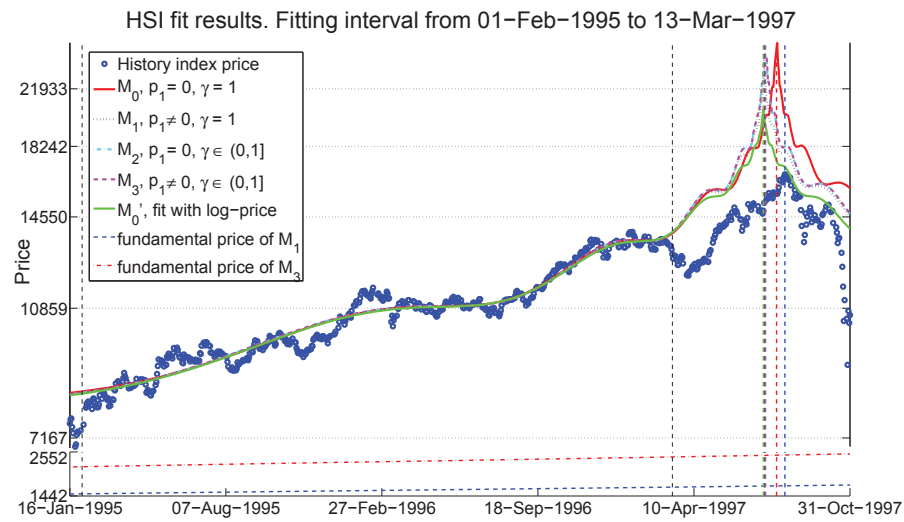
Figure 3.1: Calibration of the different models to the Hong Kong Hang Seng Index. The fit interval is shown with vertical black dashed lines. The fitted critical time t_c when the crash is most probable according the modified JLS models are marked by vertical dashed lines with the same color as the corresponding fits with each model. The historical close prices are shown as blue empty circles. The fundamental price for M_1 and M_3 are also shown as the almost horizontal dashed lines (beware of the break in the vertical scales for low values).
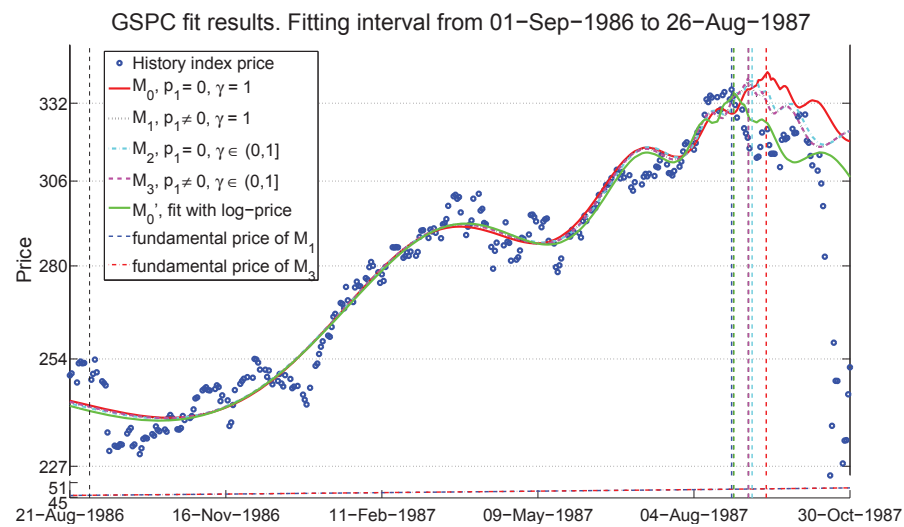
Figure 3.2: Same as Fig. 3.1 for the S & P 500 Index.

HSI	t_c	$|t_c - t_p|$	m	ω	ϕ	$\frac{p_f(t_1)}{p(t_1)}$	$\frac{p_f(t_p)}{p(t_p)}$	γ	$RC_{[2\text{months}]}$	$RC_{\max}$	RMS
M_0	27-Jul-1997	10	0.19	6.97	0.00	-	-	-	0.46	0.62	0.0320
M_1	11-Jul-1997	26	0.25	6.63	0.78	0.20	0.10	-	0.52	0.69	0.0320
M_2	12-Jul-1997	25	0.03	6.64	0.87	-	-	0.13	0.46	0.62	0.0319
M_3	12-Jul-1997	25	0.03	6.65	4.04	0.29	0.15	0.11	0.54	0.73	0.0319
M_0'	09-Jul-1997	28	0.39	6.53	3.30	-	-	-	0.41	0.55	0.0323

Table 3.1: Results of the calibration of models $M_0 - M_3$ for the Hong Kong Hang Seng index (HSI) from Feb. 1, 1995 to March 13, 1997. t_c is the critical time of a given model corresponding to the end of the bubble and the time at which the crash is the most probable. t_1 is the beginning of the fitting interval. t_p is the time when the asset value peaks before the crash. The relative amplitude of the crash following the peak of the bubble is given by $RC_{[2\text{months}]}$ and $RC_{\max}$, which are calculated using expression (3.13) from the following drawdown amplitudes: (i) $DD_{[2\text{months}]}$ is the two-months drop measured from the peak; (ii) $DD_{\max}$ is the peak-to-valley drawdown from the peak to the minimum of the asset price. RMS is the root mean square of the distances between historical prices and the model values, i.e., the square root of the sum of the squares of terms given by Eq. (3.12), for t going from t_1 to t_2, where t_2 is the last date of the time window used for the analyses. The model denoted M_0' corresponds to model M_0 with a different calibration method, as explained in the text.

GSPC	t_c	$|t_c - t_p|$	m	ω	ϕ	$\frac{p_f(t_1)}{p(t_1)}$	$\frac{p_f(t_p)}{p(t_p)}$	γ	$RC_{[2\text{months}]}$	$RC_{\max}$	RMS
M_0	13-Sep-1987	19	0.70	6.62	0.00	-	-	-	0.34	0.35	0.0196
M_1	03-Sep-1987	9	0.68	6.10	0.00	0.18	0.14	-	0.40	0.40	0.0190
M_2	05-Sep-1987	11	0.63	6.09	0.00	-	-	0.72	0.34	0.35	0.0191
M_3	03-Sep-1987	9	0.64	6.10	0.00	0.18	0.14	0.64	0.40	0.40	0.0190
M_0'	26-Aug-1987	1	0.68	5.59	0.14	-	-	-	0.32	0.33	0.0187

Table 3.2: Same as Tab. 3.1 for the S&P 500 index (GSPC) from Sept. 1, 1986 to Aug. 26, 1987.

SSEC	t_c	$|t_c - t_p|$	m	ω	ϕ	$\frac{p_f(t_1)}{p(t_1)}$	$\frac{p_f(t_p)}{p(t_p)}$	γ	$RC_{[\text{2months}]}$	$RC_{\max}$	RMS
M_0	29-Jul-2009	2	0.63	16.60	0.00	-	-	-	0.23	0.23	0.0258
M_1	24-Jul-2009	3	0.77	15.86	1.94	0.36	0.19	-	0.29	0.29	0.0256
M_2	21-Jul-2009	6	0.69	15.52	6.28	-	-	0.99	0.23	0.23	0.0257
M_3	24-Jul-2009	3	0.65	15.96	2.49	0.92	0.49	0.20	0.45	0.45	0.0254
M_0'	24-Jul-2009	3	0.68	15.86	5.12	-	-	-	0.23	0.23	0.0256

Table 3.3: Same as Tab. 3.1 for the Shanghai Composite index (SSEC) from Oct. 24, 2008 to July 10, 2009.
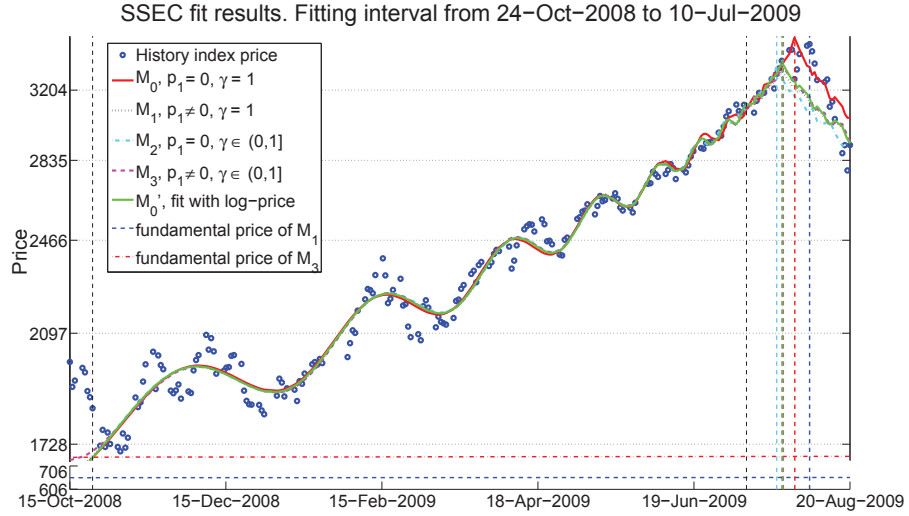
Figure 3.3: Same as Fig. 3.1 for the Shanghai Composite Index.

estimate that the bubble component might have been already accounting for 71% to 80% of the observed price. At the end of the bubble, the bubble component is between 85% to 90% of the observed price. Similar values are found for the two other case studies. An exception is for the Shanghai Composite index bubble, for which model M_3 suggests that the fundamental price was 92% of the observed price at the beginning of the calibrating interval and about half of the observed price at its peak.

The models provide a method to measure the amplitude of the crash that follows the bubble peak. Consider two types of drawdown after the peak: (i) $DD_{[2\text{months}]}$ is the two-months drop measured from the peak; (ii) $DD_{\max}$ is the peak-to-valley drawdown from the peak to the minimum of the asset price after the crash. We calculate the magnitude of the crash compared to the over-valued prices as follows. The ratio between the crash magnitude and over-valued prices is estimated as:

$$RC_i = \frac{DD_i}{p_{\text{obs}}(t_p) - p_1 \prod_{s=t_1+1}^{t}(1 + r_f(s))^{\frac{1}{365}}} \qquad i \in \{[2\text{months}], \max\}. \qquad (3.13)$$

During the crashes, the hazard rate in Eq. (3.4) should be 1. Then comparing the definition of RC and Eq. (3.4), one can easily find that $\kappa = RC$ for the models whose $\gamma = 1$ (M_0, M_1, M_0'). For the other models, κ is different from RC. These values are reported in Tab. 3.1–3.3.

According to the specification of [78], we should verify that the calibrations discussed above are self-consistent, i.e., the residuals are stationary. This verification step was proposed by [78] as a possible solution to the problems identified by [115] and [116] resulting from the calibration of non-stationary prices.

In order to check that the normalized residuals are stationary for all the four models, we use the Phillips-Perron and the Dickey-Fuller unit root tests. The null hypothesis H_0 is that the normalized residuals are not stationary, i.e. they have a unit root. In order to have reasonable statistics, we consider time windows of fixed length of 175, 250 or 550 trading days. We identify these windows in time series much larger than the (t_1, t_2) intervals used to identify the bubbles (given at the top of Sec. 3.1.2). The interval lengths correspond to the different values of $t_2 - t_1$ for the respective case studies. We choose overlapping intervals with the start of neighboring intervals separated by 25 days. There are 303 windows of size 550 trading days for the HSI from Jan. 1, 1987 to Feb. 25, 2010; 800 windows for the GSPC index from Feb. 2, 1954 to Feb. 10, 2010 with size of 250 trading days; 167 windows of SSEC from Aug. 3, 1997 to Jan. 22, 2010 of size of 175 trading days. Note that we choose these dates as the window boundaries because: (i) the chosen (t_1, t_2) intervals identified at the top of Sec. 3.1.2 should be one of the windows we get here; (ii) up to the data collection date (Feb. 26, 2010), we want to get as many windows as we can. Using the statistical confidence level of 99%, we determine the fraction of those windows which reject the Phillips-Perron and the Dickey-Fuller unit root tests (H_1), i.e., which qualify as stationary. The results are presented in Tab. 3.4. We conclude that most of the residuals are found stationary, which support the validity of our calibration procedure.

Previous works have identified the domain of parameters of the calibration of the JLS model M_0 which is the most relevant [50]. These conditions, referred to as the LPPL (log-period power law) conditions, are

$$B > 0; \quad 0.1 \le m \le 0.9; \quad 6 \le \omega \le 13; \quad -1 \le C \le 1 . \qquad (3.14)$$

Imposing that the calibrations obey these LPPL conditions (3.14), we find in Tab. 3.5 that the fraction of the above windows analyzed in Tab. 3.4 which fulfill the stationary conditions is significantly increased, augmenting our trust of the quality of the calibration and of the relevance of this class of models.

Percentage of stationary	M_0	M_1	M_2	M_3
303 HSI windows from Jan. 1, 1987 to Feb. 25, 2010, length 550.				
Phillips-Perron	96.7%	98.0%	96.7%	97.7%
Dickey-Fuller	96.7%	98.0%	96.7%	97.7%
800 GSPC windows from Feb. 2, 1954 to Feb. 10, 2010, length 250.				
Phillips-Perron	90.6%	91.0%	91.8%	91.8%
Dickey-Fuller	90.6%	91.0%	91.8%	91.8%
167 SSEC windows from Aug. 3, 1997 to Jan. 22, 2010, length 175.				
Phillips-Perron	96.4%	97.0%	96.4%	97.0%
Dickey-Fuller	96.4%	97.0%	96.4%	97.0%

Table 3.4: Percentage of stationary residuals for the Phillips-Perron and Dickey-Fuller tests. Significance level: 99%.

Percentage of stationary under LPPL constrains	M_0	M_1	M_2	M_3
303 HSI windows from Jan. 1, 1987 to Feb. 25, 2010, length 550.				
P_{LPPL}	0.99%	0.99%	2.64%	1.98%
Phillips-Perron	100%	100%	100%	100%
Dickey-Fuller	100%	100%	100%	100%
800 GSPC windows from Feb. 2, 1954 to Feb. 10, 2010, length 250.				
P_{LPPL}	4.50%	6.00%	4.50%	5.87%
Phillips-Perron	95.7%	100%	97.9%	100%
Dickey-Fuller	95.7%	100%	97.9%	100%
167 SSEC windows from Aug. 3, 1997 to Jan. 22, 2010, length 175.				
P_{LPPL}	4.19%	4.79%	8.38%	9.58%
Phillips-Perron	93.8%	92.9%	100%	100%
Dickey-Fuller	93.8%	92.9%	100%	100%

Table 3.5: Percentage of stationary residuals, as qualified by the Phillips-Perron and Dickey-Fuller tests, which obey the LPPL conditions (3.14). The variable P_{LPPL} gives the fraction of fits that satisfy the conditions (3.14), independently of whether their residuals are stationary or not. Significance level: 99%.

3.1.3 Statistical comparisons of the four generalized JLS models

Standard Wilks test of nested hypotheses assuming independent and normally distributed residuals

Let us consider the five pairs of models with nested structure: $(M_0 \subset M_1)$, $(M_0 \subset M_2)$, $(M_1 \subset M_3)$, $(M_2 \subset M_3)$, and $(M_0 \subset M_3)$. Let us denote M_l as the model with the smaller number of parameters and M_h that with the larger number of parameters. For each pair, we use Wilks test of nested hypotheses in terms of the log-likelihood ratios to decide between the two hypotheses:

H_0: M_l is sufficient and M_h is not necessary.

H_1: M_l is not sufficient and M_h is needed.

We first present in this subsection the tests assuming that the residuals of the calibration of the models to the asset price time series are normally and independently distributed. In the next subsection, we loosen this restriction.

For each model M_i, $i = 0, 1, 2, 3$, let us denote the normalized residuals defined by expression Eq. (3.12) by $R_i(t)$ and assume that they are i.i.d. Gaussian. For sufficiently large time windows, and noting N the number of trading days in the fitted time window $[t_1; t_2]$, the Wilks log-likelihood ratio reads

$$T = 2 \log \frac{L_{h,max}}{L_{l,max}} = 2N \ln \frac{\sigma_l}{\sigma_h} + \frac{\sum_{t=1}^{N} R_l^2(t)}{\sigma_l^2} - \frac{\sum_{t=1}^{N} R_h^2(t)}{\sigma_h^2} \ , \qquad (3.15)$$

where R_l and σ_l (respectively R_h and σ_h) are the residuals and their corresponding standard deviation for M_l (respectively M_h).

In the large N limit, and under the above conditions of asymptotic independence and normality, the T-statistics is distributed with a χ_k^2 distribution with k degrees of freedom, where k is the difference between the number of parameters in M_h and M_l. We have $k = 1$ for the pairs (M_0, M_1), (M_0, M_2), (M_1, M_3), (M_2, M_3), and $k = 2$ for (M_0, M_3). The p-values associated with the T-statistics given by (3.53) for each of the five pairs are reported in Tab. 3.6. The summary of that table is:

- Hong Kong Hang Seng index (HSI) from Feb. 1, 1995 to March 13, 1997: Model M_0 is never rejected and the standard JLS model is sufficient.

	(M_0, M_1)	(M_0, M_2)	(M_1, M_3)	(M_2, M_3)	(M_0, M_3)
HSI	0.4710	0.2210	0.3221	0.9626	0.4723
GSPC	0.0003	0.0006	0.7930	0.2150	0.0012
SSEC	0.1405	0.2494	0.0863	0.0516	0.0775

Table 3.6: p-value of the null hypothesis H_0 for pairs of models (M_l, M_h) that M_l is sufficient and M_h is not necessary, using Wilks log-likelihood ratio statistics. Low p-value indicates the improvement of M_h compared to M_l is significant and H_0 is rejected.

- S&P 500 index (GSPC) from Sept. 1, 1986 to Aug. 26, 1987: Model M_0 is re-jected with strong statistical confidence in favor of M_1, M_2 and M_3. However, when comparing M_1 and M_2 to M_3, we find that M_3 is not necessary. There-fore, we conclude that the structure of the S&P 500 index bubble requires the introduction of either a fundamental price p_1 or of a nonlinear crash amplitude as a function of mispricing (price for M_0 and M_2), but that both ingredients together are not necessary.

- Shanghai Composite index (SSEC) from Oct. 24, 2008 to July 10, 2009: Only M_3 improves on M_0 at a confidence level of 92.3% that can be considered as acceptable, while M_1 and M_2 are not significantly better than M_0 for standard confidence levels. Consistent with M_3 being rather significantly better than M_0, it is also better than M_1 and M_2, which are themselves not significantly improving on M_0. There seems to exist both a fundamental value component and a nonlinear over-reaction to mispricing in the unfolding of this Chinese bubble.

Comparison between models by bootstrapping to account for non-normality and dependence between residuals

Consider a pair of models $(M_l \subset M_h)$. Let us assume that M_l is the correct gen-erating model of the data. The calibration of M_l to the data gives a specific set of parameters as well as a specific realization of residuals. We then use this specifi-cation of the model M_l and its residuals to generate 1000 synthetic time series. A given synthetic time series is the calibrated M_l time series on which we add residuals obtained by randomly reshuffling the previously obtained residuals. Thus, the 1000

synthetic time series differ from each other only by the reshuffling of the residuals. We then calibrate the two models M_l and M_h on each of these 1000 synthetic time series and calculate the difference of the sum of the square of residuals of the fits of these two models. We thus have a list of 1000 different d_n, $n = 1, ..., 1000$. Comparing with the corresponding difference d_{fit} (between M_l and M_h) gives us a realistic estimation of the p-value for the null hypothesis that M_l is the correct generating model of the data. Specifically, the p-value is the fraction among the 1000 d_n's that are *larger* than d_{fit}. For instance, if all values d_n are smaller than d_{fit}, we obtain $p = 0$, i.e., it is very improbable that the difference in quality of fit between M_l and M_h results solely from the structure of the models and of the residues. We can reject the null and conclude that M_h is a better necessary model.

The second test we perform starts with the hypothesis that the true generating process is M_h. Thus, the 1000 synthetic time series are now generated by using model M_h calibrated on the data and its residuals. Then, the p-value for this null is determined as the fraction among the 1000 d_n's that are *smaller* than d_{fit}.

Tab. 3.7 summarizes the results, which improve on those shown in Tab. 3.6 by relaxing the conditions of normality and of independence between the daily residuals of the calibration. The bootstraps are performed by reshuffling the residuals of the fit "every day" or in blocks of 25 continuous days ("every 25 days"), which is in blocks of 25 continuous days. The later allows us to keep the dependence structure over 25 days to test its possible impact on the p-values. Reshuffling every day destroys any dependence in the residuals, while keeping their one-point (possibly non-Gaussian) statistics.

For HSI, taking into account the dependence structure of the residuals up to 25 days confirm the results already found in Tab. 3.6 that the standard JLS model M_0 is sufficient to explain the observed financial bubble. For GSPC, the results also confirm those of the Wilks test in Tab. 3.6, that M_1 and M_2 improve significantly on M_0, while M_3 is not necessary. For SSEC, also in agreement with Tab. 3.6, model M_3 is found to be the best and to be significant at the 95% confidence level.

Overall, these tests confirm that the generalized JLS models seem to provide useful improvements over the standard JLS model, both in terms of their explanatory power and in the extraction of additional information, specifically the fundamental price p_1 and a possible nonlinear dependence of the crash amplitude as a function

	(M_0, M_1)	(M_0, M_2)	(M_0, M_3)	(M_1, M_3)	(M_2, M_3)
HSI shuffle every day					
M_l true	0	0	0	0.05	0.75
M_h true	0	0	0	0.10	0.60
HSI shuffle every 25 days					
M_l true	0.46	0.20	0.42	0.26	0.76
M_h true	0.42	0.12	0.38	0.18	0.70
GSPC shuffle every day					
M_l true	0	0	0	0.35	0.45
M_h true	0.05	0	0	0.45	0.40
GSPC shuffle every 25 days					
M_l true	0.05	0	0.05	0.40	0.50
M_h true	0	0	0	0.50	0.45
SSEC shuffle every day					
M_l true	0	0	0	0.05	0.35
M_h true	0	0.05	0	0.05	0.50
SSEC shuffle every 25 days					
M_l true	0.14	0.08	0.04	0.04	0.38
M_h true	0.12	0.06	0.06	0.08	0.40

Table 3.7: p-values calculated by bootstraping (see text for explanation). Low p-value indicates the improvement of M_h compared to M_l is significant.

of mispricing.

3.1.4   Conclusion

In this section, we generalized the JLS model by inferring the fundamental value and crash nonlinearity from bubble calibration. In the generalized model, one can not only predict the crash time of a stock, but also estimate the fundamental value of that stock. Furthermore, the crash nonlinearity can also be estimated.

Three historical bubbles from different markets are tested by the generalized models. All the results suggest that the new models perform very well in describing bubbles, predicting crash time and estimating fundamental value and the crash nonlinearity.

The performance of the new models is tested both under the Gaussian and non-Gaussian residual assumptions. Under the Gaussian residual assumption, nested hypothesis testing with the Wilks statistics is used and the p-values suggest models with more parameters are necessary. Under non-Gaussian residual assumption, we use bootstrap method and get the type I and II errors of the hypothesis. All those tests confirm that the generalized JLS models provide useful improvements over the standard JLS model.

3.2   The role of the diversification risk in the financial bubbles

We present an extension of the JLS model in this section, in the spirit of the approach developed by Zhou and Sornette [105] to include additional pricing factors.

The literature on factor models is huge and we refer e.g. to Ref.[117] and references therein for a review of the literature. One of the most famous factor model, now considered as a standard benchmark, is the three-factor Fama-French model [118, 119, 120, 121] augmented by the momentum factor [122].

Recently, the concept of the Zipf factor has been introduced [123, 124]. The key idea of the Zipf factor is that, due to the concentration of the market portfolio when the distribution of the capitalization of firms is sufficiently heavy-tailed as is the case empirically, a risk factor generically appears in addition to the simple market factor, even for very large economies. Malevergne et al. [123, 124] proposed a simple proxy for the Zipf factor as the difference in returns between the equal-weighted and the value-weighted market portfolios. Malevergne et al. [123, 124] have shown that the resulting two-factor model (market portfolio + the new factor termed "Zipf factor") is as successful empirically as the three-factor Fama-French model. Specifically, tests of the Zipf model with size and book-to-market double-sorted portfolios as well as industry portfolios finds that the Zipf model performs as well as the Fama-French model in terms of the magnitude and significance of pricing errors and explanatory power, despite that it has only two factors instead of three.

In the present section, we would like to introduce a new model by combining the Zipf factor with the JLS model. The new model keeps all the dynamical characteristics of a bubble described in the JLS model. In addition, the new model can also provide the information about the concentration of stock gains over time from the knowledge of the Zipf factor. This new information is very helpful to understand the risk diversification and to explain the investors' behavior during the bubble generation.

This section is constructed as follows. Sec. 3.2.1 describe the definition of the Zipf factor as well as the new model. Two approaches of the model derivation are presented in this section. Sec. 3.2.2 introduce the calibration method of this new

model. Then we test the new model with two famous Chinese stock bubbles in the history in Sec. 3.2.3 and discuss the role of the Zipf factor in these two bubbles. Sec. 3.2.4 concludes.

3.2.1   The model

We introduce the new model in this section. Our goal is to combine the Zipf factor $z(t)dt$ with the JLS model of the bubble dynamics. To be specific, we introduce the following definition.

Definition 1: *The Zipf factor $z(t)dt$ is defined as proportional to the difference between the returns of the capitalization-weighted portfolio and the equal-weighted portfolio for the last time step:*

$$z(t)dt := \frac{dp}{p(t)} - \frac{dp_e}{p_e(t)} \ , \tag{3.16}$$

where p (respectively p_e) is the price of the capitalization-weighted (respectively equal-weighted) portfolio, $dp := p(t) - p(t - dt)$ and $dp_e := p_e(t) - p_e(t - dt)$. The weights of the portfolios are normalized so that their two prices are identical at the day preceding the beginning time t_0 of the time series: $p_e(t_0) = p(t_0)$.

Definition 2: *The integrated Zipf factor $\zeta(t)$ is obtained by taking the integral of the Zipf factor defined by expression (3.16):*

$$\zeta(t) := \ln p(t) - \ln p_e(t) \ . \tag{3.17}$$

By definition, the Zipf factor describes the exposition to a lack of diversification due to the concentration of the stock market on a few very large firms.

The dynamics of stock markets during a bubble regime is then described as

$$\frac{dp(t)}{p(t)} = \mu(t)dt + \gamma z(t)dt + \sigma(t)dW - \kappa dj \ , \tag{3.18}$$

where p is the portfolio price, μ is the drift (or trend) whose accelerated growth describes the presence of a bubble (see below), γ is the factor loading on the Zipf's factor and dW is the increment of a Wiener process (with zero mean and unit variance). The term dj represents a discontinuous jump such that $dj = 0$ before the crash and $dj = 1$ after the crash occurs. The loss amplitude associated with

the occurrence of a crash is determined by the parameter κ. The assumption of a constant jump size is easily relaxed by considering a distribution of jump sizes, with the condition that its first moment exists. Then, the no-arbitrage condition is expressed similarly with κ replaced by its mean. Each successive crash corresponds to a jump of dj by one unit. The dynamics of the jumps is governed by a crash hazard rate $h(t)$. Since $h(t)dt$ is the probability that the crash occurs between t and $t + dt$ conditional on the fact that it has not yet happened, we have $E_t[dj] = 1 \times h(t)dt + 0 \times (1 - h(t)dt)$, where $E_t[.]$ denotes the expectation operator. This leads to

$$\mathrm{E}_t[dj] = h(t)dt \ . \tag{3.19}$$

Noise traders exhibit collective herding behaviors that may destabilize the market in this model. We assume that the aggregate effect of noise traders can be accounted for by the following dynamics of the crash hazard rate

$$h(t) = B'(t_c - t)^{m-1} + C'(t_c - t)^{m-1} \cos(\omega \ln(t_c - t) - \phi') \ . \tag{3.20}$$

The intuition behind this specification Eq. (3.20) has been presented at length by Johansen et al. [46, 48, 47], and further developed by Sornette and Johansen [125], Ide and Sornette [73] and Zhou and Sornette [105]. In a nutshell, the power law behavior $\sim (t_c - t)^{m-1}$ embodies the mechanism of positive feedback posited to be at the source of the bubbles. If the exponent $m < 1$, the crash hazard may diverge as t approaches a critical time t_c, corresponding to the end of the bubble. The cosine term in the r.h.s. of Eq. (3.20) takes into account the existence of a possible hierarchical cascade of panic acceleration punctuating the course of the bubble, resulting either from a preexisting hierarchy in noise trader sizes [82] and/or from the interplay between market price impact inertia and nonlinear fundamental value investing [73].

We assume that all the investors of the market have already taken the diversification risk into account, so that the no-arbitrage condition reads $\mathrm{E}_t[\frac{dp(t)}{p(t)} - \gamma z(t)dt] = 0$, where the expectation is performed with respect to the risk-neutral measure, and in the frame of the risk-free rate. This is the condition that the price process concerning the diversification risk should be a martingale. Taking the expectation of

expression Eq. (3.18) under the filtration (or history) until time t reads

$$\mathrm{E}_t\left[\frac{dp}{p} - \gamma z dt\right] = \mu(t)dt + \sigma(t)\mathrm{E}_t[dW] - \kappa\mathrm{E}_t[dj] \; . \tag{3.21}$$

Since $\mathrm{E}_t[dW] = 0$ and $\mathrm{E}_t[dj] = h(t)dt$ (equation (3.19)), together with the no-arbitrage condition $\mathrm{E}_t[dp(t)] = 0, \forall t$, this yields

$$\mu(t) = \kappa h(t) \; . \tag{3.22}$$

This result (3.22) expresses that the return $\mu(t)$ is controlled by the risk of the crash quantified by its crash hazard rate $h(t)$. The excess return $\mu(t) = \kappa h(t)$ is the remuneration that investors require to remain invested in the bubbly asset, which is exposed to a crash risk.

Now, conditioned on the fact that no crash occurs, Eq. (3.18) is simply

$$\frac{dp(t)}{p(t)} - \gamma z(t) = \mu(t)dt + \sigma(t)dW = \kappa h(t)dt + \sigma(t)dW \; , \tag{3.23}$$

where the Zipf factor $z(t)$ is given by expression (3.16). Its conditional expectation leads to

$$\mathrm{E}_t\left[\frac{dp(t)}{p(t)} - \gamma z(t)\right] = \kappa h(t)dt \tag{3.24}$$

Substituting with the expression Eq. (3.20) for $h(t)$ and (3.16) for $z(t)$, and integrating, yields the log-periodic power law (LPPL) formula as in the JLS model, but here augmented by the presence of the Zipf factor, which adds the term proportional to the Zipf factor loading γ:

$$\mathrm{E}_t[\ln p(t) - \gamma\zeta(t)] = A + B(t_c - t)^m + C(t_c - t)^m \cos(\omega\ln(t_c - t) - \phi) \; , \tag{3.25}$$

where $\zeta(t)$ is defined by expression (3.17) and the r.h.s. of Eq. (3.25) is the primitive of expression Eq. (3.20) so that $B = -\kappa B'/m$ and $C = -\kappa C'/\sqrt{m^2 + \omega^2}$. This expression Eq. (3.25) describes the average price dynamics only up to the end of the bubble.

The same structure as Eq. (3.25) is obtained using a stochastic discount factor (stochastic pricing kernel) following the derivation of Zhou and Sornette [105], as shown below:

Under the stochastic pricing kernel theory, the no-arbitrage condition is presented as follows. The product of the stochastic pricing kernel (stochastic discount factor)

$D(t)$ and the value process $p(t)$, of any admissible self-financing trading strategy implemented by trading on a financial asset, should be a martingale:

$$D(t)p(t) = \mathrm{E_t}[D(t')p(t')], \qquad \forall t' > t .$$

(3.26)

Let us assume that the dynamics of the stochastic pricing kernel is formulated as:

$$\frac{dD(t)}{D(t)} = -r(t)dt - \gamma z(t)dt - \lambda(t)dW + \nu d\hat{W} ,$$

(3.27)

where $r(t)$ is the interest rate and $z(t)$ is the Zipf factor defined as (3.16). The process $\lambda(t)$ denotes the market price of risk, as measured by the covariance of asset returns with the stochastic discount factor and $d\hat{W}$ represents all other stochastic factors acting on the stochastic pricing kernel. By definition, dW is independent to $d\hat{W}$ at any time $t \geq 0$:

$$\mathrm{E_t}[dW \cdot d\hat{W}] = \mathrm{E_t}[dW] \cdot \mathrm{E_t}[d\hat{W}] = 0 , \forall t \geq 0.$$

(3.28)

We further use the standard form of the price dynamics in the JLS model [47, 48, 46]:

$$\frac{dp}{p} = \mu dt + \sigma(t)dW - \kappa dj ,$$

(3.29)

where W is the same Brownian motion as in Eq. (3.27). The term dj represents the jump process, valued 0 when there is no crash and 1 when the crash occurs. The dynamics of the jumps is governed by the crash hazard rate $h(t)$ defined in Eq. (3.20) with:

$$\mathrm{E}_t[dj] = h(t)dt .$$

(3.30)

According to the stochastic pricing kernel theory, $D \times p$ should be a martingale. Taking the future time t' in Eq. (3.26) as the increment of the current time t, then

$$
\begin{aligned}
\mathrm{E}&\left[\frac{p(t+dt)D(t+dt) - p(t)D(t)}{p(t)D(t)}\right] \\
=\ &\mathrm{E}\left[\frac{(p(t)+dp)(D(t)+dD) - p(t)D(t)}{p(t)D(t)}\right] \\
=\ &\mathrm{E}\left[\frac{p(t)dD + D(t)dp + dDdp}{p(t)D(t)}\right] \\
=\ &\mathrm{E}\left[\frac{dD}{D} + \frac{dp}{p} + \frac{dDdp}{Dp}\right] \\
=\ &0 .
\end{aligned}
$$

(3.31)

To satisfy this equation, the coefficient of dt should be zero, that is $-r(t) + \mu(t) + \gamma z(t) + \kappa h(t) + \sigma(t)\lambda(t) = 0$. This yields

$$\mu(t) = r(t) + \gamma z(t) - \kappa h(t) - \sigma(t)\lambda(t) \ . \tag{3.32}$$

When there is no crash ($dj = 0$), the expectation of the price process is obtained by integrating Eq. (3.29):

$$\mathrm{E_t}\left[\ln p(t)\right] = \int (\gamma z(t) + \kappa h(t) + r(t) + \sigma(t)\lambda(t))dt \ . \tag{3.33}$$

For $r(t) = 0$ and $\lambda(t) = 0$, we obtain:

$$\begin{aligned}
\mathrm{E_t}\left[\ln p(t)\right] &= \int (\gamma z(t) + \kappa h(t))dt \\
&= \gamma\zeta(t) + \int \kappa h(t)dt \\
&= \gamma\zeta(t) + A + B(t_c - t)^m + C(t_c - t)^m \cos(\omega \ln(t_c - t) - \phi) \ ,
\end{aligned} \tag{3.34}$$

which recovers Eq. (3.25).

The JLS model does not specify what happens beyond t_c. This critical t_c is the termination of the bubble regime and the transition time to another regime. This regime could be a big crash or a change of the growth rate of the market. Merrill Lynch EMU (European Monetary Union) Corporates Non-Financial Index in 2009 [64] provides a vivid example of a change of regime characterized by a change of growth rate rather than by a crash or rebound. For $m < 1$, the crash hazard rate accelerates up to t_c but its integral up to t which controls the total probability for a crash to occur up to t remains finite and less than 1 for all times $t \leq t_c$. It is this property that makes it rational for investors to remain invested knowing that a bubble is developing and that a crash is looming. Indeed, there is still a finite probability that no crash will occur during the lifetime of the bubble. The condition that the price remains finite at all time, including t_c, imposes that $m > 0$.

Within the JLS framework, a bubble is qualified when the crash hazard rate accelerates. According to Eq. (3.20), this imposes $m < 1$ and $B' > 0$, hence $B < 0$ since $m > 0$ by the condition that the price remains finite. We thus have a first condition for a bubble to occur

$$0 < m < 1 \ . \tag{3.35}$$

By definition, the crash rate should be non-negative. This imposes [83]

$$b \equiv -Bm - |C|\sqrt{m^2 + \omega^2} \geq 0 . \tag{3.36}$$

3.2.2 Calibration method

There are eight parameters in this LPPL model augmented by the introduction of the Zipf's factor, four of which are the linear parameters $(\gamma, A, B$ and $C)$. The other four $(t_c, m, \omega$ and $\phi)$ are nonlinear parameters.

We first slave the linear parameters to the nonlinear ones. The method here is the same as used by Johansen et al. [47]. The detailed equations and procedure is as follows. We rewrite Eq. (3.25) as:

$$\mathrm{E}[\ln p(t)] = \gamma\zeta(t) + A + Bf(t) + Cg(t) := RHS(t) . \tag{3.37}$$

We have also defined

$$f(t) = (t_c - t)^m , \qquad g(t) = (t_c - t)^m \cos(\omega \ln(t_c - t) - \phi) . \tag{3.38}$$

The minimization of the sum of the squared residuals should satisfy

$$\frac{\partial \Sigma_t [\ln p(t) - RHS(t)]^2}{\partial \theta} = 0, \quad \forall\, \theta \in \{\gamma, A, B, C\}. \tag{3.39}$$

The linear parameters γ, A, B and C are determined as the solutions of the linear system of four equations:

$$\Sigma_{t=t_1}^{t_2} \begin{pmatrix} \zeta^2(t) & \zeta(t) & \zeta(t)f(t) & \zeta(t)g(t) \\ \zeta(t) & 1 & f(t) & g(t) \\ \zeta(t)f(t) & f(t) & f^2(t) & f(t)g(t) \\ \zeta(t)g(t) & g(t) & f(t)g(t) & g^2(t) \end{pmatrix} \begin{pmatrix} \gamma \\ A \\ B \\ C \end{pmatrix} = \Sigma_{t=t_1}^{t_2} \begin{pmatrix} \zeta(t)\ln p(t) \\ \ln p(t) \\ f(t)\ln p(t) \\ g(t)\ln p(t) \end{pmatrix} . \tag{3.40}$$

This provides four analytical expressions for the four linear parameters (γ, A, B, C) as a function of the remaining nonlinear parameters t_c, m, ω, ϕ. The resulting cost function (sum of square residuals) becomes function of just the four nonlinear parameters t_c, m, ω, ϕ. This achieves a very substantial gain in stability and efficiency as the search space is reduced to the 4 dimensional parameter space (t_c, m, ω, ϕ). A heuristic search implementing the taboo algorithm [84] is used to find initial estimates of the parameters which are then passed to a Levenberg-Marquardt algorithm [85, 86] to minimize the residuals (the sum of the squares of the differences) between

the model and the data. The calibration is performed for the time window delineated by $[t_1, t_2]$, where t_1 is the starting time and t_2 is the ending time of the price time being fitted by expression Eq. (3.25) or equivalently Eq. (3.37).

The bounds of the search space are:

$$t_c \in [t_2, t_2 + 0.375(t_2 - t_1)] \qquad (3.41)$$

$$m \in [10^{-5}, 1 - 10^{-5}] \qquad (3.42)$$

$$\omega \in [0.01, 40] \qquad (3.43)$$

$$\phi \in [0, 2\pi - 10^{-5}] \qquad (3.44)$$

We choose these bounds because m has to be between 0 and 1 according to the discussion before; the log-angular frequency ω should be greater than 0. The upper bound 40 is large enough to catch high-frequency oscillations (though we later discard fits with $\omega > 20$); the phase ϕ should be between 0 and 2π; The predicted critical time t_c should be after the end t_2 of the fitted time series. Finally, the upper bound of the critical time t_c should not be too far away from the end of the time series since predictive capacity degrades far beyond t_2. Jiang et al. [50] have found empirically that a reasonable choice is to take the maximum horizon of predictability to extent to about one-third of the size of the fitted time window.

3.2.3 Application to the Shanghai Composite Index (SSEC)

Construction of the capitalization-weighted and equally-weighted portfolios

We use the Shanghai Composite Index as the market proxy to test the JLS model augmented with the Zipf factor. The Shanghai Composite Index is a capital-weighted measure of stock market performance. On December 19, 1990, the base value of the Shanghai Composite Index I was fixed to 100. We note the base date as t_B. Denoting by K_B, the total market capitalization of the firms entering in the Shanghai Composite index on t_B December 19, 1990, the value $p(t)$ of the Shanghai Composite Index at any later time t is given by

$$p(t) = \frac{K(t)}{K_B} \times 100, \qquad (3.45)$$

where $K(t)$ is the current total market capitalization of the constituents of the Shanghai Composite index. Here, time is counted in units of trading days. Calling

$p_j(t)$ (respectively $s_j(t)$), the share price (respectively total number of shares) of firm j at time t, we have the total capitalization of firm j at time t

$$K_j(t) = p_j(t)s_j(t) \ , \tag{3.46}$$

and the total market capitalization at time t

$$K(t) = \sum_{j=1}^{M(t)} K_j(t) \ , \tag{3.47}$$

where $M(t)$ is the number of the stocks listed in the index at time t.

At the time when the calibrations were performed, the SSEC market included 884 active stocks. Since December 19, 1990, 36 firms were delisted and another 11 were temporarily stopped. Based on the rule of the index calculation, the terminated stocks are deleted from the total market capitalization after the termination is executed, while the last active capitalization of the temporarily stopped stocks are still included in the total market capitalization.

The equal-weighted price p_e entering in the definition of the Zipf factor is constructed according to the formula:

$$p_e(t) = p(t_0) \times \exp\left[\sum_{i=t_1}^{t} r_e(i)\right] \ , \tag{3.48}$$

where t_1 is the beginning of the fitted window and t_0 is the trading day immediately preceding t_1. We use this measure of p_e to make sure that the equal-weighted price and the value-weighted price are identical at t_0. This implies that $\zeta(t_0)$ is set to be 0 (recall that ζ is defined by expression (3.17)). The return $r_e(i)$ is defined by

$$r_e(i) = \frac{1}{M(i)} \sum_{j=1}^{M(i)} \left[\ln K_j(i) - \ln K_j(i-1)\right] \ . \tag{3.49}$$

In expression (3.49), $K_j(i)$ is the total capitalization value of firm j at time i and $M(i)$ is the number of the stocks which are listed in the index for both time i and $i-1$. Formula (3.49) together with (3.48) means that the Zipf factor is a portfolio that puts an equal amount of wealth at each time step (by a corresponding dynamical reallocation depending on the relative performance of the $M(i)$ stocks as a function of time) on each of the $M(i)$ stocks entering in the definition of the Shanghai Composite Index, so that the Zipf portfolio is maximally diversified (neglecting here

the impact of cross-correlations between the assets). Putting expression (3.49) inside (3.48) yields

$$p_e(t) = p(t_0) \times \prod_{i=t_1}^{t} \left[\left(\prod_{j=1}^{M(i)} \frac{K_j(i)}{K_j(i-1)} \right)^{1/M(i)} \right]. \tag{3.50}$$

When the number of the stocks remains unchanged from t_0 to t, i.e.

$$M(i) = M, \qquad \forall i \in [t_0, t] , \tag{3.51}$$

expression (3.50) can be simplified as:

$$p_e(t) = p(t_0) \times \left[\prod_{j=1}^{M} \left(\frac{K_j(t)}{K_j(t_0)} \right) \right]^{1/M} , \tag{3.52}$$

showing that $p_e(t)$ is the geometrical mean of the capitalizations of the stocks constituting the Shanghai Composite Index, as compared with the index which is proportional to the arithmetic mean of the firm capitalizations.

Empirical test of the JLS model augmented by the Zipf factor

The Shanghai Composite Index had two famous bubbles in recent history as described in Tab. 3.8. Both of them are tested in this paper. The time series are fitted with both the original JLS model and the new model. The 10 best initial guesses from the heuristic search algorithm are kept. The results are shown in Fig. 3.4–3.5.

Example	Calibration start at t_1	Prediction start at t_2	Peak date of the bubble
Bubble 1	Aug-01-2006	Sep-28-2007	16-Oct-2007
Bubble 2	Oct-31-2008	Jul-01-2009	Aug-04-2009

Table 3.8: Information on the tested bubbles of SSEC.

We use the standard Wilks test of nested hypotheses to check the improvement of the new factor model. This test assumes independent and normally distributed residuals. The null hypothesis is:

H_0:   the original JLS model is sufficient and the new factor model is not necessary.

The alternative hypothesis reads:

H_1:   The original JLS model is not sufficient and the new factor model is needed.
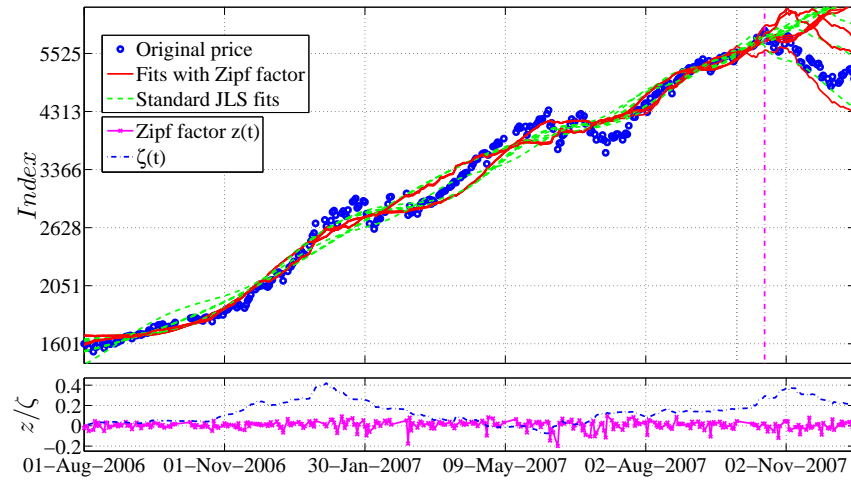
Figure 3.4: Calibration of the new factor model and the original JLS model to the Shanghai Composite Index (SSEC) between Aug-01-2006 and Sep-28-2007. (Upper panel) The beginning of the fit interval is the left boundary of the plot, while the end of the fit interval is indicated by the vertical thick black dotted line. The real critical time t_c when the crash started is marked by the vertical magenta dot-dashed line. The historical close prices are shown as blue full circles. The best 10 fits of the original JLS model are shown as the green dashed lines and the best 10 fits of the new factor model are shown as the red solid lines. (Lower panel) The corresponding Zipf factor (magenta solid line with 'x' symbol) and ζ function (blue dot-dashed line) during this period.
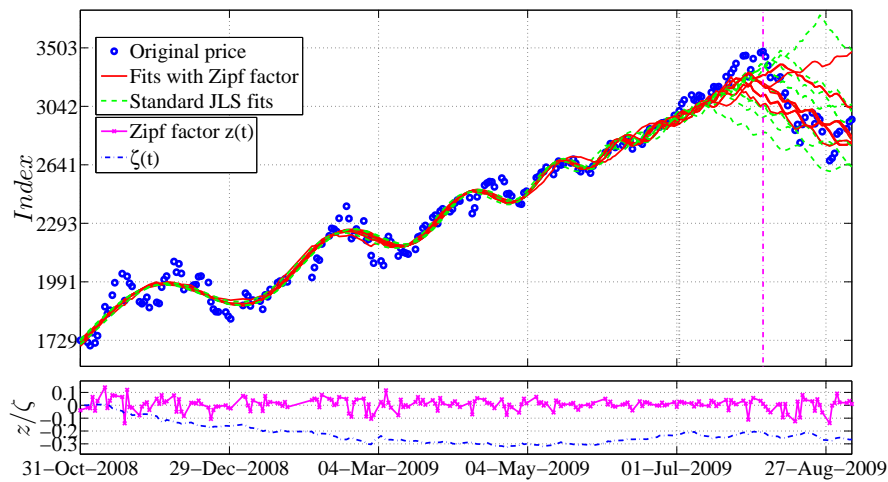
Figure 3.5: Calibration of the new factor model and the original JLS model to the Shanghai Composite Index (SSEC) between Oct-31-2008 and Jul-01-2009. (upper) The beginning of the fit interval is the left boundary of the plot, while the end of the fit interval is indicated by the vertical thick black dotted line. The real critical time t_c when the crash started is marked by the vertical magenta dot-dashed line. The historical close prices are shown as blue full circles. The best 10 fits of the original JLS model are shown as the green dashed lines and the best 10 fits of the new factor model are shown as the red solid lines. (lower) The corresponding Zipf factor (magenta solid line with 'x' symbol) and ζ function (blue dot-dashed line) during this period.

For sufficiently large time windows, and noting T the number of trading days in the fitted time window $[t_1, t_2]$, the Wilks log-likelihood ratio reads

$$W = 2\log\frac{L_{Zipf,max}}{L_{JLS,max}} = 2T\ln\frac{\sigma_{JLS}}{\sigma_{Zipf}} + \frac{\sum_{t=1}^{T} R_{JLS}^2(t)}{\sigma_{JLS}^2} - \frac{\sum_{t=1}^{T} R_{Zipf}^2(t)}{\sigma_{Zipf}^2} \;, \quad (3.53)$$

where R_{JLS} and σ_{JLS} (respectively R_{Zipf} and σ_{Zipf}) are the residuals and their corresponding standard deviation for the original JLS model (respectively the new factor model).

In the large T limit, and under the above conditions of asymptotic independence and normality, the W-statistics is distributed with a χ_k^2 distribution with k degrees of freedom, where k is the difference between the number of parameters in two models. In our case, the new factor model has one more parameter, which is γ. Therefore, W in Eq.(3.53) should follow the χ_1^2 distribution.

Only considering the best fit for each of the two models, we obtain a p-value associated with the empirical value of the W-statistics equal to 2.64×10^{-7} for bubble 1 and 0.2517 for bubble 2. Thus, the null hypothesis is rejected and the Zipf factor is necessary for the best fit of bubble 1, while the null hypothesis is not rejected and the Zipf factor is not necessary for the best fit of bubble 2. This result is also consistent with the two values found for γ, where $\gamma = 0.44$ for bubble 1 and $\gamma = -0.028$ for bubble 2, showing the Zipf factor in bubble 1 plays an important role in the improvement of the fit quality.

Keeping the best 10 fits as we described before increases the statistical power of the Wilks test (simply by having more statistical data) and we want to show that the new JLS model with the Zipf factor is an significant improvement. For this, we combine all of the residuals from the best 10 fits to the data into a large residual sample and calculate the Wilks log-likelihood ratio W for this large sample as defined by expression (3.53). The corresponding p-values are 0 for bubble 1 and 0.0119 for bubble 2. This means the new factor model performs better than the original JLS model for both cases when we consider the overall qualify of the best 10 fits.

A natural and interesting test is to find out if the new model with Zipf factor has a better predictability of the critical time. To achieve this goal, two examples are fitted by both models within different time windows obtained by varying their

start time t_1 and the end time t_2. We consider 15 different values of t_1 and of t_2 in steps of 3 days, yielding 225 time series for each example. We keep the best 10 fits for each time series and get 2250 predicted critical time t_c with each model and for each example. The results in Tab. 3.9 show that the mean value and the standard deviation of the critical time t_c for both models are similar. The new model including the Zipf factor neither improves nor deteriorates the predictability of the critical time for these two examples.

Example	Peak date	Mean(std) of t_c, new	Mean(std) of t_c, original
Bubble 1	16-Oct-2007	07-Oct-2007(55.6)	18-Oct-2007(54.1)
Bubble 2	Aug-04-2009	04-Jul-2009(33.6)	05-Jul-2009(32.4)

Table 3.9: Prediction of the critical time for both models ("new" is stand for the new model with Zipf factor while "original" is stand for the standard JLS model). For each example, 225 time series are generated by varying the start time t_1 and end time t_2 of the windows in which the calibration is performed. The mean value and the standard deviation of the predicted critical time t_c among 2250 predictions are shown in the table.

However, the new model makes it possible to determine the concentration of stock gains over time from the knowledge of the Zipf factor. The two bubbles are found to differ by the sign and contribution of the Zipf factor as well as the factor load γ.

For bubble 1, the integrated Zipf factor ζ is positive as shown in Fig. 3.4, corresponding to the fact that valuation gains were more concentrated on the large firms of the Shanghai index, especially in two periods, Dec. 2006–Jan. 2007 and Oct. 2007–Dec. 2007. The factor load γ of the best fit in the example shown in Fig. 3.4 is 0.44. And the statistics of γ from all the 2250 fits of bubble 1 is shown in the second row of Tab. 3.10. All these results indicate that the Zipf factor load γ in bubble 1 is statistically large and positive. This implies the existence of a lack-of-diversification premium that contributes significantly to the overall price level in addition to the bubble component.

A possible interpretation of the important of the Zipf factor is based on the importance that investors started to attribute to the role of large companies in driving the appreciation of the SSEC index during the first bubble. The so-called 80-20 rule started to be hot among investors in discussions and interpretation of the

rising SSEC index. It was widely pointed out that the growth of the SSEC index was driven essentially by 20% of the stocks while the other 80% constituents of the index remains approximately flat (known as the 80-20 quotation of the Chinese stock market [1]). It is plausible that the widespread acknowledgement of the 80-20 rule led many investors to discount the risk of a lack of diversification, therefore enhancing the role of the Zipf factor. This is consistent with our observation that the Zipf factor load γ is large and positive during the first bubble period.

Example	$Mean of \gamma$	Median of γ	std of γ
Bubble 1	0.35	0.56	0.43
Bubble 2	-0.14	-0.11	0.15

Table 3.10: Statistics of the Zipf factor load γ from 2250 fit results. Most of the values for γ for the period during the development of bubble 1 are positive and their average value is large. This means that the Zipf factor plays an important role during the development of bubble 1. The concentration of the stock market on a small number of large firms has a significant impact on the price change of the stock index. In contrast, for bubble 2, the average value of γ is relatively small and the exposition to the risk associated with a lack of diversification is found to be insignificant in pricing the value of the market.

In contrast, the integrated Zipf factor ζ remained negative over the lifetime of bubble 2 as shown in Fig. 3.5, implying that the gains of the Shanghai index were more driven by small and medium size firms. The factor load γ is -0.028 for the best fit shown in Fig. 3.5 and the mean value of γ for bubble 2 is small and negative (see Tab. 3.10). The overall contribution of the Zipf factor to the stock change is therefore small and negative (due to the product of a negative integrated Zipf factor by a negative factor loading), which makes the remuneration of investors due to their exposition to the diversification risk still positive but small.

At the time when bubble 2 started, the world economy has been seriously shaken by the developing subprime crisis. The demand for Chinese product exports decreased dramatically. To compensate for the loss from collapsing exports, the Chinese government launched a 4 trillion Chinese yuan stimulus with the aim to boost the domestic demand. Small companies that are usually more vulnerable to a lack of access to capital profited proportionally more than their larger counterpart from this injection of capital in the economy. This is reflected in relative better perfor-

---

[1]http://www.hudong.com/wiki/二八现象

mance of small and medium size firms in the stock market, leading to a slightly negative value of the integrated Zipf factor ζ during the development of bubble 2. Although the small companies benefit more, the stimulus was designed to boost the whole economy. The diversification risk turned out to be relatively minor at that time, explaining the small value of the Zipf factor load.

3.2.4 Conclusion

We have introduced a new model that combines the Zipf factor embodying the risk due to lack of diversification with the JLS model of rational expectation bubbles with positive feedbacks. The new model keeps all the dynamical characteristics of a bubble described in the JLS model. In addition, the new model can also provide information about the concentration of stock gains over time from the knowledge of the Zipf factor. This new information is very helpful to understand the risk diversification and to explain the investors' behavior during the bubble generation. We have applied this new model to two famous Chinese stock bubbles and found that the new model provide sensible explanation for the diversification risk observed during these two bubbles.

4

Systematic Diagnosis and Prediction of Rebounds and Crashes in Financial Markets

In this chapter, we introduce a pattern recognition method, which is originally developed by Israel Gelfand and his collaborators to predict the earthquakes. Gelfand is a famous mathematician who shared the first Wolf Prize in Mathematics with Carl Ludwig Siegel for his work in functional analysis, group representation, and for his seminal contributions to many areas of mathematics and its applications. He also did many important works in many areas outside mathematics such as biology, medicine and earthquake predictions. This pattern recognition method together with the JLS model enables us to perform systematic diagnosis and prediction of rebounds and crashes in financial markets.

In Sec. 4.1, we introduce the concept of "negative bubbles" as the mirror (but not necessarily exactly symmetric) image of standard financial bubbles, in which positive feedback mechanisms may lead to transient accelerating price falls. To model these negative bubbles, we adapt the JLS model of rational expectation bubbles with a hazard rate describing the collective buying pressure of noise traders. The price fall occurring during a transient negative bubble can be interpreted as an effective random down payment that rational agents accept to pay in the hope of profiting from the expected occurrence of a possible rally. We validate the model by showing that it has significant predictive power in identifying the times of major market rebounds. This result is obtained by using a general pattern recognition method that

combines the information obtained at multiple times from a dynamical calibration of the JLS model. Error diagrams, Bayesian inference and trading strategies suggest that one can extract genuine information and obtain real skill from the calibration of negative bubbles with the JLS model. We conclude that negative bubbles are in general predictably associated with large rebounds or rallies, which are the mirror images of the crashes terminating standard bubbles.

Then in Sec. 4.2, we extend our work by testing both rebounds and crashes in 10 major equity markets. A simple trading strategy based on the prediction results of both rebounds and crashes is designed. The performance of the trading strategy as well as the error diagram confirms that our method is very efficient in terms of diagnosing and predicting market rebounds and crashes systematically.

4.1 Diagnosis and Prediction of Rebounds in Financial Markets

In this section, we explore the hypothesis that financial bubbles have mirror images in the form of "negative bubbles" in which positive feedback mechanisms may lead to transient accelerating price falls. We adapt the JLS model of rational expectation bubbles [46, 48, 47] to negative bubbles. The crash hazard rate becomes the rally hazard rate, which quantifies the probability per unit time that the market rebounds in a strong rally. The upward accelerating bullish price characterizing a bubble, which was the return that rational investors require as a remuneration for being exposed to crash risk, becomes a downward accelerating bearish price of the negative bubble, which can be interpreted as the cost that rational agents accept to pay to profit from a possible future rally. During this accelerating downward trend, a tiny reversal could be a strong signal for all the investors who are seeking the profit from the possible future rally. These investors will long the stock immediately after this tiny reversal. As a consequence, the price rebounds very rapidly.

This section contributes to the literature by augmenting the evidence for transient pockets of predictability that are characterized by faster-than-exponential growth or decay. This is done by adding the phenomenology and modeling of "negative bubbles" to the evidence for characteristic signatures of (positive) bubbles. Both

positive and negative bubbles are suggested to result from the same fundamental mechanisms, involving imitation and herding behavior which create positive feedbacks. By such a generalization within the same theoretical framework, we hope to contribute to the development of a genuine science of bubbles.

The rest of this section is organized as follows. Sec. 4.1.1 gives a brief literature review on the research of rebounds in the financial market. Sec. 4.1.2 presents the modified JLS model for negative bubbles and their associated rebounds (or rallies). The subsequent sections test the JLS model for negative bubbles by providing different validation steps, in terms of prediction skills of actual rebounds and of abnormal returns of trading strategies derived from the model. Sec. 4.1.3 describes the method we have developed to test whether the adapted JLS model for negative bubbles has indeed skills in forecasting large rebounds. This method uses a robust pattern recognition framework build on the information obtained from the calibration of the adapted JLS model to the financial prices. Sec. 4.1.4 presents the results of the tests concerning the performance of the method of Sec. 4.1.3 with respect to the advanced diagnostic of large rebounds. Sec. 4.1.5 develops simple trading strategies based on the method of Sec. 4.1.3, which are shown to exhibit statistically significant returns, when compared with random strategies without skills with otherwise comparable attributes. Sec. 4.1.6 concludes.

4.1.1   Literature review on market rebounds

The rebounds in the financial markets have been studied widely in both theoretical and empirical aspects.

On the theoretical side, there are several competing explanations for price decreases followed by reversals: liquidity and time-varying risk. [126] stresses the importance of liquidity: as more people sell, agents who borrowed money to buy assets are forced to sell too. When forced selling stops, this trend reverses. [127] shows that it is risky to be a fundamental trader in this environment and that price reversals after declines are likely to be higher when there is more risk in the price, as measured by volatility.

On the empirical front concerning the forecast of reversals in price drops, [31] shows that the simplest way to predict prices is to look at past performance. [128] shows that price-dividend ratios forecast future returns for the market as a whole.

Our approach in this section has the advantage in both theoretical and empirical aspects. Theoretically, we suggest that the negative bubbles may generated due to the imitation and herding behavior among the noisy investors which create positive feedbacks. During this accelerating downward trend, a tiny reversal could be a strong signal for all the investors who are seeking the profit from the possible future rally. While empirically, the previous approaches do not aim at predicting and cannot determine the most probable rebound time for a single ticker of the stock. The innovation of our methodology in this respect is to provide a very detailed method to detect rebound of any given ticker.

4.1.2   Theoretical model for detecting rebounds

In the JLS framework, financial bubbles are defined as transient regimes of faster-than-exponential price growth resulting from positive feedbacks. We refer to these regimes as "positive bubbles." We propose that positive feedbacks leading to increasing amplitude of the price momentum can also occur in a downward price regime and that transient regimes of faster-than-exponential *downward* acceleration can exist. We refer to these regimes as "negative bubbles." In a "positive" bubble regime, the larger the price is, the larger the increase of future price. In a "negative bubble" regime, the smaller the price, the larger is the decrease of future price. In a positive bubble, the positive feedback results from over-optimistic expectations of future returns leading to self-fulfilling but transient unsustainable price appreciations. In a negative bubble, the positive feedbacks reflect the rampant pessimism fueled by short positions leading investors to run away from the market which spirals downwards also in a self-fulfilling process.

The symmetry between positive and negative bubbles is obvious for currencies. If a currency A appreciates abnormally against another currency B following a faster-than-exponential trajectory, the value of currency B expressed in currency A will correspondingly fall faster-than-exponentially in a downward spiral. In this example, the negative bubble is simply obtained by taking the inverse of the price, since the value of currency A in units of B is the inverse of the value of currency B in units of A. Using logarithm of prices, this corresponds to a change of sign, hence the "mirror" effect mentioned above.

Recall that the dynamics of the stock market in the JLS model is described as:

$$\frac{dp}{p} = \mu(t)dt + \sigma(t)dW - \kappa dj \;, \tag{4.1}$$

It provides a suitable framework to describe negative bubbles, with the only modifications that both the expected excess return $\mu(t)$ and the crash amplitude κ become negative (hence the term "negative" bubble). Thus, μ becomes the expected (negative) return (i.e., loss) that investors accept to bear, given that they anticipate a potential rebound or rally of amplitude $|\kappa|$. Symmetrically to the case of positive bubbles, the price loss before the potential rebound plays the role of a random payment that the investors honor in order to remain invested and profit from the possible rally. The hazard rate $h(t)$ now describes the probability per unit time for the rebound to occur:

$$h(t) = B'(t_c - t)^{m-1} + C'(t_c - t)^{m-1} \cos(\omega \ln(t_c - t) - \phi') \;. \tag{4.2}$$

The fundamental JLS equation remains the same as:

$$\ln \mathrm{E}[p(t)] = A + B(t_c - t)^m + C(t_c - t)^m \cos(\omega \ln(t_c - t) - \phi) \;. \tag{4.3}$$

The only difference is that the inequalities

$$B > 0 \;, \quad b < 0 \tag{4.4}$$

being the opposite to those corresponding to a positive bubble as described in the preceding subsection.

An example of the calibration of a negative bubble with the JLS model (4) to the S&P 500 index from 1973-01-01 to 1974-10-01 is shown in the upper panel of Fig. 4.1. During this period, the S&P 500 index decreased at an accelerating pace. This price fall was accompanied by very clear oscillations that are log-periodic in time, as described by the cosine term in formula (4). Notice that the end of the decreasing market is followed by a dramatic rebound in index price. We hypothesize that, similar to a crash following an unsustainable super-exponential price appreciation (a positive bubble), an accelerating downward price trajectory (a negative bubble) is in general followed by a strong rebound. Furthermore, in order to suggest that this phenomenon is not an isolated phenomenon but actually happens widely in all kinds of markets, another example in the foreign exchange market is presented in

the lower panel of Fig. 4.1. The USD/EUR change rate from 2006-07-01 to 2008-04-01 also underwent a significant drawdown with very clear log-periodic oscillations, followed by a strong positive rebound. One of the goals of this paper is to identify such regions of negative bubbles in financial time series and then use a pattern recognition method to distinguish ones that were (in a back-testing framework) followed by significant price rises.

In financial markets, large positive returns are less frequent than large negative returns, as expressed for instance in the skewness of return distributions. However, when studying drawdowns and drawups (i.e., runs of same sign returns). Johansen and Sornette found that, for individual companies, there are approximately twice as many large rallies as crashes with amplitude larger than 20% with durations of a few days [129].

4.1.3   Rebound prediction method

We adapt the pattern recognition method of [130] to generate predictions of rebound times in financial markets on the basis of the detection and calibration of negative bubbles, defined in the previous section. We analyze the S&P 500 index prices, obtained from Yahoo! finance for ticker '^GSPC' (adjusted close price)[1]. The start time of our time series is 1950-01-05, which is very close to the first day when the S&P 500 index became available (1950-01-03). The last day of our tested time series is 2009-06-03.

Fitting methods

We first divide our S&P 500 index time series into different sub-windows (t_1, t_2) of length $dt \equiv t_2 - t_1$ according to the following rules:

1. The earliest start time of the windows is $t_1 = $ 1950-01-03. Other start times t_1 are calculated using a step size of $dt_1 = 50$ calendar days.

2. The latest end time of the windows is $t_2 = $ 2009-06-03. Other end times t_2 are calculated with a negative step size $dt_2 = -50$ calendar days.

3. The minimum window size $dt_{\min} = 110$ calendar days.

4. The maximum window size $dt_{\max} = 1500$ calendar days.
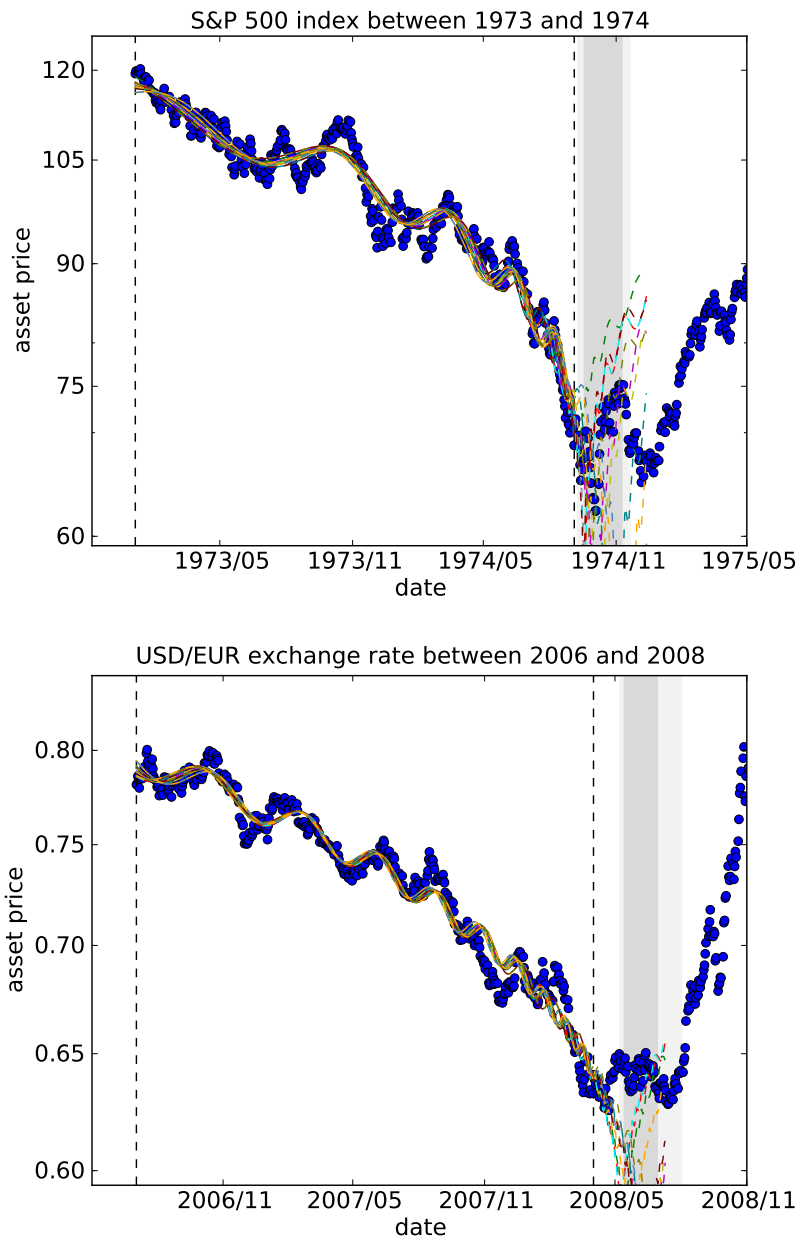
---

[1] http://finance.yahoo.com/q/hp?s=^GSPC

Figure 4.1: (upper) Significant drawdown of nearly 50% from 1973-01-01 to 1974-
10-01 (time window delineated by the two black dashed vertical lines) with very
clear log-periodic oscillations, followed by a strong positive rebound. The best
fits from taboo search are used to form a 90% confidence interval for the critical
time t_c shown by the light shadow area. The dark shadow area corresponds to the
20-80 quantiles region of the predicted rebounds. (lower) The same phenomenon is
observed in foreign exchange market. The plot shows the fitted results for USD/EUR
change rate from 2006-07-01 to 2008-04-01. The USD/EUR change rate performed
a significant drawdown with very clear log-periodic oscillations, followed by a strong
positive rebound.

These rules lead to 11,662 windows in the S&P 500 time series.

For each window, the log of the S&P 500 index is fit with the JLS equation Eq. (4.3). The fit is performed in two steps. First, the linear parameters A, B and C are slaved to the non-linear parameters by solving them analytically as a function of the nonlinear parameters. We refer to [47] (page 238 and following ones), which gives the detailed equations and procedure. Then, the search space is obtained as a 4 dimensional parameter space representing m, ω, ϕ, t_c. A heuristic search implementing the Tabu algorithm [84] is used to find initial estimates of the parameters which are then passed to a Levenberg-Marquardt algorithm [85, 86] to minimize the residuals (the sum of the squares of the differences) between the model and the data. The bounds of the search space are:

$$m \quad \in \quad [0.001, 0.999] \tag{4.5}$$

$$\omega \quad \in \quad [0.01, 40] \tag{4.6}$$

$$\phi \quad \in \quad [0.001, 2\pi] \tag{4.7}$$

$$t_c \quad \in \quad [t_2, t_2 + 0.375(t_2 - t_1)] \tag{4.8}$$

We choose these bounds because m has to be between 0 and 1 according to the discussion before; the log-angular frequency ω should be greater than 0. The upper bound 40 is large enough to catch high-frequency oscillations (though we later discard fits with $\omega > 20$); phase ϕ should be between 0 and 2π; as we are predicting a critical time in financial markets, the critical time should be after the end of the time series we are fitting. Finally, the upper bound of the critical time should not be too far away from the end of the time series since predictive capacity degrades far beyond t_2. We have empirically found elsewhere [50] one-third of the interval width to be a good cut-off.

The combination of the heuristic and optimization results in a set of parameters A, B, C, m, ω, ϕ and t_c for each of the 11,662 windows. Of these parameter sets, 2,568 satisfy the negative bubble condition Eq. (4.4). In Fig. 4.2, we plot the histogram of critical time t_c for these negative bubble fits and the *negative* logarithm of the S&P 500 time series. Peaks in this time series, then, indicate minima of the prices, many of these peaks being preceded by a fast acceleration with upward curvature indicating visually a faster-than-exponential growth of $-p(t)$. This translates into
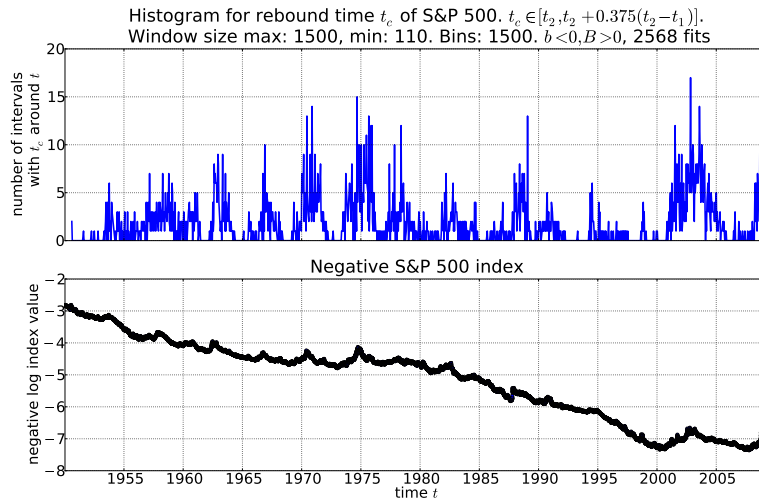
Figure 4.2: (upper) Histogram of the critical times t_c over the set of 2,568 time intervals for which negative bubbles are detected by the condition that the fits of $\ln p(t)$ by Eq. (4.3) satisfy condition Eq. (4.4). (lower) Plot of $-\ln p(t)$ versus time for the S&P 500 index. Note that peaks in this figure correspond to valleys in actual price.

accelerating downward prices. Notice that many of these peaks of $-\ln p(t)$ are followed by sharp drops, that is, fast rebounds in the regular $+\ln p(t)$. We see that peaks in $-\ln p(t)$ correspond to valleys in the negative bubble t_c histogram, implying that the negative bubbles qualified by the JLS model are often followed by rebounds. This suggests the possibility to diagnose negative bubbles and their demise in the form of a rebound or rally. If correct, this hypothesis would extend the proposition [50, 65], that financial bubbles can be diagnosed before their end and their termination time can be determined with an accuracy better than chance, to negative bubble regimes associated with downward price regimes. We quantify this observation below.

Definition of rebound

The aim is first to recognize different patterns in the S&P 500 index from the 11,662 fits and then use the subset of 2,568 negative bubble fits to identify specific negative bubble characteristics. These characteristics will then be used to 'predict' (in a back-testing sense) negative bubbles and rebounds in the future.

We first define a rebound, note as Rbd. A day d is a rebound Rbd if the price on

that day is the minimum price in a window of 200 days before and 200 days after it. That is,

$$\text{Rbd} = \{d \mid P_d = \min\{P_x\}, \forall x \in [d - 200, d + 200]\} \tag{4.9}$$

where P_d is the adjusted closing price on day d. We find 19 rebounds of the ± 200-days type[2] in the 59 year S&P 500 index history. Our task is to diagnose such rebounds in advance. We could also use other numbers instead of 200 to define a rebound. The predictability is stable with respect to a change of this number. This is because we learn from the learning set with a certain number type of rebounds and try to predict the rebounds of the same type. Later we will also show the results for ± 365-days type of rebounds.

Definitions and concepts needed to set up the pattern recognition method

In what follows we describe a hierarchy of descriptive and quantitative terms as follows.

- **learning set.** A subset of the whole set which only contains the fits with critical times in the past. We learn the properties of historical rebounds from this set and develop the predictions based on these properties.

- **classes.** Two classes of fits are defined according to whether the critical time of a given fit is near some rebound or not, where 'near' will be defined below.

- **groups.** A given group contains all fits of a given window size.

- **informative parameters.** Informative parameters are the distinguishing parameters of fits in the same group but different classes.

- **questionnaires.** Based on the value of an informative parameter, one can ask if a certain trading day is a start of rebound or not. The answer series generated by all the informative parameters is called questionnaire.

- **traits.** Traits are extracted from questionnaire. They are short and contain crucial information and properties of a questionnaire.

---

[2]Ten rebounds in the back tests before 1975.1.1: 1953-09-14; 1957-10-22; 1960-10-25; 1962-06-26; 1965-06-28; 1966-10-07; 1968-03-05; 1970-05-26; 1971-11-23; 1974-10-03 and nine rebounds after 1975.1.1 in the prediction range: 1978-03-06; 1980-03-27; 1982-08-12; 1984-07-24; 1987-12-04; 1990-10-11; 1994-04-04; 2002-10-09; 2009-03-09.

- **features.** Traits showing the specific property of a single class are selected to be the feature of that class.

- **rebound alarm index.** An index developed from features to show the probability that a certain day is a rebound.

In this paper, we will show how all the above objects are constructed. Our final goal is to make predictions for the rebound time. The development of the rebound alarm index will enable us to achieve our goal. Several methodologies are presented to quantify the performance of the predictions.

Classes

In the pattern recognition method of [130], one should define the learning set to find characteristics that will then be used to make predictions. We designate all fits before Jan. 1, 1975 as the learning set Σ_1:

$$\Sigma_1 = \{f \mid t_{c,f}, t_{2,f} < Jan.1, 1975\} \tag{4.10}$$

There are 4,591 fits in this set, which we all use without any pre-selection. No pre-selection for instance using Eq. (4.4) is applied, on the basis of the robustness of the pattern recognition method. We then distinguish two different classes from Σ_1 based on the critical time t_c of the fits. For a single fit f with critical time $t_{c,f}$, if this critical time is within D days of a rebound, then we assign fit f to Class I, represented by the symbol C_I. Otherwise, f is assigned to Class II, represented by the symbol C_{II}. For this study, we chose $D = 10$ days because D too big will lose precision and D too small will take the noise into account. In this case, Class I fits are those with t_c within 10 days of one of the 19 rebounds. We formalize this rule as:

$$
\begin{aligned}
C_I &= \{f \mid f \in \Sigma_1, \exists d \in \text{Rbd}, s.t. |t_{c,f} - d| \leq D\}, & (4.11) \\
C_{II} &= \{f \mid f \in \Sigma_1, |t_{c,f} - d| > 10, \forall d \in \text{Rbd}\}, & (4.12) \\
D &= 10 \text{ days.} & (4.13)
\end{aligned}
$$

To be clear, Class I is formed by all the fits in learning set Σ_1 which have a critical time t_c within 10 days of one of the rebounds. All of the fits in the learning set which are not in Class I are in Class II.

Groups

We also categorize all fits into separate *groups* (in addition to the two *classes* defined above) based on the length of the fit interval, $L_f = dt = t_2 - t_1$. We generate 14 groups, where a given group G_i is defined by:

$$G_i = \{f \mid L_f \in [100i, 100i + 100], i = 1, 2, ..., 14, f \in \Sigma_1\} \qquad (4.14)$$

All 4,591 fits in the learning set are placed into one of these 14 groups.

Informative Parameters

For each fit in the learning set, we take 6 parameters to construct a flag that determines the characteristics of classes. These 6 parameters are m, ω, ϕ and B from Eq. (4.3), b (the negative bubble condition) from Eq. (2.21) and q as the residual of the fit.

We categorize these sets of 6 parameters for fits which are in the same group and same class. Then for each class-group combination, we calculate the probability density function (pdf) of each parameter using the adaptive kernel method [131], generating 168 pdfs (6 parameters $\times$ 2 classes $\times$ 14 groups).

We compare the similarity (defined below) of the pdfs of each of the six parameters that are in the same group (window length) but different classes (proximity of t_c to a rebound date). If these two pdfs are similar, then we ignore this parameter in this group. If the pdfs are different, we record this parameter of this group as an *informative parameter*. The maximum number of possible informative parameters is 84 (6 parameters $\times$ 14 groups).

We use the Kolmogorov-Smirnov method [132] to detect the difference between pdfs. If the maximum difference of the cumulative distribution functions (integral of pdf) between two classes exceeds 5%, then this is an informative parameter. We want to assign a uniquely determined integer IP_l to each informative parameter. We can do so by using three indexes, i, j and l. The index i indicates which group, with $i \in [1, 14]$. The index j indicates the parameter, where $j = 1, 2, 3, 4, 5, 6$ refer to m, ω, ϕ, B, b, q, respectively. Finally, l represents the actual informative parameter. Assuming that there are L informative parameters in total and using the indexes,

IP_l is then calculated via

$$IP_l = 6i + j \qquad (4.15)$$

for $l \in [1, L]$.

Given the L informative parameters IP_l, we consider the pdfs for the two different classes of a single informative parameter. The set of abscissa values within the allowed range given by Eq. (4.5–4.8), for which the pdf of Class I is larger than the pdf of Class II, defines the domain $Rg_{I,l}$ ('good region') of this informative parameter which is associated with Class I. The other values of the informative parameters for which the pdf of Class I is smaller than the pdf of Class II define the domain $Rg_{II,l}$ which is associated with Class II. These regions play a crucial role in the generation of questionnaires in the next section.

Our hypothesis is that many "positive" and "negative bubbles" share the same structure described by the JLS model, because they result from the same underlying herding mechanism. However, nothing a priori imposes that the control parameters should be identical. Note that our pattern recognition methodology specifically extract the typical informative parameter ranges that characterize the "negative bubbles".

Intermediate summary

We realize that many new terms are being introduced, so in an attempt to be absolutely clear, we briefly summarize the method to this point. We sub-divide a time series into many windows (t_1, t_2) of length $L_f = t_2 - t_1$. For each window, we obtain a set of parameters that best fit the model Eq. (4.3). Each of these windows will be assigned one of two *classes* and one of 14 *groups*. Classes indicate how close the modeled critical time t_c is to a historical rebound, where Class I indicates 'close' and Class II indicates 'not close'. Groups indicate the length of the window. For each fit, we create a set of six parameters: m, ω, ϕ and B from Eq. (4.3), b (the negative bubble condition) from Eq. (2.21) and q as the residual of the fit. We create the pdfs of each of these parameters for each fit and define *informative parameters* as those parameters for which the pdfs differ significantly according to a Kolmogorov-Smirnov test. For each informative parameter, we find the regions of the abscissa of the pdf for which the Class I pdf (fits with t_c close to a rebound) is

greater than the Class II pdf. For informative parameter l (defined in Eq. (4.15)), this region is designated as $Rg_{I,l}$. In the next section, we will use these *regions* to create *questionnaires* that will be used to predictively identify negative bubbles that will be followed by rebounds.

Another important distinction to remember at this point is that the above method has been used to find *informative parameters* that will be used below. Informative parameters are associated with a *class* and a *group*.

Questionnaires

Using the informative parameters and their pdfs described above, we can generate *questionnaires* for each day of the learning or testing set. Questionnaires will be used to identify negative bubbles that will be followed by rebounds. The algorithm for generating questionnaires is the following:

1. Obtain the maximum (t_{cmax}) and minimum (t_{cmin}) values of t_c from some subset Σ_{sub}, either the 'learning' set or the 'predicting (testing)' set of all 11,662 fits.

2. Scan each day t_{scan} from t_{cmin} to t_{cmax}. There will be $N = t_{cmax} - t_{cmin} + 1$ days to scan. For each scan day, create a new set $S_{t_{scan}}$ consisting of *all* fits in subset Σ_{sub} that have a t_c near the scan day t_{scan}, where 'near' is defined using the same criterion used for defining the two classes, namely $D = 10$ days:

$$S_{t_{scan}} = \{f \mid |t_{c,f} - t_{scan}| \leq D, f \in \Sigma_{sub}\} \tag{4.16}$$

   The number $\#S_{t_{scan}}$ of fits in each set can be 0 or greater. The sum of the number of fits found in all of the sets $\sum_{t_{scan}=t_{cmin}}^{t_{cmax}} \#S_{t_scan}$ can actually be greater than the total number of fits in Σ_{sub} since some fits can be in multiple sets. Notice that the fits in each set $S_{t_{scan}}$ can (and do) have varying window lengths. At this point, only the proximity to a scan day is used to determine inclusion in a scan set.

3. Assign a group to each of the fits in S_{tscan}. Recall that groups are defined in Eq. (4.14) and are based on the window length $L_f = dt = t_2 - t_1$.

4. Using all sets S_{tscan}, for each informative parameter IP_l found in Sec. 4.1.3, determine if it belongs to Class I (close to a rebound) or Class II (not close

to a rebound). There are 3 possible answers: 1 = 'belongs to Class I', -1 = 'belongs to Class II' or 0 = 'undetermined'.

The status of 'belonging to Class I' or not is determined as follows. First, find all values of the informative parameter IP_l in a particular scan set $S_{t_{scan}}$. For instance, if for a particular scan day t_{scan}, there are n fits in the subset Σ_{sub} that have t_c 'near' t_{scan}, then the set $S_{t_{scan}}$ contains those n fits. These n fits include windows of varying lengths so that the windows themselves are likely associated with different groups. Now consider a given informative parameter IP_l and its underlying parameter j (described in Sec. 4.1.3) that has an associated 'good region', $Rg_{I,l}$. Remember that this informative parameter IP_l has an associated group. Count the number p of the n fits whose lengths belong to the associated group of IP_l. If more of the values of the underlying parameter of p lie within $Rg_{I,l}$ than outside of it, then IP_l belongs to Class I and, thus, the 'answer' to the question of 'belonging to Class I' is $a = 1$. If, on the other hand, more values lie outside the 'good region' $Rg_{I,l}$ than in it, the answer is $a = -1$. If the same number of values are inside and outside of $Rg_{I,l}$ then $a = 0$. Also, if no members of $S_{t_{scan}}$ belong to the associated group of IP_l then $a = 0$.

To assist more in that understanding, let us have a look at an example. Assume that the informative parameter information tells us parameter m in Group 3 is the informative parameter IP_{19} and $m \in [A, B]$ is the 'good region' $Rg_{I,l}$ of Class I. We consider a single t_{scan} and find that there are two fits in $S_{t_{scan}}$ in this group with parameter m values of m_1 and m_2. We determine the 'answer' $a = a_{IP_{19}}$ as follows:

- If $m_1, m_2 \in [A, B]$, we say that based on IP_{19} (Group 3, parameter m) that fits near t_{scan} belong to Class I. Mark this answer as $a_{IP_{19}} = 1$.

- If $m_1 \in [A, B]$ and $m_2 \notin [A, B]$, we say that fits near t_{scan} cannot be identified and so $a_{IP_{19}} = 0$.

- If $m_1, m_2 \notin [A, B]$, fits near t_{scan} belong to Class II and $a_{IP_{19}} = -1$.

More succinctly,

$$a_{IP_{19}} = \begin{cases} 1 & \text{if } m_1, m_2 \in [A, B] \\ 0 & \text{if } m_i \in [A, B], m_j \notin [A, B], i \neq j, i, j \in \{1, 2\} \\ -1 & \text{if } m_1, m_2 \notin [A, B] \end{cases} \quad (4.17)$$

For each of the informative parameters, we get an answer a that says that fits near t_{scan} belong to Class I or II (or cannot be determined). For a total of L informative parameters, we get a questionnaire A of length L:

$$A_{t_{scan}} = a_1 a_2 a_3 ... a_L, a_i \in \{-1, 0, 1\} \tag{4.18}$$

Qualitatively, these questionnaires describe our judgment to whether t_{scan} is a rebound or not. This judgment depends on the observations of informative parameters.

Traits

The concept of a *trait* is developed to describe the property of the questionnaire for each t_{scan}. Each questionnaire can be decomposed into a fixed number of traits if the length of questionnaire is fixed.

From any questionnaire with length L, we generate a series of traits by the following method. Every trait is a series of 4 to 6 integers, $\tau = p, q, r, (P, Q, R)$. The first three terms p, q and r are simply integers. The term (P, Q, R) represents a string of 1 to 3 integers. We first describe p, q and r and then the (P, Q, R) term.

The integers p, q and r have limits: $p \in 1, 2, \ldots, L, q \in p, p+1, \ldots, L, r \in q, q+1, \ldots, L$. We select all the possible combinations of bits from the questionnaire $A_{t_{scan}}$ with the condition that each time the number of selected questions is at most 3. We record the numbers of the selected positions and sort them. The terms p, q and r are selected position numbers and defined as follows:

- If only one position i_1 is selected: $r = q = p = i_1$

- If two i_1, i_2 are selected: $p = i_1, r = q = i_2 (i_1 < i_2)$

- If three i_1, i_2, i_3 are selected: $p = i_1, q = i_2, r = i_3 (i_1 < i_2 < i_3)$

The term (P, Q, R) is defined as follows:

$$r = q = p, \quad (P, Q, R) = a_p \tag{4.19}$$

$$r = q, q \neq p, \quad (P, Q, R) = a_p, a_q \tag{4.20}$$

$$r \neq q, q \neq p, \quad (P, Q, R) = a_p, a_q, a_r \tag{4.21}$$

As an example, A = (0,1,-1,-1) has traits in Tab. 4.1.

p	q	r	(P,Q,R)
1	1	1	0
1	2	2	0,1
1	2	3	0,1,-1
1	2	4	0,1,-1
1	3	3	0,-1
1	3	4	0,-1,-1
1	4	4	0,-1
2	2	2	1
2	3	3	1,-1
2	3	4	1,-1,-1
2	4	4	1,-1
3	3	3	-1
3	4	4	-1,-1
4	4	4	-1

Table 4.1: Traits for series A = (0,1,-1,-1)

For a questionnaire with length L, there are $3L + 3^2\binom{L}{2} + 3^3\binom{L}{3}$ possible traits. However, a single questionnaire has only $L + \binom{L}{2} + \binom{L}{3}$ traits, because (P,Q,R) is defined by p,q and r. In this example, there are 14 traits for questionnaire (0,1,-1,-1) and 174 total traits for all possible $L = 4$ questionnaires.

Features

At the risk of being redundant, it is worth briefly summarizing again. Until now we have: L informative parameters $IP_1, IP_2, \ldots, IP_L$ from 84 different parameters (84 = 6 parameters × 14 Groups) and a series of questionnaires $A_{t_{scan}}$ for each t_{scan} from t_{cmin} to t_{cmax} using set $S_{t_{scan}}$. These questionnaires depend upon which subset Σ_{sub} of fits is chosen. Each questionnaire has a sequence of traits that describe the property of this questionnaire in a short and clear way. Now we generate *features* for both classes.

Recall that the subset of fits $\Sigma_{feature}$ that we use here is that which contains all fits which have a critical time t_c earlier than $t_p = $ 1975-01-01, $\Sigma_{feature} = \{f \mid t_{c,f} < t_p\}$. By imposing that t_2 and $t_{c,f}$ are both smaller than t_p, we do not use any future information. Considering the boundary condition of critical times in Eq. (4.8), the end time of a certain fit t_2 is less than or equal to t_c. Additionally, we select only those critical times such that $t_{c,f} < t_p, \forall f \in \Sigma_{feature}$.

Assume that there are two sets of traits T_I and T_{II} corresponding to Class I and Class II, respectively. Scan day by day the date t from the smallest t_c in $\Sigma_{feature}$ until t_p. If t is near a rebound (using the same $D = 10$ day criterion as before), then all traits generated by questionnaire A_t belong to T_I. Otherwise, all traits generated by A_t belong to T_{II}.

Count the frequencies of a single trait τ in T_I and T_{II}. If τ is in T_I for more than α times and in T_{II} for less than β times, then we call this trait τ a *feature F_I* of Class I. Similarly, if τ is in T_I for less than α times and in T_{II} for more than β times, then we call τ a *feature F_{II}* of Class II. The pair (α, β) is defined as a *feature qualification*. We will vary this qualification to optimize the back tests and predictions.

Rebound alarm index

The final piece in our methodology is to define a *rebound alarm index* that will be used in the forward testing to 'predict' rebounds. Two types of rebound alarm index are developed. One is for the back tests before 1975-01-01, as we have already used the information before this time to generate informative parameters and features. The other alarm index is for the prediction tests. We generate this prediction rebound alarm index using only the information before a certain time and then try to predict rebounds in the 'future' beyond that time.

4.1.4   Results

Features of learning set

Recall that a *feature* is a trait which frequently appears in one class but rarely in the other class. Features are associated with feature qualification pairs (α, β). Using all the fits from subset $\Sigma_{feature}$ found in Sec. 4.1.3, we generate the questionnaires for each day in the learning set, i.e., the fits with t_c before 1975-01-01. Take all traits from the questionnaire A_t for a particular day t and compare them with features F_I and F_{II}. The number of traits in F_I and F_{II} are called $\nu_{t,I}$ and $\nu_{t,II}$. Then we define:

$$RI_t = \begin{cases} \frac{\nu_{t,I}}{\nu_{t,I}+\nu_{t,II}} & \text{if } \nu_{t,I} + \nu_{t,II} \geq 0 \\ 0 & \text{if } \nu_{t,I} + \nu_{t,II} = 0 \end{cases} \qquad (4.22)$$

From the definition, we can see that $RI_t \in [0, 1]$. If RI_t is high, then we expect that this day has a high probability that the rebound will start.

We choose feature qualification pair (10, 200) here, meaning that a certain trait must appear in trait Class I at least 11 times *and* must appear in trait Class II less than 200 times. If so, then we say that this trait is *a feature of Class I*. If, on the other hand, the trait appears 10 times or less in Class I *or* appears 200 times or more in Class II, then this trait is *a feature of Class II*. The result of this feature qualification is shown in Fig. 4.3. Note that the choice (10, 200) is somewhat arbitrary and does not constitute an in-sample optimization on our part. This can be checked from the error diagrams presented below, which scan these numbers: one can observe in particular that the pair (10, 200) does not give the best performance. We have also investigated the impact of changing other parameters and find a strong robustness.
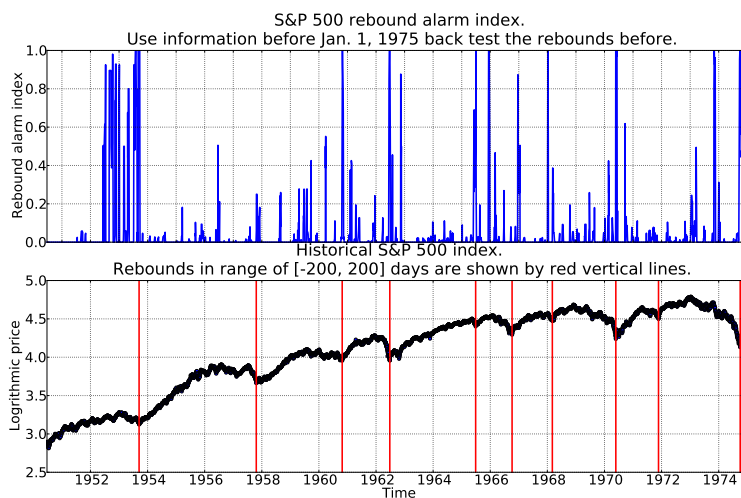

Figure 4.3: Rebound alarm index and log-price of the S&P 500 Index for the learning set, where t_2 and t_c are both before Jan. 1, 1975. (upper) Rebound alarm index for the learning set using feature qualification pair $(10, 200)$. The rebound alarm index is in the range $[0, 1]$. The higher the rebound alarm index, the more likely is the occurrence of a rebound. (lower) Plot of $\ln p(t)$ versus time of S&P Index. Red vertical lines indicate rebounds defined by local minima within plus and minus 200 days around them. Note that these rebounds are the historical "change of regime" rather than only the jump-like reversals. The jump-like reversals, 1972, 1974 as examples, are included in these rebounds. They are located near clusters of high values of the rebound alarm index of the upper figure.

With this feature qualification, the rebound alarm index can distinguish rebounds with high significance. If the first number α is too big and the second number β is too small, then the total number of Class I features will be very small and the number of features in Class II will be large. This makes the rebound alarm index always close to 0. In contrast, if α is too small and β is too large, the rebound alarm index will often be close to 1. Neither of these cases, then, is qualified to be a good rebound alarm index to indicate the start of the next rebound. However, the absolute values of feature qualification pair are not very sensitive within a large range. Only the ratio α/β plays an important role. Fig. 4.4–4.7 show that varying α and β in the intervals $10 \le \alpha \le 20$ and $200 \le \beta \le 1000$ does not change the result much. For the sake of conciseness, only the rebound alarm index of feature qualification pair $(10, 200)$ is shown in this paper.
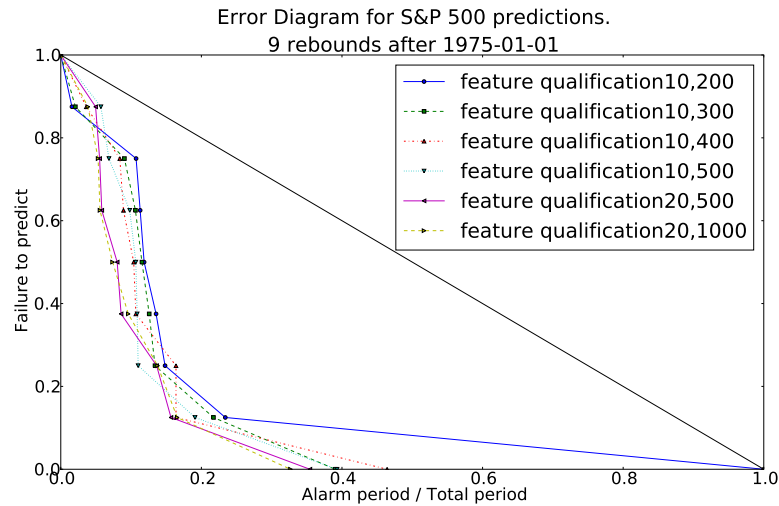

Figure 4.4: Error diagram for predictions after Jan. 1, 1975 with different types of feature qualifications. Feature qualification α, β means that, if the occurrence of a certain trait in Class I is larger than α and less than β, then we call this trait a feature of Class I and vice versa. See text for more information.

Predictions

Once we generate the Class I and II features of the learning set for values of t_c before t_p (Jan. 1, 1975), we then use these features to generate the predictions on the data after t_p. Recall that the windows that we fit are defined such that the end time t_2 increases 50 days from one window to the next. Also note that all predictions
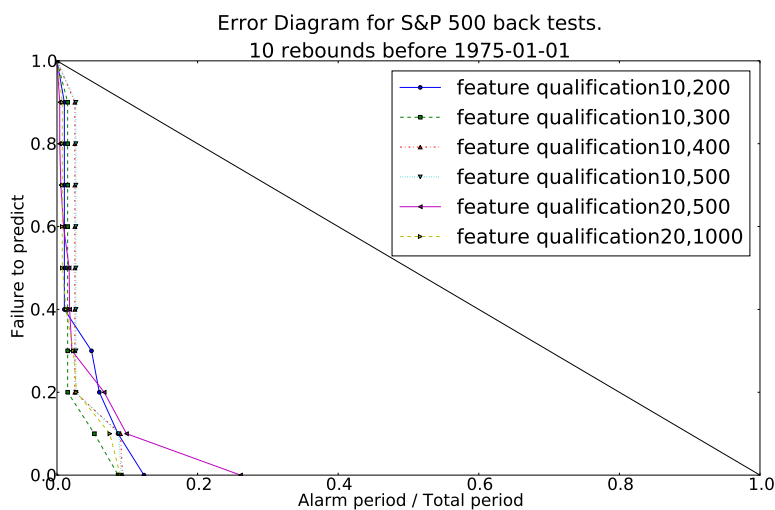
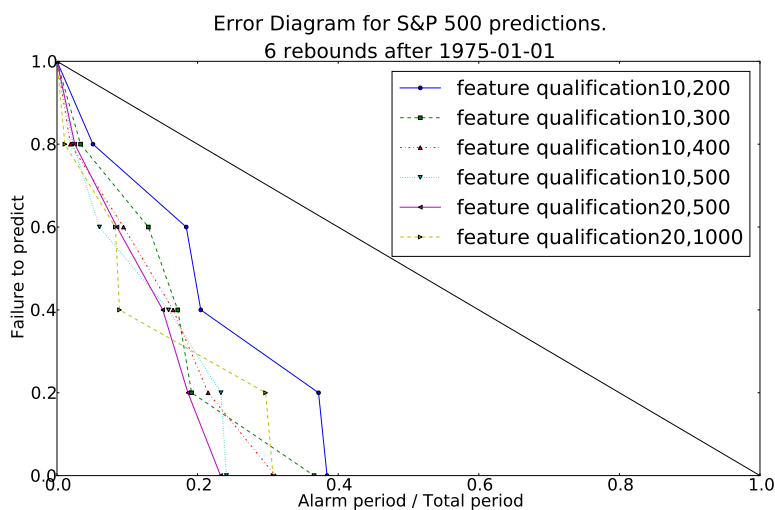Figure 4.5: Same as Fig. 4.4 but for the learning set before Jan. 1, 1975.

Figure 4.6: Same as Fig. 4.4 but with the different definition of a rebound determined as the day with the smallest price within the 365 days before it and the 365 days after it.
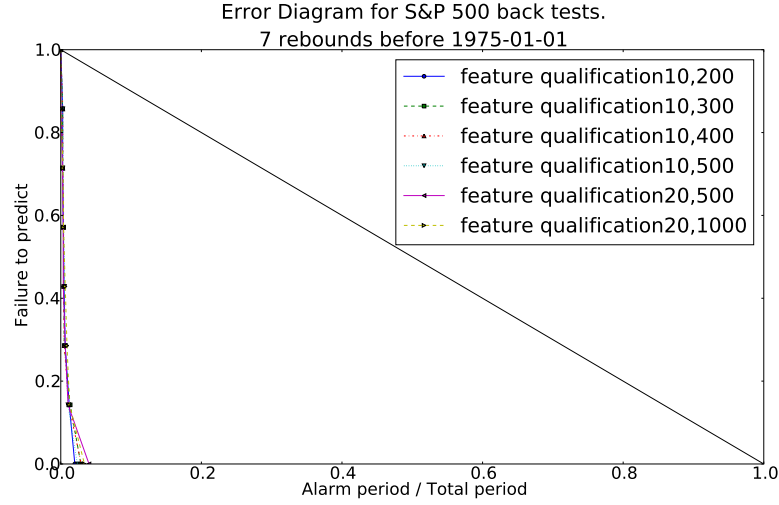
Figure 4.7: Same as Fig. 4.6 for the learning set before Jan. 1, 1975.

made on days between these 50 days will be the same because there is no new fit information between, say, t_2^n and t_2^{n-1}.

Assume that we make a prediction at time t:

$$t \in (t_2, t_2 + 50], \quad t > t_p \tag{4.23}$$

Then the fits set $\Sigma_{t_2} = \{f \mid t_{2,f} \leq t_2\}$ is made using the past information before prediction day t. We use Σ_{t_2} as the subset Σ_{sub} mentioned in Sec. 4.1.3 to generate the questionnaire on day t and the traits for this questionnaire. Comparing these traits with features F_I and F_{II} allows us to generate a rebound alarm index RI_t using the same method as described in Sec. 4.1.4.

Using this technique, the prediction day t_2 is scanned from 1975-01-01 until 2009-07-22 in steps of 50 days. We then construct the time series of the *rebound alarm index* over this period and with this resolution of 50 days. The comparison of this rebound alarm index with the historical financial index (Fig. 4.8) shows a good correlation, but there are also some false positive alarms (1977, 1998, 2006), as well as some false negative missed rebounds (1990). Many false positive alarms such as in 1998 and 2006 are actually associated with rebounds. But these rebounds have smaller amplitudes than our qualifying threshold targets. Concerning the false negative (missed rebound) in 1990, the explanation is probably that the historical prices preceding this rebound does not follow the JLS model specification. Rebounds

may result from several mechanisms and the JLS model only provides one of them, arguably the most important. Overall, the predictability of the rebound alarm index shown in Fig. 4.8, as well as the relative cost of the two types of errors (false positives and false negatives) can be quantified systematically, as explained in the following sections. The major conclusion is that the rebound alarm index has a prediction skill much better than luck, as quantified by error diagrams.
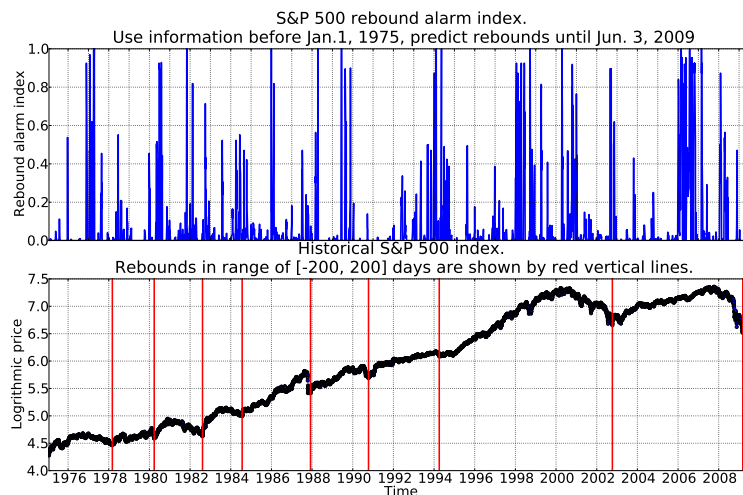

Figure 4.8: Rebound alarm index and log-price of S&P 500 Index for the predicting set after Jan. 1, 1975. (upper) Rebound alarm index for predicting set using feature qualification pair $(10, 200)$. The rebound alarm index is in the range [0,1]. The higher the rebound alarm index, the more likely is the occurrence of a rebound. (lower) Plot of $\ln p(t)$ versus time of the S&P Index. Red vertical lines indicate rebounds defined by local minima within in plus and minus 200 days. They are located near clusters of high values of the rebound alarm index of the upper figure.

Error Diagram

We have qualitatively seen that the feature qualifications method using back testing and forward prediction can generate a rebound alarm index that seems to detect and predict well observed rebounds in the S&P 500 index. We now quantify the quality of these predictions with the use of error diagrams [133, 134]. We create an error diagram for predictions after 1975-01-01 with a certain feature qualification in the following way:

1. Count the number of rebounds after 1975-01-01 as defined in Sec. 4.2.1 and expression (4.33). There are 9 rebounds.

2. Take the rebound alarm index time series (after 1975-01-01) and sort the set of all alarm index values in decreasing order. There are 12,600 points in this series and the sorting operation delivers a list of 12,600 index values, from the largest to the smallest one.

3. The largest value of this sorted series defines the first threshold.

4. Using this threshold, we declare that an alarm starts on the first day that the unsorted rebound alarm index time series exceeds this threshold. The duration of this alarm D_a is set to 41 days, since the longest distance between a rebound and the day with index greater than the threshold is 20 days. Then, a prediction is deemed successful when a rebound falls inside that window of 41 days.

5. If there are no successful predictions at this threshold, move the threshold down to the next value in the sorted series of alarm index.

6. Once a rebound is predicted with a new value of the threshold, count the ratio of unpredicted rebounds (unpredicted rebounds / total rebounds in set) and the ratio of alarms used (duration of alarm period / 12,600 prediction days). Mark this as a single point in the error diagram.

In this way, we will mark 9 points in the error diagram for the 9 rebounds.

The aim of using such an error diagram in general is to show that a given prediction scheme performs better than random. A random prediction follows the line $y = 1 - x$ in the error diagram. A set of points below this line indicates that the prediction is better than randomly choosing alarms. The prediction is seen to improve as more error diagram points are found near the origin (0, 0). The advantage of error diagrams is to avoid discussing how different observers would rate the quality of predictions in terms of the relative importance of avoiding the occurrence of false positive alarms and of false negative missed rebounds. By presenting the full error diagram, we thus sample all possible preferences and the unique criterion is that the error diagram curve be shown to be statistically significantly below the anti-diagonal $y = 1 - x$.

In Fig. 4.4, we show error diagrams for different feature qualification pairs (α, β). Note the 9 points representing the 9 rebounds in the prediction set. We also plot

the 11 points of the error diagrams for the learning set in Fig. 4.5.

As a different test of the quality of this pattern recognition procedure, we repeated the entire process but with a rebound now defined as the minimum price within a window of 2×365 days[3] instead of 2×200 days, as before. These results are shown in Fig. 4.6–4.7.

Bayesian inference

Given a value of the *predictive* rebound alarm index, we can also use the *historical* rebound alarm index combined with Bayesian inference to calculate the probability that this value of the rebound alarm index will actually be followed by a rebound. We use predictions near the end of November, 2008 as an example. From Fig. 4.8, we can see there is a strong rebound signal in that period. We determine if this is a true rebound signal by the following method:

1. Find the highest rebound alarm index Lv around the end of November 2008.

2. Calculate D_{total}, the number of days in the interval from 1975-01-01 until the end of the prediction set, 2009-07-22.

3. Calculate D_{Lv}, the number of days which have a rebound alarm index greater than or equal to Lv.

4. The probability that the rebound alarm index is higher than Lv is estimated by

$$P(RI \geq Lv) = \frac{D_{Lv}}{D_{total}} \tag{4.24}$$

5. The probability of a day being near the bottom of a rebound is estimated as the number of days near real rebounds over the total number of days in the predicting set:

$$P(rebound) = \frac{D_{rw}N_{rebound}}{D_{total}}, \tag{4.25}$$

where $N_{rebound}$ is the number of rebounds we can detect after 1975-01-01 and D_{rw} is the rebound width, i.e. the number of days near the real rebound

---

[3]seven rebounds in the back tests before 1975.1.1: 1953-09-14; 1957-10-22; 1960-10-25; 1962-06-26; 1966-10-07; 1970-05-26; 1974-10-03, and six rebounds after 1975.1.1 in the prediction range: 1978-03-06; 1982-08-12; 1987-12-04; 1990-10-11; 2002-10-09; 2009-03-09.

in which we can say that this is a successful prediction. For example, if we say that the prediction is good when the predicted rebound time and real rebound time are within 10 days of each other, then the rebound width $D_{rw} = 10 \times 2 + 1 = 21$.

6. The probability that the neighbor of a rebound has a rebound alarm index larger than Lv is estimated as

$$P(RI \geq Lv | rebound) = \frac{N_0}{N_{rebound}} \qquad (4.26)$$

where N_0 is the number of rebounds in which

$$\sup_{|d-rebound| \leq 20} RI_d \geq Lv. \qquad (4.27)$$

7. Given that the rebound alarm index is higher than Lv, the probability that the rebound will happen in this period is given by Bayesian inference:

$$P(rebound | RI \geq Lv) = \frac{P(rebound) \times P(RI \geq Lv | rebound)}{P(RI \geq Lv)} \qquad (4.28)$$

Averaging $P(rebound | RI \geq Lv)$ for all the different feature qualifications gives the probability that the end of November 2008 is a rebound as 0.044. By comparing with observations, we see that this period is not a rebound. We obtain a similar result by increasing the definition of rebound from 200 days before and after a local minimum to 365 days, yielding a probability of 0.060.

When we *decrease* the definition to 100 days, the probability that this period is a rebound jumps to 0.597. The reason for this sudden jump is shown in Fig. 4.9 where we see the index around this period and the S&P 500 index value. From the figure, we find that this period is a local minimum within 100 days, not more. This is consistent with what Bayesian inference tells us. However, we have to address that the more obvious rebound in March 2009 is missing in our rebound alarm index. Technically, one can easily find that this is because the end of crash is not consistent with the beginning of rebound in this special period.

In this case, we then test all the days after 1985-01-01 systematically by Bayesian inference using only prediction data (rebound alarm index) after 1975-01-01. To show that the probability that $RI \geq Lv$ is stable, we cannot start Bayesian inference too close to the initial predictions so we choose 1985-01-01 as the beginning time.
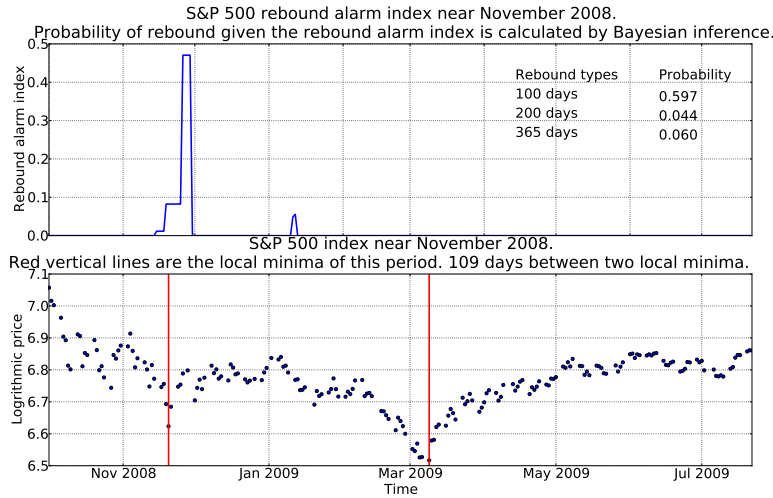
Figure 4.9: Rebound alarm index and market price near and after November 2008.

We have 5 'bottoms' (troughs) after this date, using the definition of a minimum within ±200 days.

For a given day d after 1985-01-01, we know all values of the rebound alarm index from 1975-01-01 to that day. Then we use this index and historical data of the asset price time series in this time range to calculate the probability that d is the bottom of the trough, given that the rebound alarm index is larger than Lv, where Lv is defined as

$$Lv = \sup_{d-t<50} RI_t \tag{4.29}$$

To simplify the test, we only consider the case of feature qualification pair (10, 200), meaning that the trait is a feature of Class I only if it shows in Class I more than 10 times and in Class II less than 200 times. Fig. 4.10 shows that the actual rebounds occur near the local highest probability of rebound calculated by Bayesian inference. This figure also illustrates the existence of false positive alarms, i.e., large peaks of the probability not associated with rebounds that we have characterized unambiguously at the time scale of ±200 days.

4.1.5 Trading strategy

In order to determine if the predictive power of our method provides a genuine and useful information gain, it is necessary to estimate the excess return it could
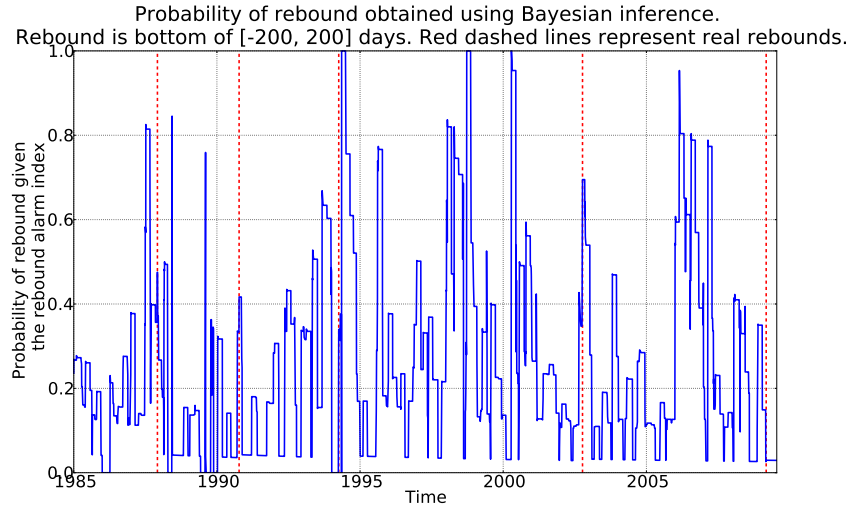
Figure 4.10: Probability of rebound as a function of time t, given the value of the rebound alarm index at t, derived by Bayesian inference applied to bottoms at the time scale of ± 200 days. The feature qualification is (10, 200). Lv is the largest rebound index in the past 50 days. The vertical red lines show the locations of the realized rebounds in the history of the S&P500 index.

generate. The excess return is the real return minus the risk free rate transformed from annualized to the duration of this period. The annualized 3-month US treasury bill rate is used as the risk free rate in this paper. We thus develop a trading strategy based on the rebound alarm index as follows. When the rebound alarm index rises higher than a threshold value Th, then with a lag of Os days, we buy the asset. This entry strategy is complemented by the following exit strategy. When the rebound alarm index goes below Th, we still hold the stock for another Hp days, with one exception. Consider the case that the rebound alarm index goes below Th at time t_1 and then rises above Th again at time t_2. If $t_2 - t_1$ is smaller than the holding period Hp, then we continue to hold the stock until the next time when the rebound alarm index remains below Th for Hp days.

The performance of this strategy for some fixed values of the parameters is compared with random strategies, which share all the properties except for the timing of entries and exits determined by the rebound alarm index and the above rules. The random strategies consist in buying and selling at random times, with the constraint that the total holding period (sum of the holding days over all trades in a given strategy) is the same as in the realized strategy that we test. Implementing

	Strategy I	Strategy II
Threshold Th	0.2	0.7
Offset Os	10	30
Holding period Hp	10	10
Number of trades	77	38
Success rate		
(fraction of trades with positive return)	66.2%	65.8%
Total holding days	1894 days	656 days
Fraction of time when invested	15.0%	5.2%
Cumulated log-return	95%	45%
cumulated excess log-return	67%	35%
Average return per trade	1.23%	1.19%
Average trade duration	24.60 days	17.26 days
p-value of cumulative excess return	0.055	0.058
Sharpe ratio per trade	0.247	0.359
Sharpe ratio of random trades		
(holding period equals average trade duration)	0.025	0.021
p-value of Sharpe ratio	0.043	0.036
Bias ratio	1.70	1.36
Bias ratio of random trades		
(holding period equals average trade duration)	1.27	1.25
p-value of bias ratio	0.105	0.309

Table 4.2: Performances of two strategies: Strategy I ($Th = 0.2, Os = 10, Hp = 10$) and Strategy II ($Th = 0.7, Os = 30, Hp = 10$).

1000 times these constrained random strategies with different random number realizations provide the confidence intervals to assess whether the performance of our strategy can be attributed to real skill or just to luck.

Results of this comparison are shown in Tab. 4.2 for two sets of parameter values. The p-value is a measure of the strategies' performance, calculated as the fraction of corresponding random strategies that are better than or equal to our strategies. The lower the p-value is, the better the strategy is compared to the random portfolios. We see that all of our strategies' cumulative excess returns are among the top 5-6% out of 1000 corresponding random strategies' cumulative excess returns. Box plots for each of the strategies are also presented in Fig. 4.11–4.12.

The cumulative returns as well as the cumulative excess returns obtained with the two strategies as a function of time are shown in Fig. 4.13–4.14. These results
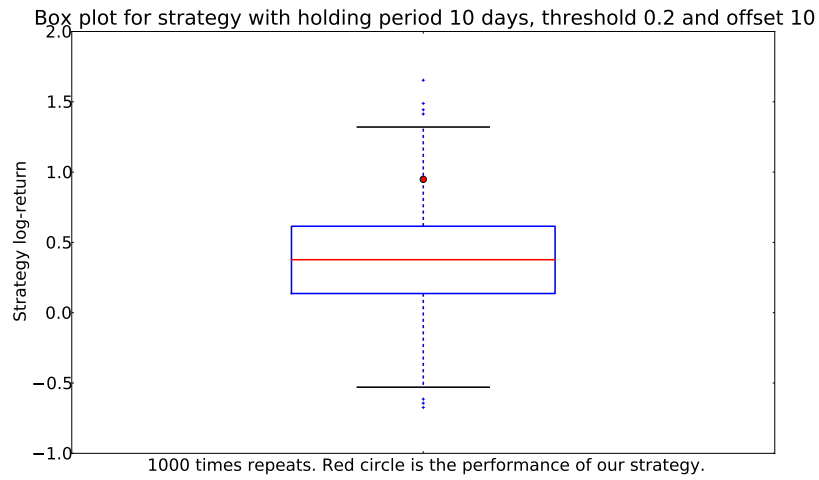
Figure 4.11: Box plot for Strategy I ($Th = 0.2, Os = 10, Hp = 10$). Lower and upper horizontal edges (blue lines) of box represent the first and third quartiles. The red line in the middle is the median. The lower and upper black lines are the 1.5 inter-quartile range away from quartiles. Points between quartiles and black lines are outliers and points out of black lines are extreme outliers. Our strategy return is marked by the red circle. This shows our strategy is an outlier among the set of random strategies. The log-return ranked 55 out of 1000 random strategies.
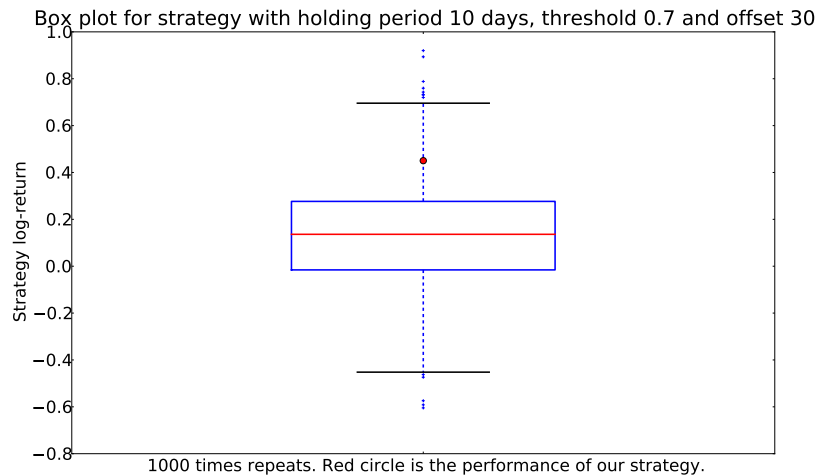

Figure 4.12: Same as Fig. 4.11 for Strategy II ($Th = 0.7, Os = 30, Hp = 10$). The log-return ranked 58 out of 1000 random strategies.

suggest that these two strategies would provide significant positive excess return. Of course, the performance obtained here are smaller than the naive buy-and-hold strategy, consisting in buying at the beginning of the period and just holding the position. The comparison with the buy-and-hold strategy would be however unfair as our strategy is quite seldom invested in the market. Our goal here is not to do better than any other strategy but to determine the statistical significance of a specific signal. For this, the correct method is to compare with random strategies that are invested in the market the same fraction of time. It is obvious that we could improve the performance of our strategy by combining the alarm indexes of bubbles and of negative bubbles, for instance, but this is not the goal here.
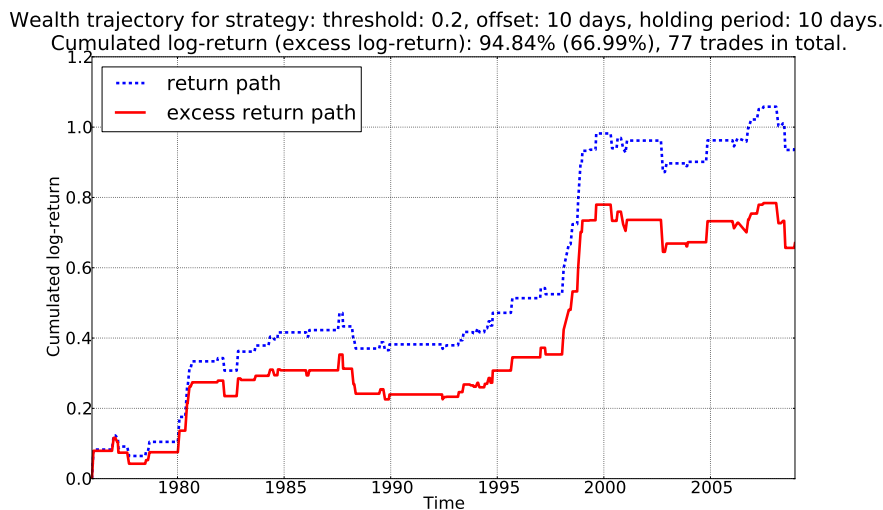

Figure 4.13: Wealth trajectory for Strategy I ($Th = 0.2, Os = 10, Hp = 10$). Major performance parameters of this strategy are: 77 trading times; 66.2% trades have positive return; 1894 total holding days, which is 15.0% of total time. Accumulated log-return is 95% and average return per trade is 1.23%. Average trade length is 24.60 days. P-value of this strategy is 0.055

We also provide the Sharpe ratio as a measure of the excess return (or risk premium) per unit of risk. We define it per trade as follows

$$S = \frac{E[R - R_f]}{\sigma} \tag{4.30}$$

where R is the return of a trade, R_f is the risk free rate (we use the 3-month US treasury bill rate) transformed from annualized to the duration of this trade given in Tab. 4.2 and σ is the standard deviation of the returns per trade. The higher the
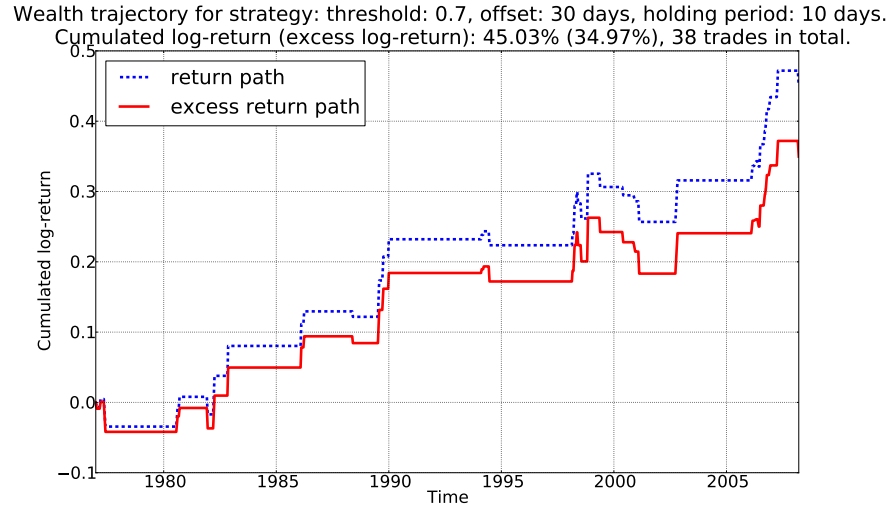
Wealth trajectory for strategy: threshold: 0.7, offset: 30 days, holding period: 10 days.
Cumulated log-return (excess log-return): 45.03% (34.97%), 38 trades in total.

Figure 4.14: Wealth trajectory for Strategy II ($Th = 0.7, Os = 30, Hp = 10$). Major performance parameters of this strategy are: 38 trading times; 65.8% trades have positive return; 656 total holding days, which is 5.2% of total time. Accumulated log-return is 45% and average return per trade is 1.19%. Average trade length is 17.26 days. P-value of this strategy is 0.058

Sharpe ratio is, the higher the excess return under the same risk.

The bias ratio is defined as the number of trades with a positive return within one standard deviation divided by one plus the number of trades which have a negative return within one standard deviation:

$$BR = \frac{\#\{r | r \in [0, \sigma]\}}{1 + \#\{r | r \in [-\sigma, 0)\}} \tag{4.31}$$

In Eq. (4.31), r is the excess return of a trade and σ is the standard deviation of the excess returns. This ratio detects valuation bias.

To see the performance of our strategies, we also check all the possible random trades with a holding period equals to the average duration of our strategies, namely 25 days and 17 days for strategy I and II respectively. The average Sharpe and bias ratios of these random trades are shown in Tab. 4.2. Both Sharpe and bias ratios of our strategies are greater than those of the random trades, confirming that our strategies deliver a larger excess return with a stronger asymmetry towards positive versus negative returns.

As another test, we select randomly the same number of random trades as in our strategies, making sure that there is no overlap between the selected trades.

We calculate the Sharpe and bias ratios for these random trades. Repeating this random comparative selection 1000 times provides us with p-values for the Sharpe ratio and for bias ratio of our strategies. The results are presented in Tab. 4.2. All the p-values are found quite small, confirming that our strategies perform well.

4.1.6 Conclusion

We have developed a systematic method to detect rebounds in financial markets using "negative bubbles," defined as the symmetric of bubbles with respect to a horizontal line, i.e., downward accelerated price drops. The aggregation of thousands of calibrations in running windows of the negative bubble model on financial data has been performed using a general pattern recognition method, leading to the calculation of a rebound alarm index. Performance metrics have been presented in the form of error diagrams, of Bayesian inference to determine the probability of rebounds and of trading strategies derived from the rebound alarm index dynamics. These different measures suggest that the rebound alarm index provides genuine information and suggest predictive ability. The implemented trading strategies outperform randomly chosen portfolios constructed with the same statistical characteristics. This suggests that financial markets may be characterized by transient positive feedbacks leading to accelerated drawdowns, which develop similarly to but as mirror images of upward accelerating bubbles. Our key result is that these negative bubbles have been shown to be predictably associated with large rebounds or rallies.

In summary, we have expanded the evidence for the possibility to diagnose bubbles before they terminate [65], by adding the phenomenology and modeling of "negative bubbles" and their anticipatory relationship with rebounds. The present paper contributes to improving our understanding of the most dramatic anomalies exhibited by financial markets in the form of extraordinary deviations from fundamental prices (both upward and downward) and of extreme crashes and rallies. Our results suggest a common underlying origin to both positive and negative bubbles in the form of transient positive feedbacks leading to identifiable and reproducible faster-than-exponential price signatures.

4.2   Detection of Crashes and Rebounds in Major Equity Markets

To test this idea and to implement a systematic forecast procedure based on the JLS model, Zhou and Sornette adapted a pattern recognition method to detect bubbles and crashes [94]. This method was originally developed by the famous mathematician I. M. Gelfand and his collaborators in 1975 [130], when they were trying to predict the earthquake in California. Since then, this method has been widely used in many kinds of predictions ranges from uranium prospecting [135] to unemployment rate [136]. Yan, Woodard and Sornette [95, 96] extended this method to negative bubbles and rebounds of financial markets, which is the content of Sec. 4.1. They also improved the method in [94] by separating the learning period and prediction period to enable a pure causal prediction.

Since the study in Sec. 4.1 only tested for rebounds in one major index (S&P 500), in this section we expand to ten major global equity markets using the pattern recognition method to detect and forecast crashes and rebounds. Our results indicate that the performance of the predictions on both crashes and rebounds for most of the indices is better than chance. That is, the end of large drawdowns and the subsequent rebounds can be successfully forecast. To demonstrate this, we design a simple trading strategy and show that it out-performs a simple buy-and-hold benchmark.

The structure of the paper is as follows: We present the pattern recognition method for the prediction of crashes and rebounds in Sec. 4.2.1. This method is the same as the one presented in Sec. 4.1.3. However, the introduction of this method in this section is a short and visible version, which can be easier understood by the readers. The quality of the prediction is tested in Sec. 4.2.2 using error diagrams to compare missed events versus total alarm time. We next introduce the trading strategy based on the alarm index and test its performance in Sec. 4.2.3. We summarize our results and conclude in Sec. 4.2.4.

4.2.1   Prediction Method

We adapt the pattern recognition method of Gelfand et al. [130] to generate predictions of crashes and rebound times in financial markets on the basis of the detection

and calibration of bubbles and negative bubbles. The prediction method used here is basically that used to detect rebounds in [95] but we now use it to detect both crashes and rebounds at the same time. Here we give a brief summary of the method, which is decomposed into five steps.

Fit the time series with the JLS model

Given a historical price time series of an index (such as the S&P 500 or the Dow Jones Industrial Average, for example), we first divide it into different sub-windows (t_1, t_2) of length $dt \equiv t_2 - t_1$ according to the following rules:

1. The earliest start time of the windows is t_{10}. Other start times t_1 are calculated using a step size of $dt_1 = 50$ calendar days.

2. The latest end time of the windows is t_{20}. Other end times t_2 are calculated with a negative step size $dt_2 = -50$ calendar days.

3. The minimum window size $dt_{\min} = 110$ calendar days.

4. The maximum window size $dt_{\max} = 1500$ calendar days.

For each sub-window generated by the above rules, the log of the index is fit with the JLS Eq. (2.9). The fitting procedure is a combination of a preliminary heuristic selection of the initial points and a local minimizing algorithm (least squares). The linear parameters are slaved by the nonlinear parameters before fitting. Details of the fitting algorithm can be found in [95, 47]. We keep the best 10 parameter sets for each sub-window and use these parameter sets as the input to the pattern recognition method.

Definition of crash and rebound

We refer to a crash as 'Crh' and to a rebound as 'Rbd'. A day d begins a crash (rebound) if the price on that day is the maximum (minimum) price in a window of 100 days before and 100 days after. That is,

$$\text{Crh} = \{d \mid P_d = \max\{P_x\}, \forall x \in [d - 100, d + 100]\} \tag{4.32}$$

$$\text{Rbd} = \{d \mid P_d = \min\{P_x\}, \forall x \in [d - 100, d + 100]\} \tag{4.33}$$

where P_d is the adjusted closing price on day d. Our task is to diagnose such crashes and rebounds in advance. We could also use other windows instead of ± 100 to define

a rebound. The results are stable with respect to a change of this number because we learn from the 'learning set' with a certain rebound window width and then try to predict the rebounds using the same window definition. The reference [95] shows the results for ±200-days and ±365-days type of rebounds.

Learning set, class, group and informative parameter

As described above, we obtain a set of parameters that best fit the model Eq. (2.9) for each window. Then we select a subset of the whole set which only contains the fits of crashes and rebounds with critical times found within the window (that is, where parameter t_c is *not* calculate to be beyond the window bounds). We learn the properties of historical rebounds from this set and develop the predictions based on these properties. We call this set the *learning set*. In this paper, a specific day for each index is chosen as the 'present time' (for backtesting purposes). All the fit windows before that day will be used as the learning set and all the fit windows after that will be used as the *testing set*, in which we will predict future rebounds. The quality of the predictability of this method can be quantified by studying the predicted results in the testing set using only the information found in the learning set.

Each of the sub-windows generated by the rules in Sec. 4.2.1 will be assigned one of two *classes* and one of 14 *groups*. Classes indicate how close the modeled critical time t_c is to a historical crash or rebound, where Class I indicates 'close' and Class II indicates 'not close' ('close' will be defined below as a parameter). Groups of windows have similar window widths. For each fit, we create a set of six parameters: m, ω, ϕ and B from Eq. (2.9), b from Eq. (2.11) and q as the residual of the fit. We will compare the probability density functions (pdf) of these parameters among the different classes and groups. The main goal of this technique is *to identify patterns of parameter pdf's that are different between windows with crashes or rebounds and windows without crashes or rebounds.* Given such a difference and a new, out-of-sample window, we can probabilistically state that a given window will or will not end in a crash or rebound.

A figure is very helpful for understanding these concepts. We show the selection of the sub-windows and sort the fits by classes and groups in Fig. 4.15. Then we create the pdf's of each of these parameters for each fit and define *informative*

parameters as those parameters for which the pdf's differ significantly according to a Kolmogorov-Smirnov test. For each informative parameter, we find the regions of the abscissa of the pdf for which the Class I pdf (fits with t_c close to an extreme) is greater than the Class II pdf. This procedure has been performed in Fig. 4.16.
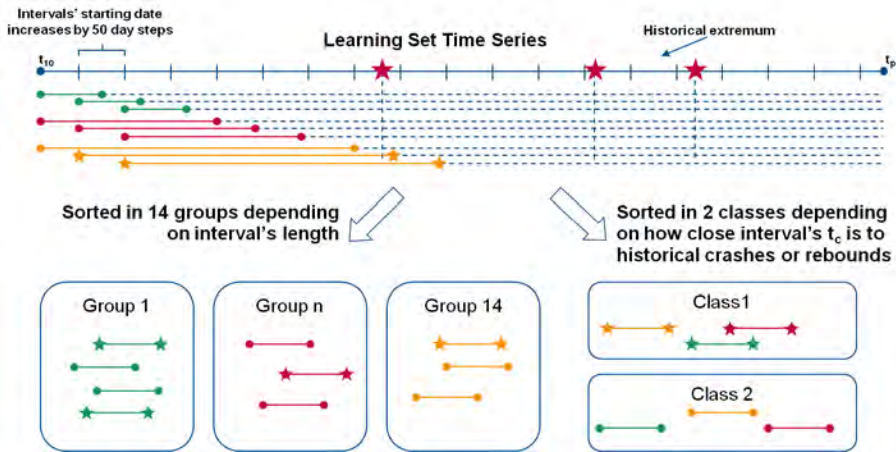

Figure 4.15: Step one of pattern recognition procedure: Create sub-windows, fit each window with the JLS model. Classify the fits in groups and classes.
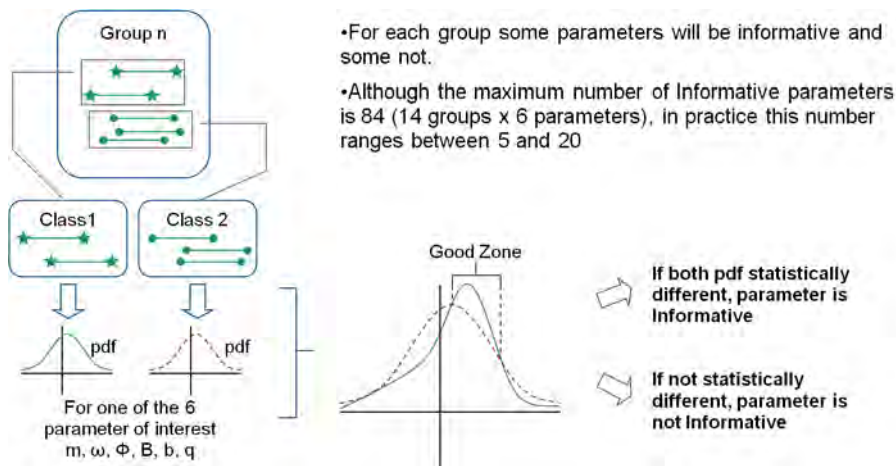

Figure 4.16: Step two of pattern recognition procedure: For each group compare fits in class I with those in class II and find out the informative parameters.

Questionnaires, traits and features

Using the informative parameters and their pdf's described above, we can generate a *questionnaire* for each day of the learning or testing set. A questionnaire is a quantitative inquiry into whether or not a set of parameters is likely to indicate a

bubble or negative bubble. Questionnaires will be used to identify bubbles (negative bubbles) which will be followed by crashes (rebounds). In short, the length of a questionnaire tells how many informative parameters there are for a given window size. An informative parameter implies that the pdf's of that parameter are very different for windows with a crash/rebound than windows without. The more values of '1' in the questionnaire, the more likely it is that the parameters are associated with a crash/rebound.

One questionnaire is constructed for each day t_{scan} in our learning set. We first collect all the fits which have a critical time near that day ('near' will be defined). Then we create a string of bits whose length is equal to the number of informative parameters found. Each bit can take a value -1, 0 or 1 (a balanced ternary system). Each bit represents the answer to the question: are more than half of the collected fits more likely to be considered as Class I? If the answer is 'yes', we assign 1 in the bit of the questionnaire corresponding to this informative parameter. Otherwise, we assign 0 when the answer cannot be determined or -1 when the answer is 'no'. A visual representation of this questionnaire process is shown in Fig. 4.17.
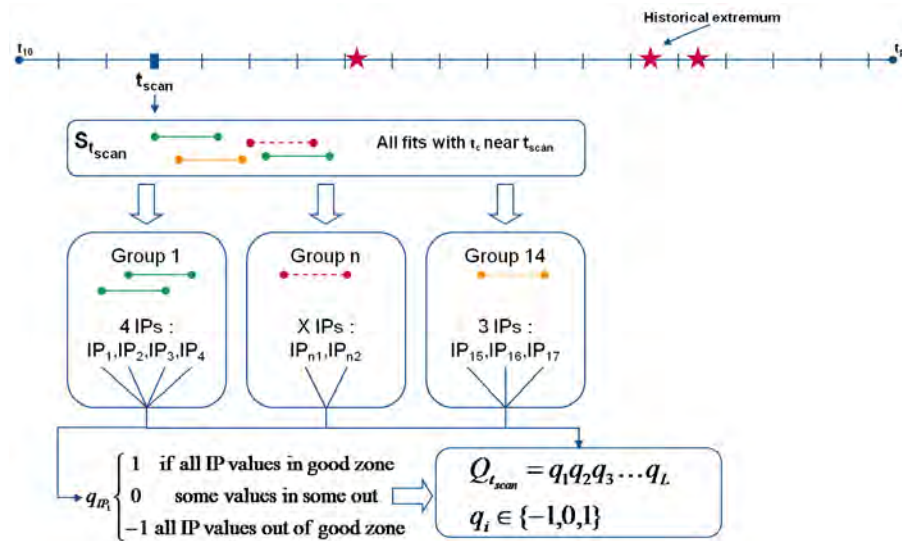

Figure 4.17: Step three of pattern recognition procedure: Generate the questionnaire for each trading day.

The concept of a *trait* is developed to describe the property of the questionnaire for each t_{scan}. Each questionnaire can be decomposed into a fixed number of traits if the length of the questionnaire is fixed. We will not give the details in how the traits

are generated in this paper. For a clear explanation of the method, please refer to Sec. 3.9 of the reference [95]. Think of a trait as a sub-set (like the 'important' short section from a very long DNA sequence) of a fixed-length questionnaire that is usually found in windows that show crashes/rebounds. Conversely, a trait can indicate windows where a crash/rebound is not found.

Assume that there are two sets of traits T_I and T_{II} corresponding to Class I and Class II, respectively. Scan day by day the date t before the last day of the learning set. If t is 'near' an extreme event (crash or rebound), then all traits generated by the questionnaire for this date belong to T_I. Otherwise, all traits generated by this questionnaire belong to T_{II}. 'Near' is defined as at most 20 days away from an extreme event. The same definition will be used later in Sec. 4.2.2 when we introduce the error diagram.

Using this threshold, we declare that an alarm starts on the first day that the unsorted crash alarm index time series exceeds this threshold. The duration of this alarm D_a is set to 41 days, since the longest distance between a crash and the day with index greater than the threshold is 20 days.

Count the frequencies of a single trait τ in T_I and T_{II}. If τ is in T_I for more than α times and in T_{II} for less than β times, then we call this trait τ a *feature* F_I of Class I. Similarly, if τ is in T_I for less than α times and in T_{II} for more than β times, then we call τ a *feature* F_{II} of Class II. The pair (α, β) is defined as a *feature qualification*. Fig. 4.18 shows the generation process of traits and features. We would like to clarify that by definition some of the traits are not from any type of feature since they are not 'extreme' and we cannot extract clear information from them.

Alarm index

The final piece in our methodology is to define an *alarm index* for both crashes and rebounds. An alarm index is developed based on features to show the probability that a certain day is considered to be a rebound or a crash. We first collect all the fits which have a predicted critical time near this specific day and generate questionnaires and traits from these fits. The rebound (crash) alarm index for a certain day is just a ratio quantified by the total number of traits from feature type F_I (a set of traits which have high probability to represent rebound (crash)) divided
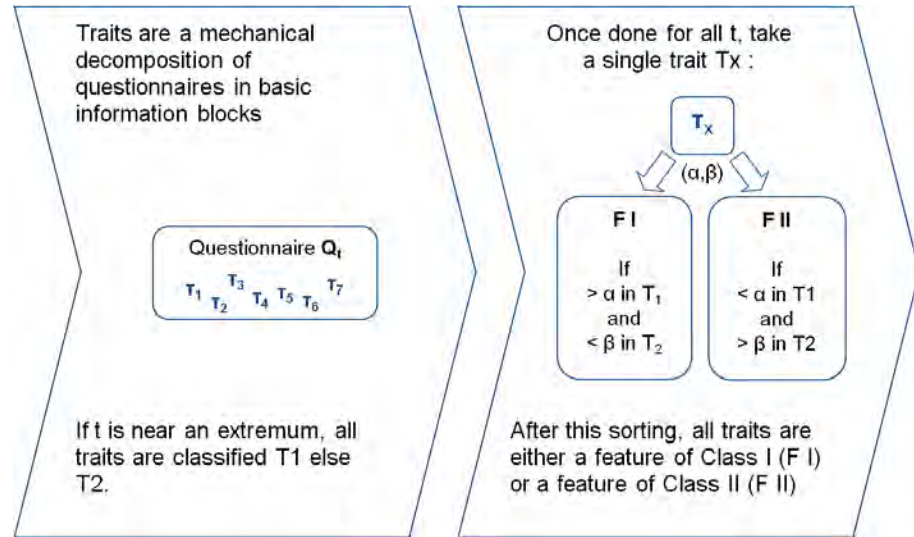
Figure 4.18: Step four of pattern recognition procedure: Create traits from questionnaires. Obtain features for each class by traits statistics.

by the total number of traits from both F_I and F_{II}. Note that F_{II} is a set of traits which have low probability to represent rebound (crash). The principles for the generation of the alarm index are summarized in Fig. 4.19.

Two types of alarm index are developed. One is for the back tests in the learning set, as we have already used the information before this time to generate informative parameters and features. The other alarm index is for the prediction tests. We generate this prediction alarm index using only the information before a certain time and then try to predict crashes and rebounds in the 'future'.

4.2.2   Prediction in major equity markets

We perform systematic detections and forecasts on both the market crashes and rebounds for 10 major global equity markets using the method we discussed in Sec. 4.2.1. The 10 indices are S&P 500 (US), Nasdaq composite (US), Russell 2000 (US), FTSE 100 (UK), CAC 40 (France), SMI (Switzerland), DAX (German), Nikkei 225 (Japan), Hang Seng (Hong Kong) and ASX (Australia). The basic information for these indices used in this study is listed in Tab. 4.3. Due to space constraints, we cannot show all results for these 10 indices here. The complete results for three indices from different continents are shown in this paper. They are Russell 2000 (America), SMI (Europe) and Nikkei 225 (Asia). Partial results for the remaining
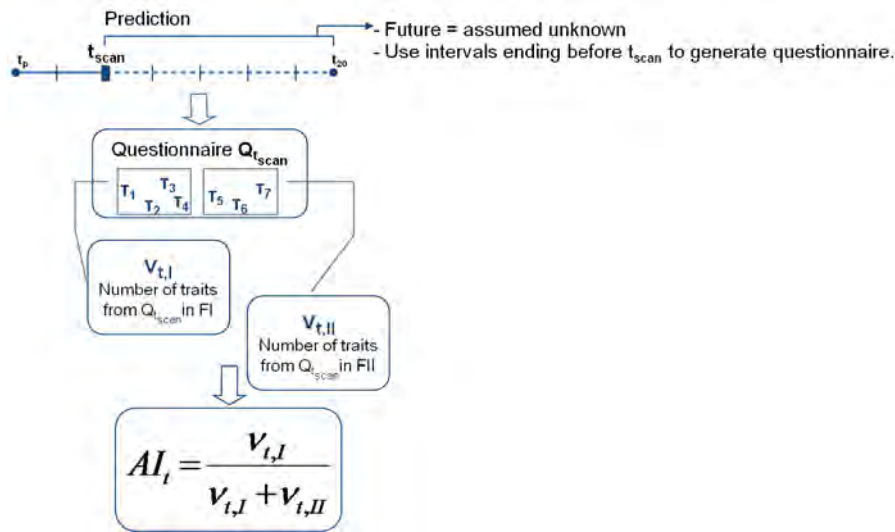
Figure 4.19: Step five of pattern recognition procedure: Construct the alarm index for each day by decomposing the questionnaire into traits for that day and compare these traits to the features of each class.

indices are shown in Tab. 4.4, which will be discussed in details later in Sec. 4.2.3.

The alarm index depends on the features which are generated using information from the learning set. Thus, the alarm index before the end of the learning set uses 'future' information. That is, the value of the alarm index on a certain day t_0 in the learning set uses prices found at $t > t_0$ to generate features. The feature definitions from the learning set are then used to define the alarm index in the *testing* set using *only* past prices. That is, the value of the alarm index on a certain day t_0 in the *testing* set uses only prices found at $t \leq t_0$ in the testing set (and the *definitions* of features found in the *learning* set). We do not use 'future' information in the testing set. In this case, the alarm index predicts crashes and rebounds in the market.

The crash and the rebound alarm index for Russell 2000, SMI and Nikkei are shown in Fig. 4.20–4.25. Fig. 4.20–4.22 show the back testing results for these three indices and Fig. 4.23–4.25 present the prediction results. In all of these results, the feature qualification pair $(7, 100)$ is used. This means that a certain trait must appear in trait Class I (crash or rebound) at least 7 times *and* must appear in trait Class II (no crash or rebound) less than 100 times. If so, then we say that this trait is a feature of Class I. If, on the other hand, the trait appears 7 times or less in Class I *or* appears 100 times or more in Class II, then this trait is a feature of

Class II. Tests on other feature qualification pairs are performed also. Due to the space constraints, we do not show the alarm index constructed by other feature qualification pairs here, but later we will present the predictability of these alarm indices by showing the corresponding error diagrams. In the rest of this paper, if we do not mention otherwise, we use $(7, 100)$ as the feature qualification pair.
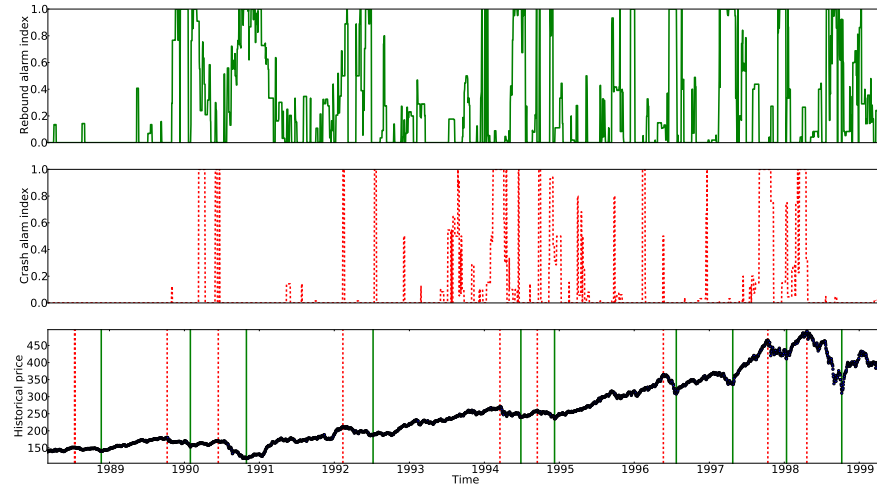

Figure 4.20: Alarm index and log-price of the Russell 2000 Index for the *learning* set, where the end date is 17-Apr-1999. (upper) Rebound alarm index for the learning set using feature qualification pair $(7, 100)$. The rebound alarm index is in the range $[0, 1]$. The higher the rebound alarm index, the more likely is the occurrence of a rebound. (middle) Crash alarm index for the learning set using feature qualification pair $(7, 100)$. The crash alarm index is in the range $[0, 1]$. The higher the crash alarm index, the more likely is the occurrence of a crash. (lower) Plot of price versus time of Russell Index (shown in blue cycles). Green solid vertical lines indicate rebounds defined by local minima within plus and minus 100 days around them. Red dashed vertical lines indicate crashes defined by local maxima within plus and minus 100 days around them. Note that these rebounds and crashes are the historical "change of regime" rather than only the jump-like reversals.

To check the quality of the alarm index quantitatively, we introduce error diagrams [133, 134]. Using Nikkei 225 as an example, we create an error diagram for crash predictions after 17-Apr-1999 with a certain feature qualification in the following way:

1. Calculate features and define the alarm index using the *learning set* between 04-Jan-1984 and 17-Apr-1999.
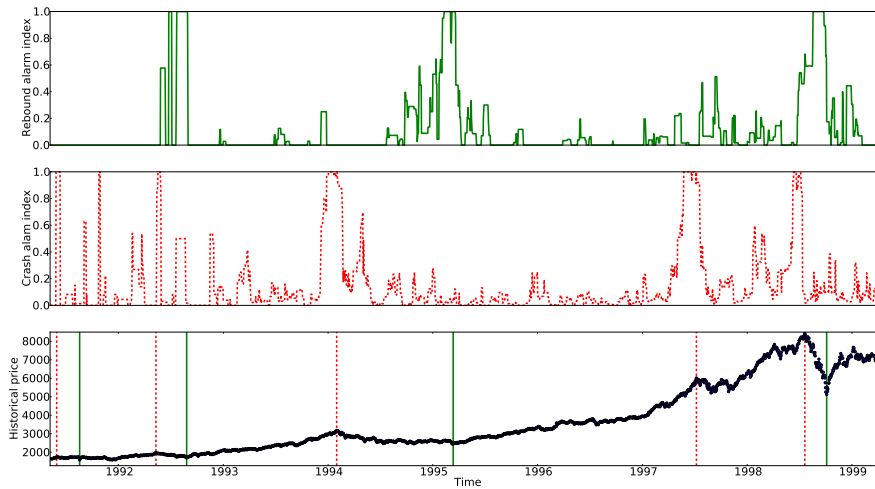
Figure 4.21: Alarm index and price of the SMI Index for the *learning* set, where the end date is 17-Apr-1999. The format is the same as Fig. 4.20.

2. Count the number of crashes after 17-Apr-1999 as defined in Sec. 4.2.1 and expression (4.32). There are 7 crashes.

3. Take the crash alarm index time series (after 17-Apr-1999) and sort the set of all alarm index values in decreasing order. There are 4,141 points in this series and the sorting operation delivers a list of 4,141 index values, from the largest to the smallest one.

4. The largest value of this sorted series defines the first threshold.

5. Using this threshold, we declare that an alarm starts on the first day that the unsorted crash alarm index time series exceeds this threshold. The duration of this alarm D_a is set to 41 days, since the longest distance between a crash and the day with index greater than the threshold is 20 days. This threshold is consistent with the previous classification of questionnaires in Sec. 4.2.1, where we define a predicted critical time as 'near' the real extreme events when its distance is less than 20 days. Then, a prediction is deemed successful when a crash falls inside that window of 41 days.

6. If there are no successful predictions at this threshold, move the threshold down to the next value in the sorted series of alarm index.
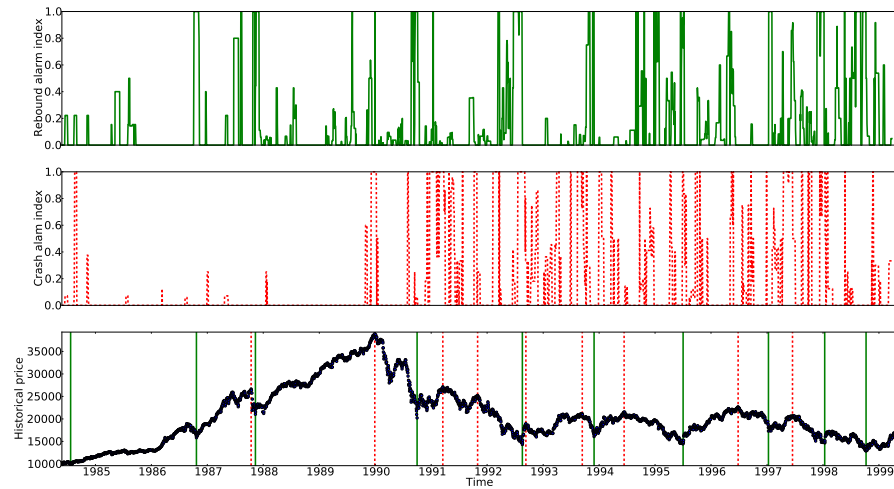
Figure 4.22: Alarm index and price of the Nikkei 225 Index for the *learning* set, where the end date is 17-Apr-1999. The format is the same as Fig. 4.20.

7. Once a crash is predicted with a new value of the threshold, count the ratio of unpredicted crashes (unpredicted crashes / total crashes in set) and the ratio of alarms used (duration of alarm period / 4,141 prediction days). Mark this as a single point in the error diagram.

In this way, we will mark 7 points in the error diagram for the 7 Nikkei 225 crashes after 17-Apr-1999.

The aim of using such an error diagram in general is to show that a given prediction scheme performs better than random. A random prediction follows the line $y = 1 - x$ in the error diagram. A set of points below this line indicates that the prediction is better than randomly choosing alarms. The prediction is seen to improve as more error diagram points are found near the origin point $(0, 0)$. The advantage of error diagrams is to avoid discussing how different observers would rate the quality of predictions in terms of the relative importance of avoiding the occurrence of false positive alarms and of false negative missed rebounds. By presenting the full error diagram, we thus sample all possible preferences and the unique criterion is that the error diagram curve be shown to be statistically significantly below the anti-diagonal $y = 1 - x$.

In Fig. 4.26–4.28, we show the results on predictions and back tests in terms of error diagrams for crashes and rebounds in each of the indices. The results
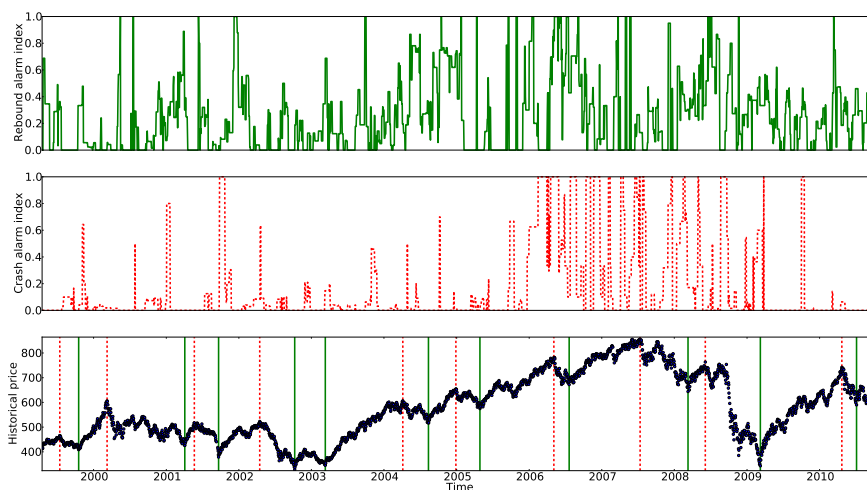
Figure 4.23: Alarm index and log-price of Russell 2000 Index for the *predicting* set after 17-Apr-1999. The format is the same as Fig. 4.20.

for different feature qualification pairs (α, β) are shown in each figure. All these figures show that our alarm index for crashes and rebounds in either back testing or prediction performs much better than random.

4.2.3   Trading Strategy

One of the most powerful methods to test the predictability of a signal is to design simple trading strategies based on it. We do so with our alarm index by using simple moving average strategies, which keep all the key features of the alarm index and avoid parametrization problems. The strategies are kept as simple as possible and can be applied to any indices.

The trading strategies are designed as follows: the daily exposure of our strategy θ is determined by the average value of the alarm index for the past n days. The rest of our wealth, $1 - \theta$, is invested in a 3-month US treasury bill.

Let us denote the average rebound and crash alarm index of the past n days as AI_R and AI_C respectively. We create three different strategies:

- A long strategy using only the rebound alarm index. We will take a long position in this strategy only. The daily exposure of our strategy is based on the average value of the past n days rebound alarm index: $\theta = AI_R$.

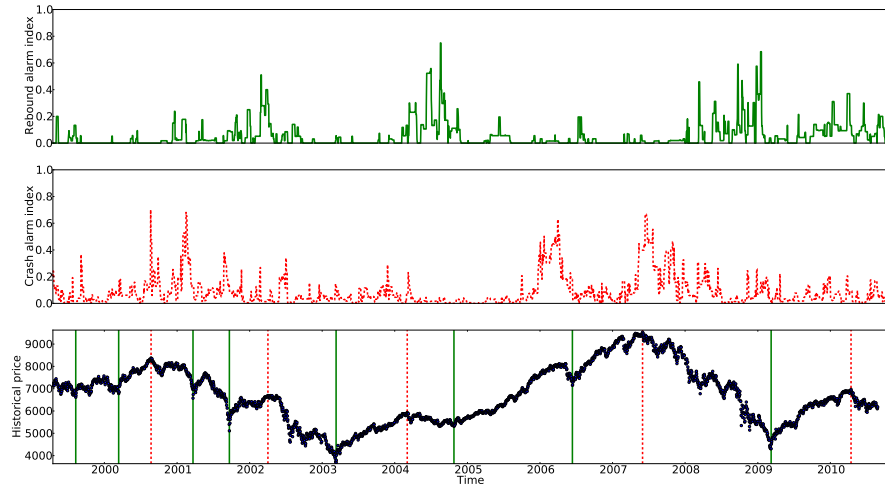- A short strategy using only the crash alarm index. We will take a short

Figure 4.24: Alarm index and price of the SMI Index for the *predicting* set after 17-Apr-1999. The format is the same as Fig. 4.20.

position in this strategy only. The daily absolute exposure of our strategy is based on the average value of the past n days crash alarm index: $|\theta| = AI_C$.

- A long-short strategy linearly combining both strategies above. When the average rebound alarm index is higher than the average crash alarm index, we take a long position and vice versa. The absolute exposure $|\theta| = |AI_R - AI_C|$.

These strategies have the advantage of having few parameters, as only the duration n needs to be determined. Despite their simplicity, they capture the two key features of the alarm index. First, we see that the alarms are clustered around certain dates. The more clustering seen, the more likely that a change of regime is coming and, therefore, the more we should be invested. Second, we see that a strong alarm close to 1 should be treated as more important than a weaker alarm while at the same time the smaller alarms still contain some information and should not be discarded.

Tab. 4.4 summarizes the Sharpe ratios for long-short strategies on the out-of-sample period (testing set) for each index. The strategy is calculated with four different moving average look-backs: $n = 20, 30, 40, 60$ days. We use the Sharpe ratios of the market during this period as the benchmark in this table. Recall that the Sharpe ratio is a measure of the excess return (or risk premium) per unit of risk
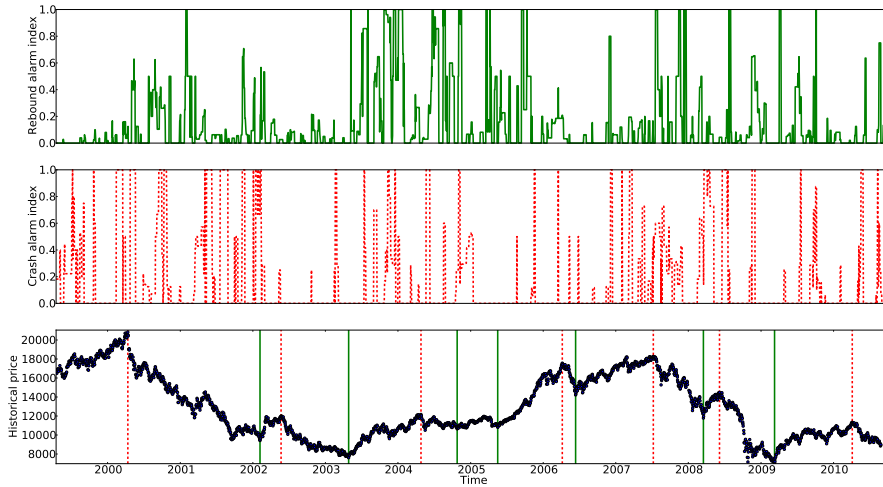
Figure 4.25: Alarm index and price of the Nikkei 225 Index for the *predicting* set after 17-Apr-1999. The format is the same as Fig. 4.20.

in an investment asset or a trading strategy. It is defined as:

$$S = \frac{R - R_f}{\sigma} = \frac{R - R_f}{\sqrt{Var[R - R_f]}} \ , \tag{4.34}$$

where R is the return of the strategy and R_f is the risk free rate. We use the US three-month treasury bill rate here as the risk free rate. The Sharpe ratio is used to characterize how well the return of an asset compensates the investor for the risk taken: the higher the Sharpe ratio number, the better. When comparing two assets with the same expected return against the same risk free rate, the asset with the higher Sharpe ratio gives more return for the same risk. Therefore, investors are often advised to pick investments with high Sharpe ratios. From Tab. 4.4, we can find that, for seven out of ten global major indices, the Sharpe ratios of our strategies (no matter which look-back duration n is chosen) are much higher than the market, which means that our strategies perform better than the simple buy and hold strategy. This result indicates that the JLS model combined with the pattern recognition method has a statistically significant power in systematic detection of rebounds and of crashes in financial markets.

The long-short strategies for CAC 40, DAX and ASX perform not as well as the market. However, this is not a statement against the prediction power of our method, but instead supports the evidence that our method detects specific signa-

Figure 4.26: Error diagram for back tests and predictions of crashes and rebounds for Russell 2000 index with different types of feature qualifications. The value of the feature qualifications are shown in the legend. The fact that all the curves lie under the line $y = 1 - x$ indicates better performance than chance in detecting crashes and rebounds using our method. (upper left) Back tests of crashes. (upper right) Back tests of rebounds. (lower left) Predictions of crashes. (lower right) Predictions of rebounds. Feature qualification (α, β) means that, if the occurrence of a certain trait in Class I is larger than α and less than β, then we call this trait a feature of Class I and vice versa. See text for more information.

Figure 4.27: Error diagram for back tests and predictions of crashes and rebounds for SMI index with different types of feature qualifications. The format is the same as Fig. 4.26.
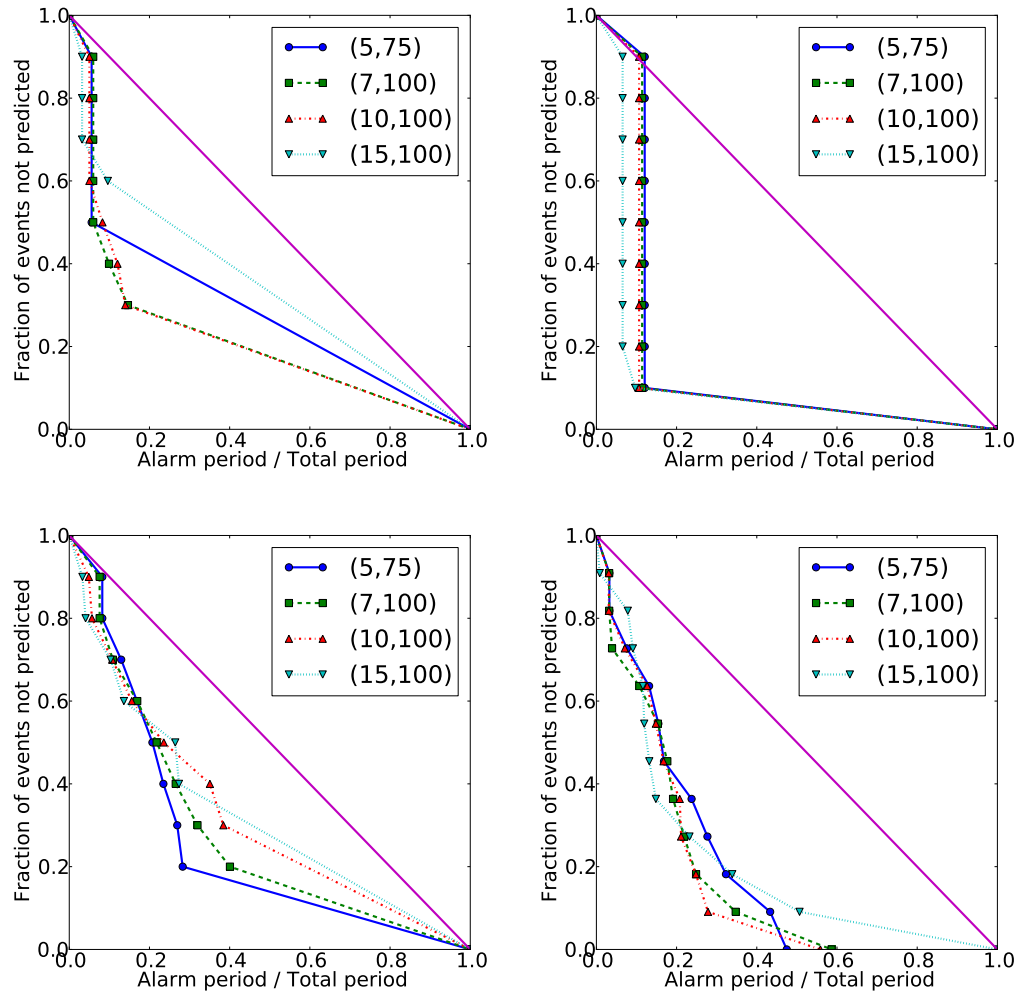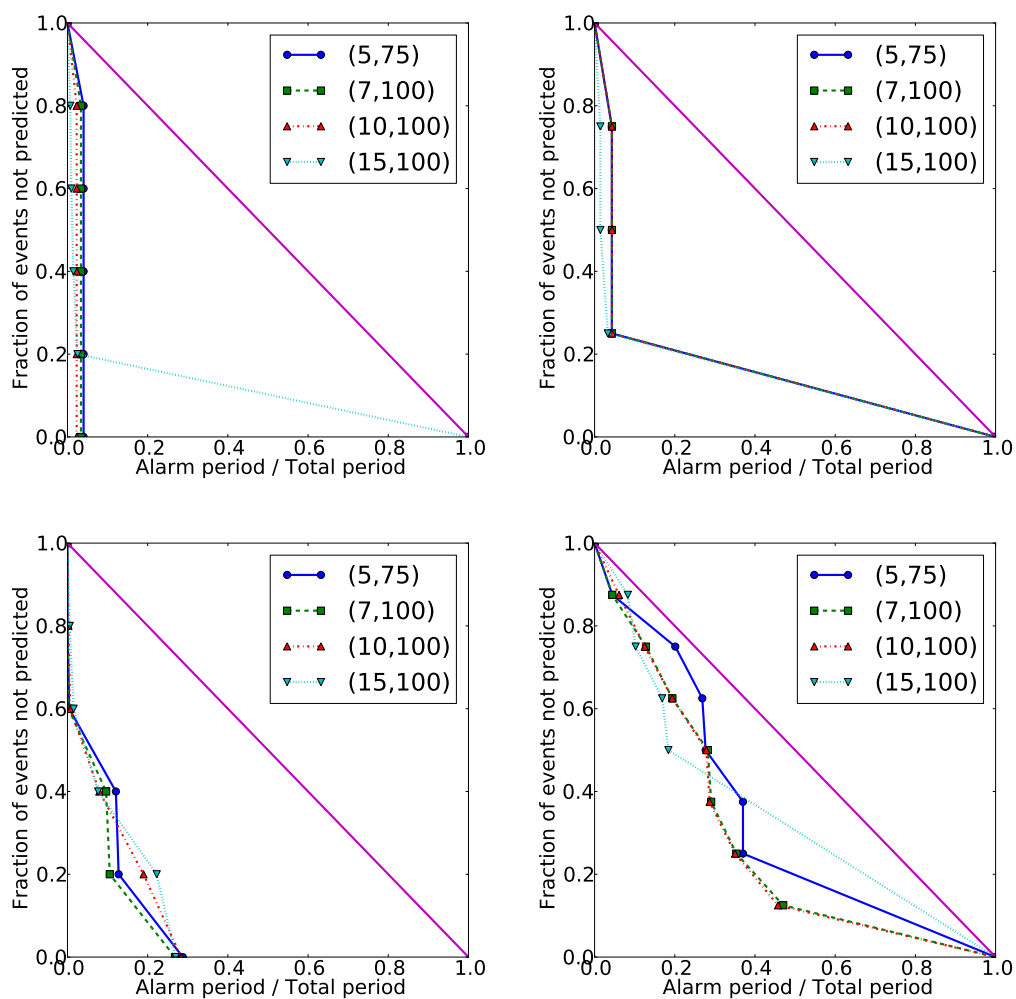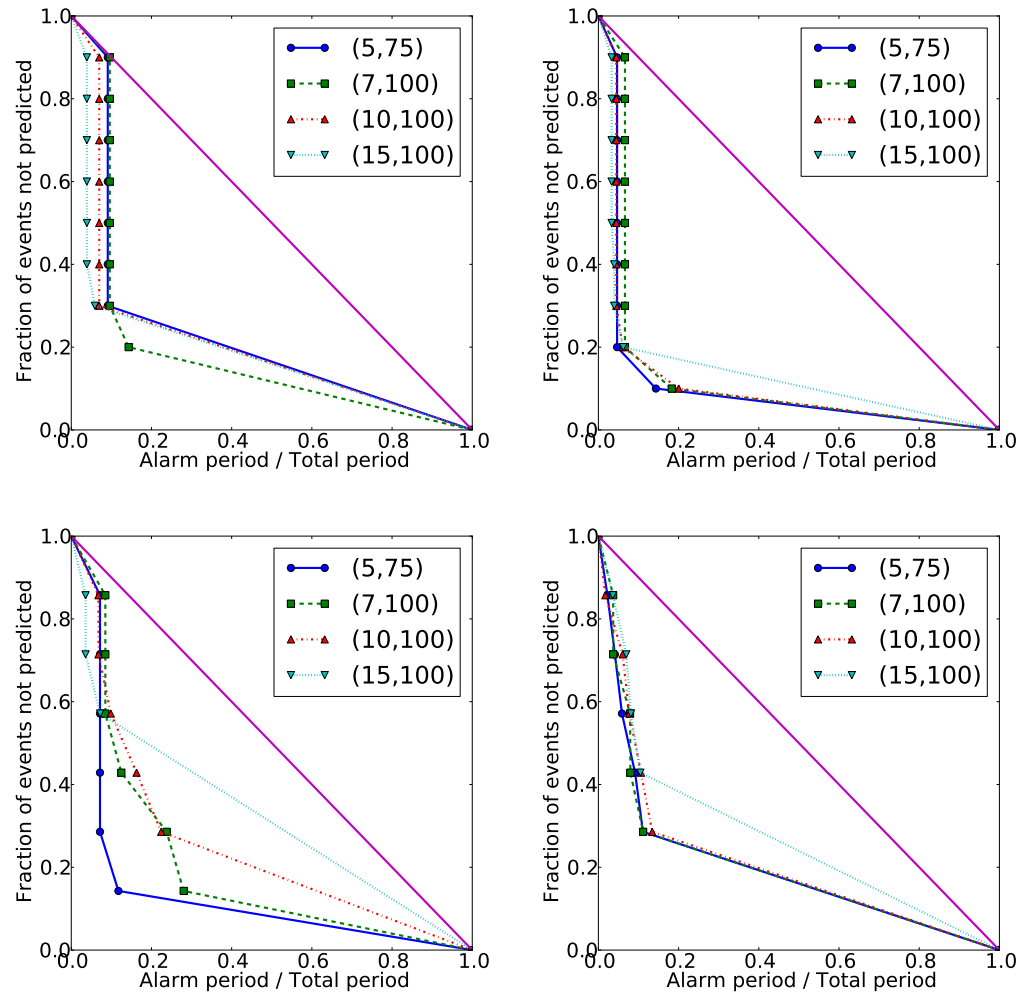
Figure 4.28: Error diagram for back tests and predictions of crashes and rebounds for Nikkei 225 index with different types of feature qualifications. The format is the same as Fig. 4.26.

tures preceding rebounds and crashes that are essentially different from high volatility indicators. Contrary to common lore and to some exceptional empirical cases [137, 75], crashes of the financial markets often happen during low-volatility periods and terminate them. By construction, both our rebound alarm index and the crash alarm index are high during such volatile periods. So if the alarm indices of both types are high at the same time, it is likely that the market is experiencing a highly volatile period. Now, we can refine the strategy and combine the evidence of a directional crash or rebound, together with a high volatility indicator. If we interpret the two co-existing evidences as a signal for a crash, we should ignore these rebound alarm index and take the short strategy mentioned before. As an application, we show the wealth trajectories of DAX based on different type of strategies in Fig. 4.29. In the beginning of 2008, both the rebound alarm index and the crash alarm index for DAX are very high, therefore, we detect this period as a highly volatile period and ignore the rebound alarm index. The short strategy gives a very high Sharpe ratio $S = 0.41$ compared to the long-short and short benchmarks where $S = 0.06$. The strategy's average weight is used to compute these benchmarks. These simple benchmarks are constantly invested by a given percentage in the market so that, over the whole time period, they give the same exposure as the corresponding strategy being tested but without the genuine timing information the strategy should contain.

As before, the detailed out-of-sample performances for each sample index (Russell 2000, SMI and Nikkei 225) are also tested. Fig. 4.30–4.32 illustrate the wealth trajectories for different strategies. In order to show the consistency of the strategies with respect to the chosen parameters in the pattern recognition method, we show the performance of the Russell 2000 index for different qualification pairs: $(15, 100)$ for rebounds and $(10, 100)$ for crashes. From these wealth trajectories, it is very obvious that our alarm indices can catch the market rebounds and crashes efficiently.

The detailed performances for these three stock indices are listed in Tabs. 4.5–4.8. We also provide the performance of the Russell 2000 index for the 'normal' qualification pair: $(7, 100)$ in Tab. 4.6 as a reference. These tables confirm again that strategies mostly succeed in capturing big changes of regime. Compared to the market, the strategies based on our alarm index perform better than the market for more than eleven years in all the important measures: Annual returns and Sharpe

ratios are larger, while volatilities, downside deviations and maximum drawdowns are smaller than the market performance.

4.2.4   Conclusion

We provided a systematic method to detect financial crashes and rebounds. The method is a combination of the JLS model for bubbles and negative bubbles, and the pattern recognition technique originally developed for earthquake predictions. The outcome of this method is a rebound/crash alarm index to indicate the probability of a rebound/crash for a certain time. The predictability of the alarm index has been tested by ten major global stock indices. The performance is checked quantitatively

Figure 4.29: Performance of trading strategy using our technique: DAX index 60 days moving average strategy using the feature qualification pair $(15, 100)$ for crashes and $(10, 200)$ for rebounds. (upper) the exposures for different strategies, where the olive solid line represents the long-short strategy, the green dotted line and red dashed line are for long and short strategy respectively. (lower) The historical price and wealth trajectories of the strategies. The blue circles represent the historical price of the index while the others are the wealth trajectories consistent with the upper figure (olive solid - long-short, green dotted - long, red dashed - short). The Sharpe ratio for the strategies are 0.07 (long-short), -0.66 (long) and 0.41 (short). The Sharpe ratio of the corresponding benchmarks, which consist of constant position in the market with exposure equal to the strategy over the whole period, are 0.06 (long-short), -0.06 (long) and 0.06 (short). And the Sharpe ratio of the index in this period is -0.06. Note that the short strategy performs better than long-short or long strategies as discussed in the text.

by error diagrams and trading strategies. All the results from error diagrams indicate that our method in detecting crashes and rebounds performs better than chance and confirm that the new method is very powerful and robust in the prediction of crashes and rebounds in financial markets. Our long-short trading strategies based on the crash and rebound alarm index perform better than the benchmarks (buy and hold strategy with the same exposure as the average exposure of our strategies) in seven out of ten indices. Highly volatile periods are observed in the indices of which the long-short trading strategy fails to surpass the benchmark. By construction of the alarm index and the fact that highly volatile periods are not coherent with bullish markets, we claim that we should ignore the rebound alarm index during such volatile periods. This statement has been proved by the short strategy which only consider the crash alarm index. Thus, our trading strategies confirm again that the alarm index has a strong ability in detecting rebounds and crashes in the financial markets.
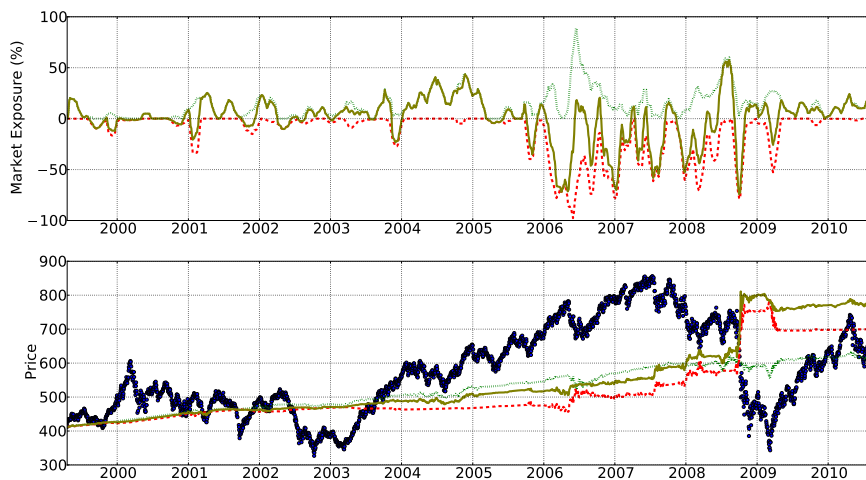
Figure 4.30: Performance of trading strategy using our technique: Russell 2000 index 30 days moving average strategy using the feature qualification pair $(15, 100)$ for crashes and $(10, 100)$ for rebounds. The format is the same as Fig. 4.29. The Sharpe ratio for the strategies are 0.47 (long-short), 0.18 (long) and 0.26 (short). The Sharpe ratio of the corresponding benchmarks, which consist of constant position in the market with exposure equal to the strategy over the whole period, are 0.03 (long-short), 0.03 (long) and -0.03 (short). And the Sharpe ratio of the index in this period is 0.03.
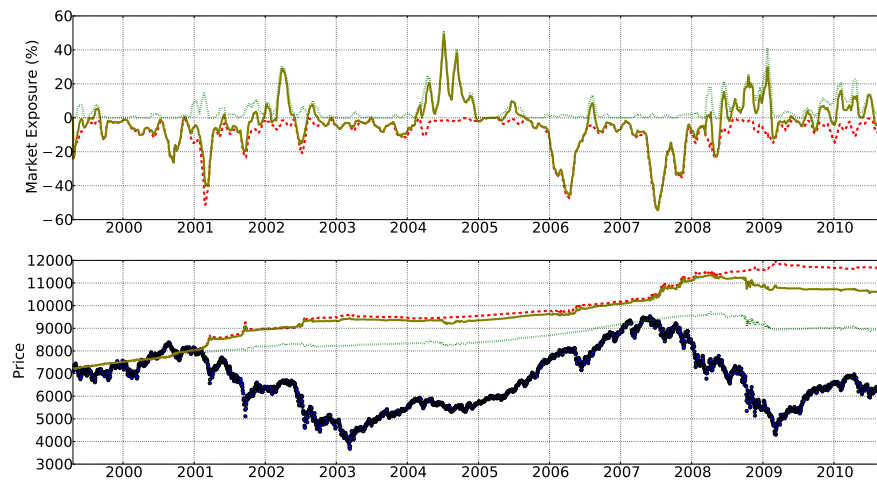
Figure 4.31: Performance of trading strategy using our technique: SMI index 20 days moving average strategy. The format is the same as Fig. 4.29. The Sharpe ratio for the strategies are 0.28 (long-short), −0.04 (long) and 0.65 (short). The Sharpe ratio of the corresponding benchmarks, which consist of constant position in the market with exposure equal to the strategy over the whole period, are 0.2 (long-short), −0.2 (long) and 0.2 (short). And the Sharpe ratio of the index in this period is −0.2.

Index name	Yahoo ticker	Learning start	Prediction start	Prediction end	win. #
S&P 500	ˆGSPC	5-Jan-1950	26-Mar-1999	3-Jun-2009	11662
Nasdaq	ˆIXIC	13-Dec-1971	20-Mar-1999	30-Jul-2010	7209
Russell 2000	ˆRUT	30-Sep-1987	17-Apr-1999	27-Aug-2010	4270
FTSE 100	ˆFTSE	3-May-1984	17-Apr-1999	27-Aug-2010	4970
CAC 40	ˆFCHI	1-Mar-1990	17-Apr-1999	27-Aug-2010	3766
SMI	ˆSSMI	9-Nov-1990	17-Apr-1999	27-Aug-2010	3626
DAX	ˆGDAXI	26-Nov-1990	17-Apr-1999	27-Aug-2010	3626
Nikkei 225	ˆN225	4-Jan-1984	17-Apr-1999	27-Aug-2010	5026
Hang Seng	ˆHSI	31-Dec-1986	17-Apr-1999	27-Aug-2010	4410
ASX	ˆAORD	6-Aug-1984	17-Apr-1999	27-Aug-2010	4914

Table 4.3: Information for the tested indices: Yahoo ticker of each index, starting time of learning and prediction periods, ending time of prediction and number of sub-windows.

Index	Strategy (duration n)				Market
	20	30	40	60	
S&P 500	0.32	0.38	0.43	0.39	-0.28
Nasdaq	0.18	0.41	0.48	0.34	-0.11
Russell 2000	0.29	0.3	0.27	0.27	0.03
FTSE 100	-0.07	-0.06	0.01	0.05	-0.22
CAC 40	-0.18	-0.35	-0.37	-0.24	-0.19
SMI	0.28	0.22	0.14	0.13	-0.20
DAX	-0.26	-0.24	-0.27	-0.19	-0.06
Nikkei 225	0.07	0.19	0.39	0.59	-0.33
Hang Seng	0.32	0.38	0.31	0.23	0.06
ASX	-0.38	-0.41	-0.33	-0.24	0.02

Table 4.4: Summary of Sharpe ratios for the market and the long-short strategies with different moving average duration n. The start and end dates of the strategies are 26-Mar-1999 – 3-Jun-2009 for S&P 500, 20-Mar-1999 – 30-Jul-2010 for Nasdaq and 17-Apr-1999 – 27-Aug-2010 for others. The feature qualification pairs of $(7, 100)$ for both crash and rebound alarm indices are used in this calculation.
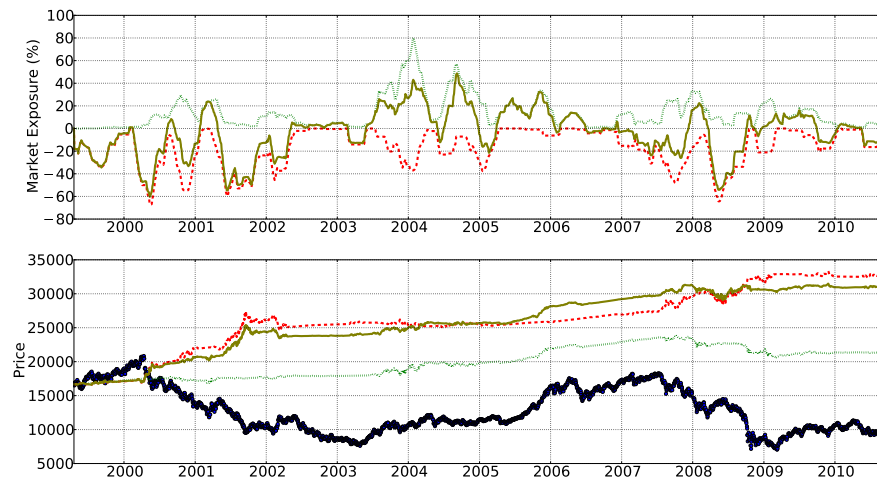
Figure 4.32: Performance of trading strategy using our technique: Nikkei 225 index 60 days moving average strategy. The format is the same as Fig. 4.29. The Sharpe ratio for the strategies are 0.59 (long-short), -0.11 (long) and 0.59 (short). The Sharpe ratio of the corresponding benchmarks, which consist of constant position in the market with exposure equal to the strategy over the whole period, are 0.33 (long-short), -0.33 (long) and 0.33 (short). And the Sharpe ratio of the index in this period is -0.33.

	Strategy (duration n)				Market
	20	30	40	60	
Ann Ret	5.3%	5.4%	4.8%	4.2%	0.1%
Vol	6.4%	5.9%	5.3%	4.1%	26.3%
Downside dev	4.2%	3.6%	3.4%	2.7%	18.9%
Sharpe	0.42	0.47	0.41	0.37	0.03
Max DD	10%	7%	7%	6%	65%
Abs Expo	16%	15%	14%	12%	
Ann turnover	328%	220%	167%	123%	

Table 4.5: Russell 2000 index long-short strategies out-of-sample performance table. Start date: 17-Apr-1999, end date 27-Aug-2010. Qualification pairs: $(15, 100)$ for rebounds and $(10, 100)$ for crashes.

	Strategy (duration n)				Market
	20	30	40	60	
Ann Ret	4.8%	4.7%	4.3%	4.0%	0.1%
Vol	7.9%	7.1%	6.5%	5.2%	26.3%
Downside dev	5.4%	4.8%	4.5%	3.6%	18.9%
Sharpe	0.29	0.30	0.27	0.27	0.03
Max DD	11%	12%	9%	9%	65%
Abs Expo	23%	21%	20%	18%	
Ann turnover	446%	306%	237%	172%	

Table 4.6: Russell 2000 index long-short strategies out-of-sample performance table. Start date: 17-Apr-1999, end date 27-Aug-2010. Qualification pairs: $(7, 100)$ for both rebounds and crashes.

	Strategy (duration n)				Market
	20	30	40	60	
Ann Ret	3.4%	3.3%	3.0%	3.0%	-3.4%
Vol	2.6%	2.6%	2.5%	2.3%	20.4%
Downside dev	1.7%	1.6%	1.6%	1.5%	14.6%
Sharpe	0.28	0.22	0.14	0.13	-0.20
Max DD	7%	6%	7%	5%	59%
Abs Expo	9%	9%	9%	9%	
Ann turnover	134%	102%	77%	55%	

Table 4.7: SMI index long-short strategies out-of-sample performance table. Start date 17-Apr-1999, end date 27-Aug-2010.

	Strategy (duration n)				Market
	20	30	40	60	
Ann Ret	3.0%	3.7%	4.8%	5.7%	-8.4%
Vol	6.3%	6.0%	5.6%	5.0%	25.4%
Downside dev	4.4%	4.1%	3.7%	3.2%	18.7%
Sharpe	0.07	0.19	0.39	0.59	-0.33
Max DD	15%	13%	10%	8%	75%
Abs Expo	19%	18%	17%	16%	
Ann turnover	417%	300%	223%	146%	

Table 4.8: Nikkei 225 index long-short strategies out-of-sample performance table. Start date 17-Apr-1999, end date 27-Aug-2010.

5

Leverage Bubble

Following [15], the term "bubble" refers to a situation in which excessive public expectations of future price increases cause prices to be temporarily elevated. For instance, during a housing price bubble, homebuyers think that a home that they would normally consider too expensive for them is now an acceptable purchase because they will be compensated by significant further price increases. They will not need to save as much as they otherwise might, because they expect the increased value of their home to do the saving for them. First-time homebuyers may also worry during a housing bubble that if they do not buy now, they will not be able to afford a home later. Furthermore, the expectation of large price increases may have a strong impact on demand if people think that home prices are very unlikely to fall, and certainly not likely to fall for long, so that there is little perceived risk associated with an investment in a home.

In this chapter, instead of emphasizing the case for the presence of a housing bubble (which was indubitably present, see [53, 51]), we argue that there was *in addition* a leverage bubble that peaked and crashed in early 2008 after building up for the years beforehand. We know that leverage is strongly related to liquidity in a market and lack of liquidity is considered a cause and/or consequence of the recent financial crisis. As we explain below, the leverage bubble formed and grew for the same reasons as described in the housing bubble example above: investors were afraid that if they did not extend their leverage (buy a house) then they would lose

money later. Further, we argue that the size of the market in *repurchase agreements* (or repos, for short) is an observable proxy of leverage in the financial system, i.e. repos market size is a very important element in calculating the overall leverage in a financial market. We will elaborate on repos below, but, briefly, a repo is simply a cash transaction for an asset combined with a forward contract to buy the asset back at a later time (hence 're-purchase'). Therefore, studying the behavior of repos market size can help to understand a process that can contribute to the birth of a financial crisis.

We hypothesize that herding behavior among large investors led to massive over-leveraging through the use of repos, resulting in a bubble (built up over the previous years) and subsequent crash in this market in early 2008. We use the JLS model of rational expectation bubbles and behavioral finance to study the dynamics of the repo market that led to the crash. As we know that the JLS model qualifies a bubble by the presence of log-periodic power law behavior in the price dynamics. We show that there was significant log-periodic power law behavior in the market before that crash and that the predicted range of times predicted by the model for the end of the bubble is consistent with the observations. We conclude that by measuring the size of the repos market and applying the JLS bubble model, we can see that the leverage crash in early 2008 was potentially a predictable event.

The chapter is constructed as follows. In Sec. 5.1, we discuss the relationship between repos market size and the overall leverage of the market. In Sec. 5.2, we apply the JLS model to total repos market size to make an ex-post forecast of the crash in early 2008. We conclude in Sec. 5.3.

5.1   Repos market size represents the leverage of the market

A repurchase agreement (repo) is the sale of securities together with an agreement for the seller to buy back the securities at a later date [1]. In other words, it is a contract obliging the seller of an asset to buy back the asset at a specified price on a given date. Therefore, a repo is equivalent to a cash transaction combined

---

[1]`http://en.wikipedia.org/wiki/Repurchase_agreement`

with a forward contract. The cash transaction results in transfer of money to the borrower in exchange for legal transfer of the security to the lender, while the forward contract ensures repayment of the loan to the lender and return of the collateral of the borrower.

To understand the possible role of repos in the generation of a bubble, we first discuss the relationship between leverage and balance sheet size. We start with a very simple case, taken from Sec. 2 of [138]. Assume that an investment bank has 100 USD in securities while its shareholder equity is 20 USD and its debt is 80 USD. Then the balance sheet of this bank looks like:

Assets	Liabilities
Securities, 100	Equity, 20
	Debt, 80

Now the leverage of the bank is:

$$\frac{assets}{equity} = \frac{100}{20} = 5. \tag{5.1}$$

Suppose that the debts of this bank are all long term debts and, therefore, we can assume that the debt remains the same in the balance sheet over the short period of time considered in the argument. Now assume that the prices of the securities increase by 10%, so that the new balance sheet is:

Assets	Liabilities
Securities, 110	Equity, 30
	Debt, 80

The leverage, then, becomes:

$$\frac{assets}{equity} = \frac{110}{30} = 3.67 < 5. \tag{5.2}$$

This shows that the leverage decreases as the assets' prices increase.

However, to an investor during the bull market, reduction of the leverage means losing money. Consider another example to demonstrate this. Suppose that two people A and B both have a house worth 1000 USD. Assume that they somehow know that the price of gold, for instance, will definitely increase in the near future.

Each of them can use her house as collateral and get a maximum 2000 USD loan from a bank (based on the recent convention of poor underwriting requirements). Investor A, being somewhat unsure of her future ability to repay her debts, applied for and received 'only' 1500 USD, which corresponds to a leverage of 1.5. Investor B, though, with no such qualms, asked for and received the maximum value of 2000 USD, for a leverage of 2. Both investors used all of the borrowed money to buy gold. After one month, the gold price, as expected, increased by 20%. Both A and B sold all of the leveraged gold and pay the money back to the bank (ignore interest rate for simplicity) and get back their houses. Investor A has made a profit of 300 USD but investor B, the bold risk-taker, has made the profit of 400 USD by simply increasing her leverage by one-third. In a sense, investor A's weak-kneed approach lost 100 USD due to failure to maximally leverage her position.

With this lesson in mind, let us now return to the investment bank. During the bull market, banks believe that the markets will continue to increase and that all of their competitors will be maximally leveraged to take advantage of the expected rise. If a bank decreases its leverage, it means it will lose money in the future (or lose opportunities with respect to competitors, since performance is relative to benchmarks and to the industry), so, guided by the practice of maximizing short-term profits by any means necessary, banks increase their leverage in order to get more return in the future. How large they will increase their leverage depends on their expectation of the future market. If the market performs very well now, they expect that the future will be very good, also (this is due to the well-documented behavior bias that investors tend to extrapolate past trends and past gains). This means that they will change their leverage based on the return *now*. Regardless of whether this is a good thing or not, for our study, we can use this because it implies that the total asset growth should be proportional to the leverage growth. This is demonstrated in Fig. 8 of [138]. In that paper, the authors used quarterly data from more than 10 years for six major U.S. investment banks: Lehman Brothers, Merrill Lynch, Morgan Stanley, Bear Stearns, Goldman Sachs and Citigroup Markets. The total asset growth of the banks is found strongly proportional to the leverage growth. So we know that when the expectation of the market is high, the investment banks tend to increase their leverage. The next question, then, is: how can a bank change its leverage?

Repos play a key role here. A typical balance sheet of an investment bank has not only the long term debt but also repos. Therefore, a typical balance sheet is as follows:

Assets	Liabilities
Trading assets	Repos
Reverse repos	Long term debt
Other assets	Equity

Recall that a repo is the sale of securities together with an agreement for the seller to buy back the securities at a later date. Long term debt is normally a small fraction of the balance sheet and can be assumed to be constant over the time scale of interest here (a few years at most). In this case, when banks want to increase or decrease their leverage, they will write repos in appropriate quantities.

We would like to emphasis one thing here: The use of repos is not the only method to change leverage. For example, the use of financial derivatives can also cause incredibly high leverage factors. However, repos trading plays a key role in changing of the leverage as the market size of repos is huge and it is a very good observable proxy of leverage in the financial system. Therefore, we use repos market size to present the leverage level in this paper.

One may argue that the haircut of the repo[2] is also a very important role for the leverage of the banks. We completely agree with this and the repurchase haircut should be counted here. However, the historical data shows that the haircut remains approximately within a range between 10% and 20% during 'normal' (i.e., non-crisis) times. During a financial crisis, the haircut will rise sharply to a very high level. When there is a shortage of liquidity, for instance, during the recent financial crisis, investors are afraid to trade. Increased haircuts and decreased repos size usually occur simultaneously. In this paper, we want to investigate the question of whether or not the dynamics of repos activity shows any precursory information before a large crash. Of course, this means we only use data before a crash to try to estimate

---

[2]The "haircut" is the difference between the true market value of the collateral and that used by the dealers in the repo contract. This haircut reflects the underlying risk of the collateral and protects the buyer against a change in its value. Haircuts are therefore specific to classes of collateral.

the time of its onset. Since the haircut is almost constant for a long time before a crash, all of the leverage information lies in the repo size of the market.

To summarize this section, we claim that:

(i) investors want to increase their leverage when their expectations of future gains of the market increase;

(ii) they will use repos to increase their leverage;

(iii) therefore, the total repo market size is a proxy to measure the overall expectation of all investors.

5.2   Predicting financial crashes with the JLS model

In the last section, we said that the repos market size represents the average leverage of the market and the leverage represents the investors' expectation of future market returns. We now discuss how the dynamics of leverage among traders could lead to a bubble and how this bubble can be identified as it grows.

We have argued before that bubbles are the result of imitation and herding behavior among investors [139, 48, 47, 5]. In the current case, investors increase their leverage when they see others doing so because, as discussed above, they think that they will lose money if they are the only ones not taking this strategy. Of course, this is a self-reinforcing (positive feedback) process: the numbers of leveraged investors and their levels of leverage will increase in a game of financial copycat. At some point, though, some investors are bound to notice that the numbers are too large and they will start to deleverage. Others nervously waiting for this signal will unload as well and the bottom will drop out. When this occurs, the repo market size goes down dramatically and the haircut of the repo increases very sharply, both leading to rapid loss of liquidity in the repo market.

This qualitative process is quantified in the JLS model to describe the herding dynamics during a bubble [48, 47]. This model combines the economic theory of rational expectation bubbles, behavioral finance on imitation and herding of investors and traders and the mathematical and statistical physics of bifurcations and phase transitions. The price dynamics in the model exhibits log-periodic power law

behavior, where a super-exponential price increase also oscillates in the log of time-to-crash (or more precisely in the log of the time to the end of the bubble, which is not necessarily a crash but rather generally a change of regime). A significant number of successful predictions of financial market crashes based on the JLS model have been made as mentioned before (see Chap. 2).

In the JLS model, (the logarithm of) price is used as a proxy for herding behavior among traders (see [46] for justifications on the use of log-price versus price). Since we argue that the repo market size is also a proxy for herding via the leverage level, we substitute it for the log-price in the JLS model. For the total repos market size $R(t)$ at time t, we use the following JLS model specification (corresponding to replacing log-price by logarithmic repos volume in the JLS equation):

$$\ln R(t) = A + B|t_c - t|^m + C|t_c - t|^m \cos(\omega \ln |t_c - t| + \phi) , \qquad (5.3)$$

where t_c is the most probable time of crash and m, ω, ϕ, A, B and C are parameters. To determine the values of these parameters, we want to minimize the sum of squares:

$$(t_c, m, \omega, \phi, A, B, C) = \qquad (5.4)$$

$$\arg\min \sum_t (\ln R(t) - A - B|t_c - t|^m - C|t_c - t|^m \cos(\omega \ln |t_c - t| + \phi))^2 .$$

We hypothesize that the run-up to the sudden large drop in the repos market in early 2008 was characterized by log-periodic power law dynamics, supporting our claim of the entanglement of expectations, leverage and herding behavior.

To test this hypothesis, we use the weekly data of US primary dealers' total repos size from 6 July 1994 to 23 June 2010.[3, 4] The data have very strong seasonal effects due to the fact that banks try to remove their repos to improve their balance sheet at the end of each quarter. To remove the seasonal effect, we used a 13 week (1 quarter) moving average.

We fit this smoothed time series with the JLS Eq. (5.3) in time windows defined

---

[3]We thank Tobias Adrian from the Federal Reserve Bank of New York for providing the data.
[4]The primary dealers list: BNP Paribas Securities Corp, Banc of America Securities LLC, Barclays Capital Inc, Cantor Fitzgerald & Co, Citigroup Global Markets Inc, Credit Suisse Securities (USA) LLC, Daiwa Capital Markets America Inc, Deutsche Bank Securities Inc, Goldman, Sachs & Co, HSBC Securities (USA) Inc, Jefferies & Company, Inc, J.P. Morgan Securities LLC, Mizuho Securities USA Inc, Morgan Stanley & Co, Incorporated Nomura Securities International, Inc, RBC Capital Markets Corporation, RBS Securities Inc, UBS Securities LLC.

by (t_1, t_2). We chose a fixed $t_2 = 13$ February 2008, approximately one month before the observed peak of the repos volume. We then repeated the analysis with an ensemble of 7 values of t_2, each separated by 7 days for the 3 weeks before and after 13 February 2008. Note that the 7 values of t_2 bracket a time span of 6 weeks, with the end of that period (5 March 2008) being just before the large drop in the repos market. An observer in the past on this date would not have noticed any unusual drop in the time series. That is, the impending crash was not obvious based on any recent trend in the data (though perhaps some market intelligence could have provided an indication). For each value of t_2, we use an ensemble of different t_1's. Each ensemble brackets a range between 6 and 18 months before the respective t_2 and values of t_1 are separated by 7 days.

The fit for a particular (t_1, t_2) interval is generated in two steps. First, the linear parameters A, B and C are slaved to the non-linear parameters by solving them analytically as a function of the nonlinear parameters. We refer to [48] (page 238 and following ones), which gives the detailed equations and procedure. Then, the search space is obtained as a 4 dimensional parameter space representing m, ω, ϕ and t_c. A heuristic search implementing the Taboo algorithm [84] is used to find 10 initial estimates of the parameters which are then passed to a Levenberg-Marquardt algorithm [85, 86] to minimize the residuals (the sum of the squares of the differences) between the model and the data. The Taboo search together with the Levenberg-Marquardt method ensure a systematic exploration of the space of solutions and provide good estimates of the uncertainty on t_c. The bounds of the search space are:

$$m \quad \in \quad [0.001, 0.999] \tag{5.5}$$

$$\omega \quad \in \quad [0.01, 40] \tag{5.6}$$

$$\phi \quad \in \quad [0.001, 2\pi - 0.001] \tag{5.7}$$

$$t_c \quad \in \quad [t_2, t_2 + 0.375(t_2 - t_1)] \tag{5.8}$$

Fig. 5.1 shows the fitting results with a fixed end of the time series $t_2 = 3$ February 2008 and the ensemble of t_1s as described above. The use of many fits provides an ensemble of t_c's, from which we can calculate quantiles of the most likely date of a crash. The 20%-80% quantile region is shown on the figure as the inner vertical

band with diagonal cross-hatching. The 5%-95% quantiles are shown as the outer vertical band with horizontal hatching. The dark vertical line to the left of the quantile windows represents the last observation used in the analysis, that is, t_2. The shaded envelopes to the right of t_2 represent 20%-80% and 5%-95% quantiles of the extrapolations of the fits. From the plot, we see that both the t_c quantiles and the extrapolation quantiles are consistent with the observed trajectory of the moving average of the repos market size.
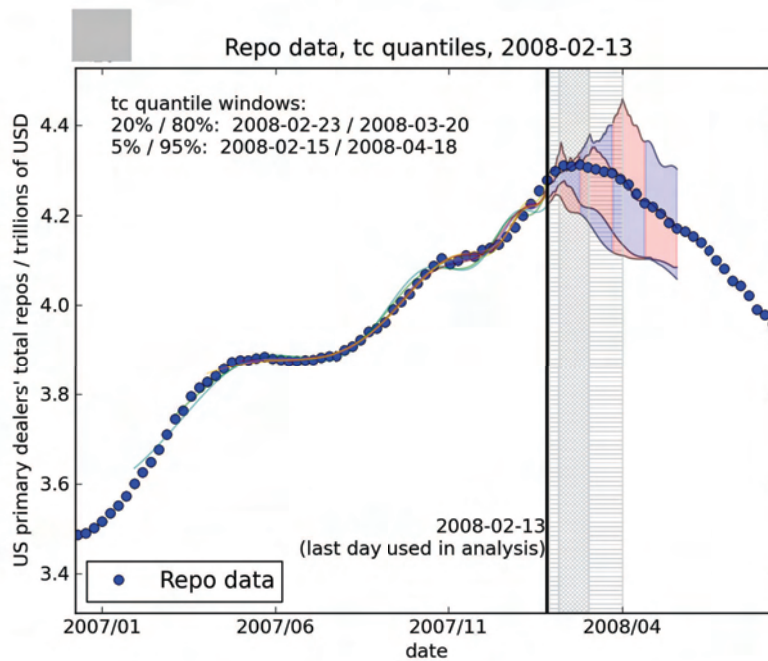

Figure 5.1: Results of the calibration of the JLS model to the time evolution of the total repos market size. The end time of the time series is fixed to t_2 =2008-02-03, shown as the dark vertical line to the left of the quantile windows. For different starting times, the probability density of the most probable time of crash t_c is shown in quantiles. The curves on the right of the dark vertical line are the extrapolated quantile repos volume, which are found consistent with the realized trajectory of the moving average of the repos market size.

One may argue that the uncertainty on the most probable critical time t_c obtained by taking several data time windows on a single time series may not be consistent with the one estimated on many artificial data sets with the same parameters. This problem is essential since in case they are not consistent with each other, the uncertainty estimates is not convincing. To prove that our estimation of the critical

time t_c is reliable, the following test has been performed:

We fix the end of the selected time window to $t_2 = 13$ February 2008, change the beginning of the time window t_1 based on the rule that each window size is between 6 and 18 months and values of t_1 are separated by 7 days. 53 time windows have been generated by this selection procedure. For each time window, we fit the repos time series with the JLS model and keep the best 10 fitted results. Therefore, 530 estimated values of t_c are obtained. We use the cumulative probability density (CDF) of these estimated t_c as the reference, CDF_{ref}.

Furthermore, we choose the fitted parameter set whose t_c is the median of the estimated critical time among all 530 sets to generate the synthetic time series which will be tested. We build up the JLS signal by this selected parameter set and add noises to generate the synthetic time series. The noises are produced by reshuffling the residuals between the repos data and the JLS signal. Two types of noises are used: the residuals are reshuffled at the daily scale and the residuals are reshuffled in blocks of 10 days in order to keep some dependence structure between the residuals.

For each type of noise, 100 synthetic time series are fit by the JLS model and 1,000 estimated critical times t_c are obtained by keeping the best 10 fits for each time series. The cumulative probability density of these estimated values of t_c from daily (respectively, 10 days) reshuffled noises is noted by CDF_1 (respectively, CDF_2).

Our goal is to prove that the two estimation methods give similar results. Fig. 5.2 shows the cumulative probability densities produced from 1) different time windows for the original time series (CDF_{ref}) and 2) a single time window for the two sets of synthetic time series (CDF_1 and CDF_2). From this figure, one can tell that the maximum difference between $CDF_{1,2}$ and CDF_{ref} is less than 10%. Therefore, we can safely conclude that both methods produce similar results. The relatively big difference between CDFs in the upper right part of the figure is due to the boundary condition of the t_c search space being different for different methods. By construction, the search space of t_c only depends on the lengths of the time series. Time series with different lengths are used to generate CDF_{ref} while the length of the synthetic time series which generate CDF_1 and CDF_2 are identical. Furthermore, CDF_2 is closer to CDF_{ref} than to CDF_1. This means that the dependence structure between residuals has influence on the t_c estimation. This finding is helpful in future studies of the JLS model fitting issues.
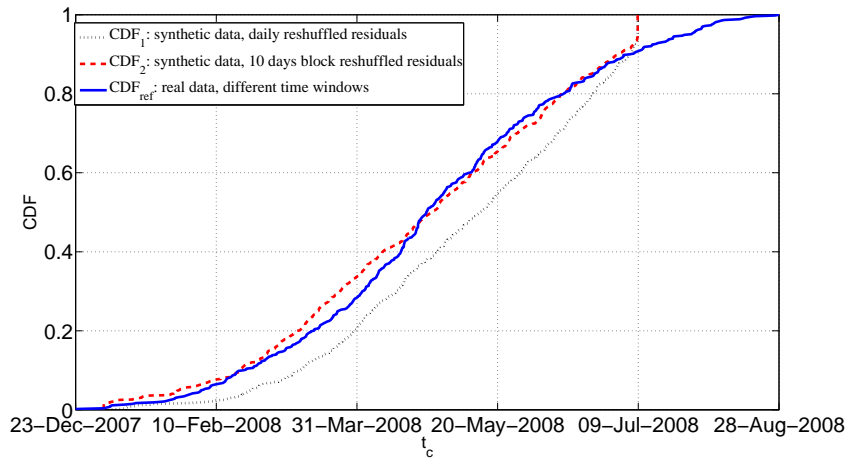
Figure 5.2: CDFs of estimated t_c with different methods. CDF_{ref} indicates the estimation from the real time series with different time windows while CDF_1 (CDF_2) refers to the estimation from the synthetic time series generated from daily (10 days) shuffled residuals. Three similar CDFs indicate that the uncertainty on the most probable critical time t_c obtained by taking several data time windows on a single time series is consistent with the one estimated on many synthetic data sets with the same parameters.

Our use of 7 values of t_2s in the 6-week window described above is to address the issue of the stability of the predicted most probable time of crash in relation to t_2. We fit the ensemble of (t_1, t_2) intervals as described above and plot the pdfs of the predicted most probable time of crash t_c for each t_2 by a non-parametric method. The pdfs are generated using the 10 best fits obtained from the Taboo search. This non-parametric method provides an excellent estimate of the distribution of t_cs. The result is shown in Fig. 5.3. From the plot, one can observe two regimes. The first four pdfs corresponding to the t_cs generated from the earliest t_2s peak practically at the same value, showing a very good stability. The last two pdf's show a tendency to shift to the future, as some of the used data starts to be sensitive to the plateauing of the repos volume. Overall, the observed stability of the predicted distributions of t_cs means the calibration of the JLS model is quite insensitive to when the prediction is made. This is proposed as an important validation step for the relevance of the JLS model. This suggests that the JLS model can be used as an advanced diagnostic of impending crashes. The present results support those accumulating within the "financial bubble experiment", which has the goal of testing such advanced forecasts

of bubbles and crashes. In the financial bubble experiment, the results are revealed only after the predicted event has passed but the original date when we produced the forecasts has been publicly, digitally authenticated [64, 65, 66].
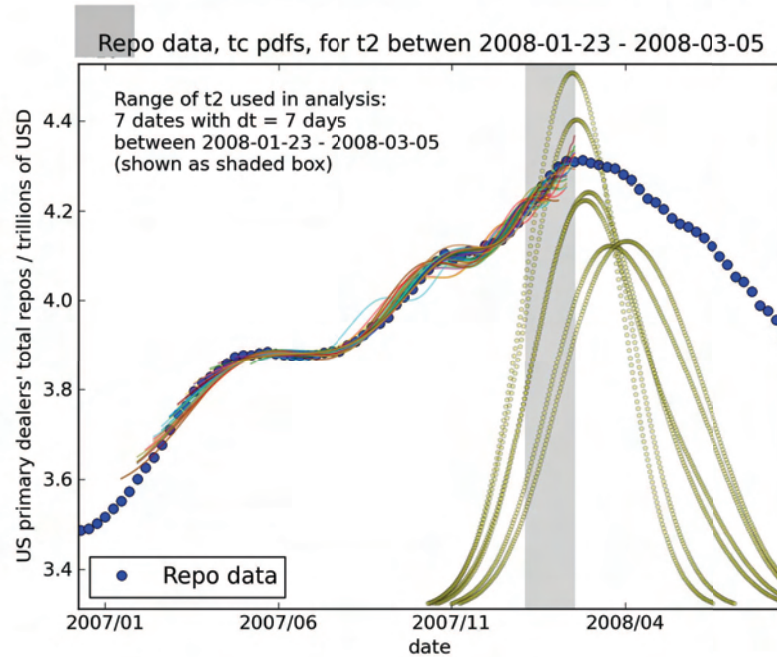

Figure 5.3: We vary the end of the window t_2 within the grey area and show the probability density of the most probable time of crash t_c for each of these t_2, as the bell-shaped curves with open circle symbols.

5.3   Conclusion

In this chapter, we discussed how leverage can influence the liquidity of the market and used the observation that a dramatic decrease of leverage coincided with the recent financial crisis. The market size of repos is a very good proxy for the overall leverage of the market. We used the JLS model of log-periodic power law dynamics on an ensemble of intervals from a time series of the total repos market size and found that the range of the most probable times of crash t_c as forecast by the fits is consistent with the observed peak and subsequent crash.

In conclusion, this chapter contributes further to our understanding of the development of financial instabilities, in providing the first quantitative study of a

leverage variable, that complements other pieces of evidence on the development of bubbles in equities (ICT and Biotech from 1995 to 2001), real-estate until mid-2006 in the USA, equities again until October 2007, commodities including cereals and precious metals as well as oil, which have been referenced by Sornette and Woodard [140].

6

Conclusion and Outlook

6.1   Summary of this thesis

The main focus of this thesis has been modeling and forecasting of bubbles and extreme events in financial systems based on the Johansen-Ledoit-Sornette (JLS) model. We discussed why the JLS model is effective in explaining the causes and dynamics of financial bubbles and followed extreme events, and how it functions as a flexible tool to detect bubbles. The present theoretical status and some calibration issues concerning the JLS model are also discussed. We have provided a guide to the advances that have punctuated the development of tests of the JLS model performed on a variety of financial markets during the last decade. We can say that the development of new versions and of methodological improvements have paralleled the occurrence of several major market crises, which have served as inspirations and catalyzers of the research. We believe that the field of financial bubble diagnosis is progressively maturing and we foresee a close future when it could become operational to help decision makers alleviate the consequences of excess leverage leading to severe market dysfunctions.

The JLS model has been theoretically and empirically extended. The generalized JLS models with the function of estimating the fundamental value of a stock, the nonlinearity of crash dynamics and risk diversification of a market have been developed and tested with famous historical bubble examples.

To show the improvement of the generalized JLS models which infer the fundamental value and crash nonlinearity, three historical bubbles from different markets were tested. The results suggest that the new models perform well in describing bubbles, predicting crash time and estimating fundamental value and the crash nonlinearity. The performance of the new models is tested also under the Gaussian and non-Gaussian residual assumptions. Under the Gaussian residual assumption, nested hypothesis testing with the Wilks statistics is used and the p-values suggest models with more parameters are necessary. Under the non-Gaussian residual assumption, we use a bootstrap method to get type I and II errors. Those tests confirm that these generalized JLS models provide useful improvements over the standard JLS model.

A new model that combines the Zipf factor embodying the risk due to lack of diversification with the JLS model is also introduced. The new model keeps all the dynamical characteristics of a bubble described in the JLS model. In addition, the new model can also provide information about the concentration of stock gains over time from the knowledge of the Zipf factor. This new information is very helpful to understand the risk diversification and to explain investors' behavior during the bubble generation. We have applied this new model to two famous Chinese stock bubbles and found it provides sensible explanation for the diversification risk observed during these two bubbles.

Furthermore, we successfully extended the standard JLS model by claiming that negative bubbles are in general predictably associated with large rebounds or rallies, which are the mirror images of the crashes terminating standard bubbles. The aggregation of thousands of calibrations in running windows of the negative bubble model on financial data has been performed using a general pattern recognition method, leading to the calculation of a rebound alarm index. Performance metrics have been presented in the form of error diagrams, of Bayesian inference to determine the probability of rebounds and of trading strategies derived from the rebound alarm index dynamics. These different measures suggest that the rebound alarm index provides genuine information and predictive ability. The implemented trading strategies outperform randomly chosen portfolios constructed with the same statistical characteristics. This suggests that financial markets may be characterized by transient positive feedbacks leading to accelerated drawdowns, which develop

similarly to but as mirror images of upward accelerating bubbles. Our key result is that these negative bubbles have been shown to be predictably associated with large rebounds or rallies.

We further detected financial crashes and rebounds in ten major global stock indices systematically using this method. A rebound/crash alarm index was calculated to indicate the probability of a rebound/crash for a certain time. The performance was checked quantitatively by error diagrams and trading strategies. The results from error diagrams indicate that our method in detecting crashes and rebounds performs better than chance and confirm that the new method is very powerful and robust in the prediction of crashes and rebounds in financial markets. Our long-short trading strategies based on the crash and rebound alarm index perform better than the benchmarks (buy and hold strategy with the same exposure as the average exposure of our strategies) in seven out of ten indices. Highly volatile periods are observed in the indices of which the long-short trading strategy fails to surpass the benchmark. By construction of the alarm index and the fact that highly volatile periods are not coherent with bullish markets, we claim that we should ignore the rebound alarm index during such volatile periods. This statement has been supported by the short strategy which only considers the crash alarm index. Thus, our trading strategies confirm again that the alarm index has a strong ability in detecting rebounds and crashes in the financial markets.

Finally, a successful ex-post prediction of the 2008 financial crash through analysis of the US repurchase agreements market with the JLS model was also presented. We discussed how leverage can influence the liquidity of the market and used the observation that a dramatic decrease of leverage coincided with the recent financial crisis. The market size of repos is a very good proxy for the overall leverage of the market. We used the JLS model of log-periodic power law dynamics on an ensemble of intervals from a time series of the total repos market size and found that the range of the most probable times of crash t_c as forecast by the fits is consistent with the observed peak and subsequent crash. This work contributes further to our understanding of the development of financial instabilities, in providing the first quantitative study of a leverage variable, that complements other pieces of evidence on the development of bubbles in equities, real-estate and commodities.

6.2   Outlook

Up to now, we have talked much about the JLS model, which says that imitation and herding behavior has direct influence on the stock price: the stock price dynamics follows a log-periodic power law in a bubble regime. This means that the JLS model only studies part of human behavior and describes only part of stock price dynamics. Thus, there are two natural extensions of the current research. First, studies on imitation and herding behavior is a small window from which we can go further to understand human behaviors. Second, we can explore other dynamics of stock markets and their relation to human behavior.

6.2.1   Future research on human dynamics

Although varying widely, human behavior still has some intrinsic characteristics which can be detected and formulated quantitatively. The JLS model is one of the successful models to describe the cumulative characteristics of human behaviors. The model provides a quantitative description of imitation and herding behavior which is log-periodic power law. However, most of the characteristics have not been well described or even studied until now. In this sense, future research on human behaviors is very important and this is the direction I want to pursue after my doctoral studies. In this section, I will first give a brief literature review on current human dynamics research, then discuss some potential topics in the future research of human dynamics by using the unique data set of mobile phone calls, texts and geolocations from the China Telecommunications Corporation.

Literature review

The bursty nature of human behavior as a consequence of a decision-based queuing process was pointed out by Barabási in 2005 [141]. When individuals execute tasks based on some perceived priority, the distribution of the timing of the tasks will be heavy tailed, with most tasks being rapidly executed while a few experiencing very long waiting times. This paper helped to motivate and guide an important facet of complexity research: human dynamics. The series of papers afterwards showed empirical research that power law distributed waiting times can be observed in many different areas, such as telephone and letter communication [142, 143, 144, 145], web browsing[146, 147, 148], online movie and music services [149, 150] and online

game behavior [151], to name a few. Almost all of these empirical studies sharply contradict the traditional hypothesis that assumes that human dynamics can be approximated by a Poisson process.

Following [141], Vázquez et al. studied the characteristics of this decision-based queuing process systematically [152, 153] and other researchers improved this process later [154, 155, 156, 157]. However, since human behavior is highly complex, many types of behavior cannot be explained by a decision-based queuing process. Therefore, many other models have been proposed, such as the self-attracting walk model [147], the adaptive interest model [158], the memory impact model [159], the seasonal inter-event time model [160] and the cascading nonhomogeneous Poisson process [161]. Recently, Jo et al. proposed that the inhomogeneity of task handling strategies of humans is the real origin of the power law distributed inter-event waiting time [162].

Compared to the temporal regularity of human dynamics, the research on human *spatial* dynamics (mobility patterns) was started quite late due to lack of data. In 2006, Brockmann et al. first introduced this topic by analyzing the circulation laws of bank notes [163]. They found that the distributions of both the travel distance and the remaining time in a small spatially confined region follow power laws with exponent 1.6. However, the circulation of bank notes is not a direct reflection of the individual travel behavior as it is difficult to know how many people make contributions to the transportation of a bank note. Starting from 2008, Barabási and his group promoted the idea that human mobility patterns can be studied based on the trajectory of mobile phone users. They found that humans follow simple reproducible patterns and that the displacements follow a truncated power law [164]. Later they pointed out that human mobility has strong regularity and predictability [165]. All of these results show that the Lévy process and the continuous time random walk model, for instance, are not enough to describe human mobility.

Theories of human mobility have been proposed by many researchers. Song et al. summarized two principles of human trajectories: new location exploration and a tendency to return to familiar locations [165, 166, 167]. They built a statistically self-consistent microscopic model for individual human mobility by adding these two principles to a continuous time random walk model. Han et al. think that the hierarchy of a transportation network leads to power law distributed human mobility

directly [168]. Hu et al. proposed that the origin of this scaling law should be due to the demand of entropy maximization [169] while Yan et al. pointed out that the spatial extension of human activity is highly dependent on the work distance and the velocity of the mobility. Therefore, a single human mobility model based on a random walk framework is not enough [170].

Empirical and theoretical studies on human dynamics in a big city

In spite of the above work, empirical studies of human mobility in big cities are still lacking. A modern megacity is usually identified with high population density and high mobility over a large spatial scale. Such specific characteristics may lead to human dynamics that is very different from that found in the general populations used in the previous studies. Also, most of the above research is based on data from developed countries, where transportation is highly developed and more related to private cars. However, transportation in Shanghai is a mixture of subways, buses, bicycles and private cars. Because of these two important differences (city size and modes of transportation), the case study on the Shanghai mobile phone data is new and potentially relevant to ever-growing city sizes worldwide.

Empirically, Jiang [171] found that both inter-event waiting times and individual mobility derived from the Shanghai mobile phone data follow a Weibull distribution, not a power law distribution, as shown in Fig. 6.1. Here, an event is defined as a phone call between any two people in the dataset and a waiting time is, then, simply the time between the beginning of successive phone calls between any two people.
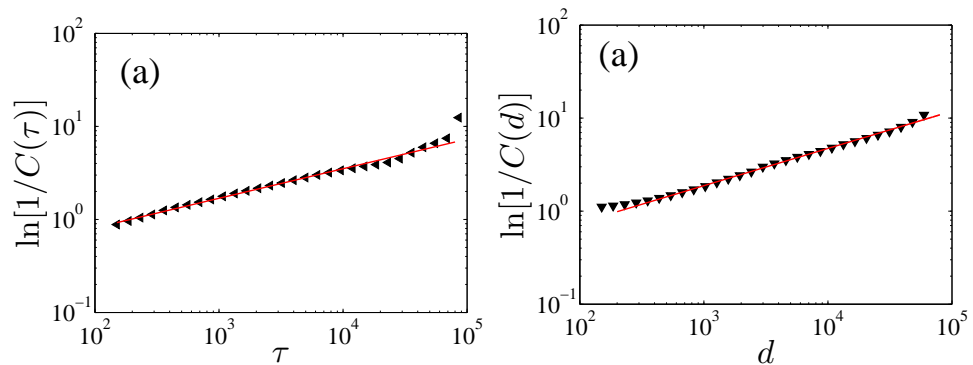

Figure 6.1: Statistics of human dynamics based on Shanghai mobile phone data. (left) The inter-event waiting time follows a Weibull distribution. (right) The individual travel distance also follows a Weibull distribution.

Theoretically, current human dynamics models lead to power law distributed waiting times and or truncated power law distributed mobility patterns. If our final results from these initial empirical studies show that the Weibull distribution, instead of power law or truncated power law, better characterizes the Shanghai mobile phone data, then new models should be introduced. A Weibull distribution implies that the cumulative distribution function $C(x) = 1 - \exp{-(x/\lambda)^k}$, where λ is the scale factor and k is the shape factor. We feel that such a result will be based on the diversity of travel modes (subways, bicycles, cars, foot), something that is not considered in current models. Jiang and I will complete this preliminary research and produce a thorough and credible model for this empirical study.

Group behavior

Almost all the current research on human dynamics focuses on individuals and their patterns. How *people interact with other people*, though, is also very important. Therefore, I would like to explore group mobility patterns by empirically calculating the distribution of the physical distance between users when interactions (i.e., phone calls) occur and then explain the possible origins behind the empirical findings.

As a bonus, with the timestamped geolocation data, we could track the dynamics of population density of phone owners within Shanghai. That is, we could observe the daily waves of human population moving into and out of a specified area in such a large city and see the differences in these dynamics between workdays and weekends.

Epidemics

Scientists would like to develop epidemic models to understand the propagation process of epidemics and, hopefully, to propose efficient policy to control and *slow down* the spread of disease. This is in contrast to studies on information propagation, for instance, that have the opposite goal of discovering the most efficient strategy to *accelerate* the diffusion of the information.

Until now, the development of epidemic models has gone through three stages: the classical models, models based on complex networks and models based on human mobility. In the first stage, the models assume that the disease propagates in a simple uniform network, where each individual has the same probability to get the

disease. In the second stage, the population structure is set as a complex network. This different setting makes for two major changes. The first is that the scale free network has no propagation threshold, i.e. the minimum propagation probability of the disease is zero. In this kind of network, a very small propagation probability can lead to a rapid burst of disease in the whole system [172]. The second change is that a small world network enhances the local propagation and rapid diffusion of the disease [173]. Some researchers also studied epidemics on actual human networks [174, 175] and time dependent networks [176]. Recently, the self-excited conditional Hawkes Poisson process has been studied as a model for the dynamics underlying an epidemic process [177, 178, 179]. However, neither the classical models nor the models based on the complex networks can accurately describe epidemics in the real world, probably because they do not consider human mobility in the model [180]. Thus, epidemic models based on human mobility have been recently proposed [181, 182, 183].

We are now experiencing the transition from the second stage to the third stage of epidemic modeling. Research on epidemics based on human mobility is just beginning. After (hopefully) understanding mobility patterns in a big city and some of the characteristics of human interactions, I would use these results to study epidemics based on the structure and mobility patterns of big cities by analyzing features of a spreading process in such a high population density city like Shanghai. I would hope to find an efficient strategy to inhibit disease propagation. In our growing, more connected, 'smaller' world, this topic is very important.

6.2.2 Interaction between open source information and stock market behavior

Another natural extension of the JLS model is to study the interaction between open source information and stock market behavior. By analyzing the open source information, which is a direct reflect of human behaviors, we may obtain more deep insight in stock dynamics.

In finance, the price of an asset is theoretically the discounted cash flow of future income. A stock price, then, should be the summation of the future discounted dividends. These future dividends are highly related to investors' current expectation of the future, which in turn is dependent on current information (i.e., news,

fundamentals, etc.). Therefore, current information plays an important role in asset pricing, specifically in stock returns. Most previous research focuses on the relationship between stock returns and *traditional information*, such as news from stock exchanges [184], news from news providing company [185], news from newspapers [186, 187] and firm-specific news [188].

In the past decades, the internet has become an important platform for publishing and receiving vast amounts and types of information. A huge amount of *open source information* is generated (and available) through the internet. A natural question is then: is open source information related to stock returns?

To answer this question, Tumarkin and Whitelaw analyzed the correlation between returns of 25 major stocks and data from the Raging Bull message board (a forum with discussions and commentary that focuses on stocks and mutual funds), concluding that open source information is mainly noise [189]. Later, Antweiler and Frank developed a bullish index of the messages using computational linguistics with the Raging Bull data and daily price data from Yahoo! Finance [190]. In contrast to Tumarkin and Whitelaw, their conclusion is that the relationship between the bullish index and stock returns is statistically significant but economically small. Recently, Preis and Stanley [191] studied the correlation between Google trends data and the S&P 500 index. They found a significant correlation between the changes in weekly transaction volume of the S&P 500 index and the changes in volume of weekly Google searches for constituent company names. However, they also found that the weekly price changes of the S&P 500 index are not correlated to the weekly search volume changes.

Though these relations were demonstrated, there are a few shortcomings. Specifically, the bullish index and the Google trend index are examples of proprietary black boxes whose derivations are not publicly known. Furthermore, due to the high level of market liquidity, the two correlations are very sensitive to the frequency of the data (i.e, hourly, daily, weekly, etc.). From an Efficient Market Hypothesis point of view, prices are updated almost as soon as a new piece of information is available. Therefore, the weekly data used in the above two studies is too coarse to fully measure correlations between new information and price changes. Finally, these studies were made on a small subset of available stocks [189, 190] or a single index [191]. Further tests on a larger data set would help in understanding this issue.

With the above discussion in mind, I would ask: is there a direct correlation between open source information and stock returns and/or volumes on daily or sub-day time scales? I would try to answer this fundamental question using a data set which addresses the problems mentioned above. I will use data from Baidu Tieba, which is the largest Chinese communication platform provided by the Chinese search engine Baidu (`http://www.baidu.com`). I have all posts from the stock forums of Baidu Tieba for the past five years. Within this data, the general 'Stock' channel has approximately 2 million posts and, further, each of the approximately 2,000 separate channels for all publicly traded Chinese stock has about 3,000 to 100,000 posts (per channel). Thus, this data set is complete in that we can test each individual Chinese stock. This data set is valuable also because of its size and time span and, most importantly, because it contains the timestamp (down to the minute) of each post which enables a much higher resolution test.

My preliminary result in Fig. 6.2 shows that both the daily price changes and the daily volume changes of the Shanghai Composite Index are strongly correlated to the amount of open source information (proxied by total number of posts per day in the 'Stock' channel). The result for the correlation of changes in transaction volume with changes in post volume is consistent with [191]. More importantly, we see a strong correlation between price changes and the open source information, which is not found in [191]. This result for the Baidu data is probably due to its higher resolution time scale (daily) and that the Google search data is only available on a weekly time scale. Coarse graining the search volume to weekly 'washes out' any correlation with daily price changes.

The above research only focuses on the correlation between the open source information and the stock price or volume changes. A more important question is: which factor is leading in this correlation? If the open source information is leading the stock changes, then we could conclude that information changes the investors' expectation of the asset and thus changes the stock prices and trading volumes. In contrast, if the stock changes lead the information (more likely), then this implies that the information (discussion) is mainly a reaction to stock changes.

To answer this question, I propose the null hypothesis that price movements (positive or negative) appear first followed by the reaction of online discussion/search. I base this on the simple assumption that large traders who move markets are not
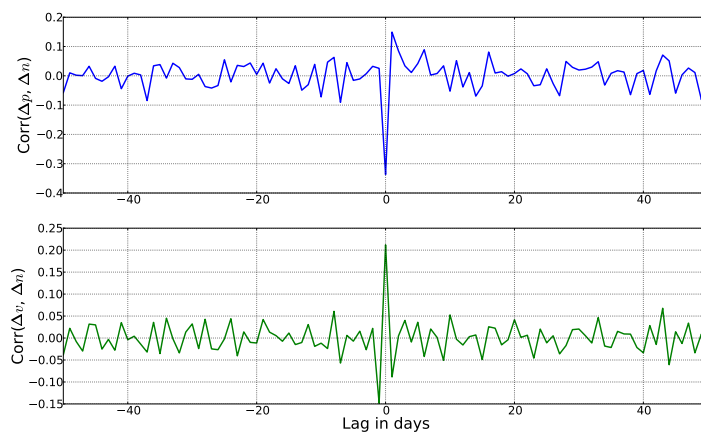
Figure 6.2: Correlation between the amount of the open source information and the stock changes. (upper) Correlation between the change in total number of daily posts in the 'Stock' channel of Baidu Tieba Δn and the Shanghai Composite Index daily return Δp. It shows a strong negative correlation at zero lag, which is an evidence of asymmetric reaction of people on good and bad news. (lower) Correlation between the change in total number of daily posts in the 'Stock' channel of Baidu Tieba Δn and the Shanghai Composite Index daily volume changes Δv. There is a strong correlation at zero lag, indicating the tracking of much discussion with much trading volume. Signals at noise levels in both figures continue for ± 100 days. Negative values of lag indicate Δn is leading.

discussing their stock picks on online public forums. If this null hypothesis is not supported (that is, if online discussion does not lag price movements) then the value of the discussion data could be tested by adding an 'open source information factor' to a simple autoregressive moving average model, which predicts the future prices (volumes) by combining the past price (volume) information. Whether the factor adds anything useful or not can be then tested by some model selection procedure (such as Akaike information criterion).

Bibliography

[1] International Monetary Fund executive summary, `http://www.imf.org/External/Pubs/FT/GFSR/2009/01/pdf/summary.pdf` (2009).

[2] M. Chadbourn, Five banks are seized, raising U.S. failures this year to 45, Bloomberg, `http://www.bloomberg.com/apps/news?pid=newsarchive&sid=aCbHA.m7rikc` (2009).

[3] J. Goldstein, New York Fed chief: We should "try to identify bubbles", National Public Radio, `http://www.npr.org/blogs/money/2010/04/the_friday_podcast.html` (2010).

[4] J. Galbraith, The great crash, 1929, Mariner Books, 1997.

[5] D. Sornette, Why Stock Markets Crash (Critical Events in Complex Financial Systems), Princeton University Press, 2003.

[6] C. Kindleberger, Manias, Panics and Crashes: A History of Financial Crises, 4th Edition, Wiley, 2000.

[7] D. Sornette, Critical market crashes, Physics Reports 378 (2003) 1–98.

[8] T. Lux, D. Sornette, On rational bubbles and fat tails, Journal of Money, Credit and Banking 34 (3) (2002) 589–610.

[9] R. Gurkaynak, Econometric tests of asset price bubbles: Taking stock, Journal of Economic Surveys 22 (1) (2008) 166–186.

[10] H. P. H. Nusteling, Welvaart en werkgelegenheid in Amsterdam, 1540-1860: Een relaas over demografie, economie en sociale politiek van een wereldstad, dutch Edition, Bataafsche Leeuw, 1985.

[11] E. Thompson, The tulip mania: Fact or artifact?, Public Choice 130 (1–2) (2007) 99–114.

[12] M. C. Taylor, Confidence Games, University of Chicago Press, 2004.

[13] J. B. De Long, A. Shleifer, The bubble of 1929: Evidence from Closed-End funds, NBER Working Paper No. 3523, `http://econpapers.repec.org/paper/nbrnberwo/3523.htm` (1990).

[14] Stock market crash of 1929, britannica Concise Encyclopedia, `http://www.britannica.com/EBchecked/topic/566754/stock-market-crash-of-1929`.

[15] K. E. Case, R. J. Shiller, Is there a bubble in the housing market?, Brookings Papers on Economic Activity 2 (2003) 299–362.

[16] M. J. Mauboussin, Rational Exuberance?, Equity research, Credit Suisse First Boston, `http://www.capatcolumbia.com/Articles/Reports/Grl_235__0.pdf` (Janurary 1999).

[17] A. Greenspan, Federal Reserve's semiannual monetary policy report, before the Committee on Banking, Housing, and Urban Affairs, U.S. Senate (February 1997).

[18] R. J. Shiller, Irrational Exuberance, 2nd Edition, Princeton University Press, 2005.

[19] J. Lintner, The aggregation of investors' diverse judgments and preferences in purely competitive security markets, Journal of Financial and Quantitative Analysis 4 (1969) 347–400.

[20] E. Miller, Risk, uncertainty and divergence of opinion, Journal of Finance 32 (1977) 1151–1168.

[21] M. Harrison, D. Kreps, Speculative investor behavior in a stock market with heterogeneous expectations, Quarterly Journal of Economics 92 (1978) 323–336.

[22] R. Jarrow, Heterogeneous expectations, restrictions on short sales, and equilibrium asset prices, Journal of Finance 35 (1980) 1105–1113.

[23] J. Chen, H. Hong, J. C. Stein, Breadth of ownership and stock returns, Journal of Financial Economics 66 (2002) 171–205.

[24] J. Scheinkman, W. Xiong, Overconfidence and speculative bubbles, Journal of Political Economy 111 (2003) 1183–1219.

[25] D. Duffie, N. Garleanu, L. H. Pedersen, Securities lending, shorting, and pricing, Journal of Financial Economics 66 (2002) 307–339.

[26] J. B. DeLong, A. Shleifer, L. H. Summers, R. J. Waldmann, Noise trader risk in financial markets, Journal of Political Economy 98(4) (1990) 703–738.

[27] N. Barberis, A. Shleifer, R. Vishny, A model of investor sentiment, Journal of Financial Economics 49(3) (1998) 307–343.

[28] K. Daniel, D. Hirshleifer, A. Subrahmanyam, Investor psychology and security market underand overreactions, Journal of Finance 53 (1998) 1839–1885.

[29] H. Hong, J. D. Kubik, J. C. Stein, Thy neighbor's portfolio: Word-of-mouth effects in the holdings and trades of money managers, Journal of Finance 60 (2005) 2801–2824.

[30] W. M. D. Bondt, R. Thaler, Does the stock market overreact?, Journal of Finance 40 (1985) 793–805.

[31] N. Jegadeesh, S. Titman, Returns to buying winners and selling losers: Implications for stock market effciency, Journal of Finance 48(1) (1993) 65–91.

[32] N. Jegadeesh, S. Titman, Profitability of momentum strategies: An evaluation of alternative explanations, Journal of Finance 54 (2001) 699–720.

[33] D. Abreu, M. K. Brunnermeier, Bubbles and crashes, Econometrica 71(1) (2003) 173–204.

[34] M. K. Brunnermeier, S. Nagel, Hedge funds and the technology bubble, Journal of Finance 59 (2004) 2013–2040.

[35] T. Kaizoji, D. Sornette, Market bubbles and crashes, in: the Encyclopedia of Quantitative Finance, Wiley, 2009, long version at `http://arxiv.org/abs/0812.2449`.

[36] U. Bhattacharya, X. Yu, The causes and consequences of recent financial market bubbles: An introduction, Review of Financial Studies 21 (1) (2008) 3–10.

[37] A. Greenspan, Economic volatility, remarks at a symposium sponsored by the Federal Reserve Bank of Kansas City, Jackson Hole, Wyoming, `http://www.federalreserve.gov/boarddocs/speeches/2002/20020830/` (August 2002).

[38] A. Goriely, C. Hyde, Necessary and sufficient conditions for finite time singularities in ordinary differential equations, Journal of Differential equations 161 (2000) 422–448.

[39] S. Gluzman, D. Sornette, Classification of possible finite-time singularities by functional renormalization, Physical Review E 6601 (2002) 016134.

[40] A. Johansen, D. Sornette, Finite-time singularity in the dynamics of the world population and economic indices, Physica A 294 (3–4) (2001) 465–502.

[41] S. Sammis, D. Sornette, Positive feedback, memory and the predictability of earthquakes, Proceedings of the National Academy of Sciences USA 99 (SUPP1) (2002) 2501–2508.

[42] D. Sornette, H. Takayasu, W.-X. Zhou, Finite-time singularity signature of hyperinflation, Physica A 325 (2003) 492–506.

[43] A. Johansen, D. Sornette, Shocks, crashes and bubbles in financial markets, Brussels Economic Review (Cahiers economiques de Bruxelles) 53(2) (2010) 201–253.

[44] D. Sornette, Discrete scale invariance and complex dimensions, Physics Reports 297 (5) (1998) 239–270.

[45] O. Blanchard, M. Watson, Bubbles, rational expectations and speculative markets, NBER Working Paper 0945, `http://papers.ssrn.com/sol3/papers.cfm?abstract_id=226909` (1983).

[46] A. Johansen, D. Sornette, Critical crashes, Risk 12 (1) (1999) 91–94.

[47] A. Johansen, O. Ledoit, D. Sornette, Crashes as critical points, International Journal of Theoretical and Applied Finance 3 (2000) 219–255.

[48] A. Johansen, D. Sornette, O. Ledoit, Predicting financial crashes using discrete scale invariance, Journal of Risk 1 (4) (1999) 5–32.

[49] D. Sornette, R. Woodard, W.-X. Zhou, The 2006-2008 oil bubble: Evidence of speculation and prediction, Physica A 388 (2009) 1571–1576.

[50] Z.-Q. Jiang, W.-X. Zhou, D. Sornette, R. Woodard, K. Bastiaensen, P. Cauwels, Bubble diagnosis and prediction of the 2005-2007 and 2008-2009 Chinese stock market bubbles, Journal of Economic Behavior and Organization 74 (2010) 149–162.

[51] W.-X. Zhou, D. Sornette, Analysis of the real estate market in Las Vegas: Bubble, seasonal patterns, and prediction of the CSW indexes, Physica A 387 (2008) 243–260.

[52] W.-X. Zhou, D. Sornette, 2000-2003 real estate bubble in the UK but not in the USA, Physica A 329 (2003) 249–263.

[53] W.-X. Zhou, D. Sornette, Is there a real estate bubble in the US?, Physica A 361 (2006) 297–308.

[54] A. Johansen, D. Sornette, Financial "anti-bubbles": log-periodicity in gold and Nikkei collapses, International Journal of Modern Physics C 10 (4) (1999) 563–575.

[55] D. Sornette, W.-X. Zhou, The US 2000-2002 market descent: How much longer and deeper?, Quantitative Finance 2 (6) (2002) 468–481.

[56] N. Vandewalle, M. Ausloos, P. Boveroux, A. Minguet, Visualizing the log-periodic pattern before crashes, European Physics Journal B 9 (1999) 355–359.

[57] A. Clark, Evidence of log-periodicity in corporate bond spreads, Physica A 338 (2004) 585–595.

[58] P. Gnaciński, D. Makowiec, Another type of log-periodic oscillations on Polish stock market, Physica A 344 (2004) 322–325.

[59] M. Bartolozzi, S. Drożdż, D. Leinweber, J. Speth, A. Thomas, Self-similar log-periodic structures in Western stock markets from 2000, International Journal of Modern Physics C 16 (2005) 1347–1361.

[60] R. Matsushita, S. da Silva, A. Figueiredo, I. Gleria, Log-periodic crashes revisited, Physica A 364 (2006) 331–335.

[61] S. Drożdż, J. Kwapień, P. Oświecimka, J. Speth, Current log-periodic view on future world market development, Acta Physica Polonica A 114 (2008) 539–546.

[62] W.-X. Zhou, D. Sornette, A case study of speculative financial bubbles in the South African stock market 2003-2006, Physica A 388 (2009) 869–880.

[63] W. Yan, R. Woodard, D. Sornette, Leverage bubble, Physica A, forthcoming. `http://arxiv.org/abs/1011.0458` (2011).

[64] D. Sornette, R. Woodard, M. Fedorovsky, S. Reimann, H. Woodard, W.-X. Zhou, The financial bubble experiment: Advanced diagnostics and forecasts of bubble terminations (the financial crisis observatory), `http://arxiv.org/abs/0911.0454` (2010).

[65] D. Sornette, R. Woodard, M. Fedorovsky, S. Reimann, H. Woodard, W.-X. Zhou, The financial bubble experiment: Advanced diagnostics and forecasts of bubble terminations volume II (master document), `http://arxiv.org/abs/1005.5675` (2010).

[66] R. Woodard, D. Sornette, M. Fedorovsky, The financial bubble experiment: Advanced diagnostics and forecasts of bubble terminations volume III (beginning of experiment + post-mortem analysis), `http://arxiv.org/abs/1011.2882` (2011).

[67] B. G. Malkiel, A random walk down Wall Street: The best and latest investment advice money can buy, 6th Edition, W. W. Norton & Company, 1996.

[68] A. Damasio, Descartes' Error: Emotion, Reason, and the Human Brain, Harper Perennial, 1995.

[69] C. F. Camerer, Strategizing in the brain, Science 300 (2003) 1673–1675.

[70] H. Gintis, S.Bowles, R. Boyd, E. Fehr (Eds.), Moral Sentiments and Material Interests — The Foundations of Cooperation in Economic Life, MIT Press, 2005.

[71] R. Dunbar, The social brain hypothesis, Evolutionary Anthropology 6 (1998) 178–190.

[72] D. Sornette, J. Andersen, A nonlinear super-exponential rational model of speculative financial bubbles, International Journal of Modern Physics C 13 (2) (2002) 171–188.

[73] K. Ide, D. Sornette, Oscillatory finite-time singularities in finance, population and rupture, Physica A 307 (2002) 63–106.

[74] A. Corcos, J.-P. Eckmann, A. Malaspinas, Y. Malevergne, D. Sornette, Imitation and contrarian behavior: Hyperbolic bubbles, crashes and chaos, Quantitative Finance 2 (2002) 264–281.

[75] J. V. Andersen, D. Sornette, Fearless versus fearful speculative financial bubbles, Physica A 337 (1–2) (2004) 565–585.

[76] H. Fogedby, Damped finite-time-singularity driven by noise, Physical Review E 68 (2003) 051105.

[77] H. Fogedby, V. Poukaradzez, Power laws and stretched exponentials in a noisy finite time singularity model, Physical Review E 66 (2002) 021103.

[78] L. Lin, R. Ren, D. Sornette, A consistent model of 'explorative' financial bubbles with mean-reversing residuals, `http://arxiv.org/abs/0905.0128` (2009).

[79] L. Lin, D. Sornette, Diagnostics of rational expectation financial bubbles with stochastic mean-reverting termination times, `http://arxiv.org/abs/0911.1921` (2009).

[80] J. Farmer, Market force, ecology and evolution, Industrial and Corporate Change 11 (5) (2002) 895–953.

[81] W.-X. Zhou, D. Sornette, R. Hill, R. Dunbar, Discrete hierarchical organization of social group sizes, Proceedings of the Royal Society B 272 (2005) 439–444.

[82] D. Sornette, A. Johansen, Large financial crashes, Physica A 245 (1997) 411–422.

[83] H.-C. G. van Bothmer, C. Meister, Predicting critical crashes? A new restriction for the free variables, Physica A 320 (2003) 539–547.

[84] D. Cvijović, J. Klinowski, Taboo search: An approach to the multiple minima problem, Science 267 (5188) (1995) 664–666.

[85] K. Levenberg, A method for the solution of certain non-linear problems in least squares, Quarterly Journal of Applied Mathematics II 2 (1944) 164–168.

[86] D. W. Marquardt, An algorithm for least-squares estimation of nonlinear parameters, Journal of the Society for Industrial and Applied Mathematics 11 (2) (1963) 431–441.

[87] J. Feigenbaum, A statistical analysis of log-periodic precursors to financial crashes, Quantitative Finance 1 (2001) 346–360.

[88] G. Chang, J. Feigenbaum, A bayesian analysis of log-periodic precursors to financial crashes, Quantitative Finance 6 (2008) 15–36.

[89] G. Chang, J. Feigenbaum, Detecting log-periodicity in a regime-switching model of stock returns, Quantitative Finance 8 (2008) 723–738.

[90] J. Fry, Statistical modelling of financial crashes, Ph.D. thesis, University of Sheffield (2007).

[91] D. Fantazzini, P. Geraskin, Everything you always wanted to know about log periodic power laws for bubble modeling but were afraid to ask, European Journal of Finance, forthcoming (2011).

[92] D. Bree, N. L. Joseph, Fitting the log periodic power law to financial crashes: a critical analysis, `http://arxiv.org/abs/1002.2010` (2010).

[93] D. Bree, D. Challet, P. P. Peirano, Prediction accuracy and sloppiness of log-periodic functions, `http://arxiv.org/abs/1006.2010` (2010).

[94] D. Sornette, W.-X. Zhou, Predictability of large future changes in major financial indices, International Journal of Forecasting 22 (2006) 153–168.

[95] W. Yan, R. Woodard, D. Sornette, Diagnosis and prediction of market rebounds in financial markets, `http://arxiv.org/abs/1001.0265` (2010).

[96] W. Yan, R. Woodard, D. Sornette, Diagnosis and prediction of tipping points in financial markets: Crashes and rebounds, Physics Procedia 3 (2010) 1641–1657.

[97] W. Yan, R. Rebib, R. Woodard, D. Sornette, Detection of crashes and rebounds in major equity markets, in preparation (2011).

[98] D. Sornette, Dragon-kings, black swans and the prediction of crises, International Journal of Terraspace Science and Engineering 2 (1) (2009) 1–18.

[99] D. Johansen, A.and Sornette, Evaluation of the quantitative prediction of a trend reversal on the Japanese stock market in 1999, International Journal of Modern Physics C 11 (2) (2000) 359–364.

[100] W.-X. Zhou, D. Sornette, Testing the stability of the 2000-2003 US stock market "antibubble", Physica A 348 (2005) 428–452.

[101] S. Gluzman, D. Sornette, Log-periodic route to fractal functions, Physical Review E 65 (2002) 036142.

[102] W.-X. Zhou, D. Sornette, Renormalization group analysis of the 2000-2002 anti-bubble in the US S&P 500 index: Explanation of the hierarchy of 5 crashes and prediction, Physica A 330 (2003) 584–604.

[103] W.-X. Zhou, D. Sornette, Evidence of intermittent cascades from discrete hierarchical dissipation in turbulence, Physica D 165 (2002) 94–125.

[104] D. Sornette, W.-X. Zhou, Evidence of fueling of the 2000 new economy bubble by foreign capital inflow: Implications for the future of the US economy and its stock market, Physica A 332 (6) (2004) 412–440.

[105] W.-X. Zhou, D. Sornette, Fundamental factors versus herding in the 2000-2005 US stock market and prediction, Physica A 360 (2009) 459–483.

[106] W. Yan, R. Woodard, D. Sornette, Role of diversification risk in financial bubbles, `http://arxiv.org/abs/1107.0838` (2011).

[107] W.-X. Zhou, D. Sornette, Non-parametric analyses of log-periodic precursors to financial crashes, International Journal of Modern Physics C 14 (8) (2003) 1107–1126.

[108] W. Yan, R. Woodard, D. Sornette, Inferring fundamental value and crash non-linearity from bubble calibration, quantitative Finance, forthcoming. `http://arxiv.org/abs/1011.5343` (2011).

[109] V. Filimonov, D. Sornette, A stable and robust calibration scheme of the log-periodic power law model, in preparation (2011).

[110] Y. Huang, A. Johansen, M. W. Lee, H. Saleur, D. Sornette, Artifactual log-periodicity in finite-size data: Relevance for earthquake aftershocks, Journal of Geophysical Research 105, (2000) 25451–25471.

[111] W.-X. Zhou, D. Sornette, Statistical significance of periodicity and log-periodicity with heavy-tailed correlated noise, International Journal of Modern Physics C 13(2) (2002) 137–170.

[112] Q. Li, J. S. Racine, Nonparametric Econometrics: Theory and Practice, Princeton University Press, 2006.

[113] L. Gazola, C. Fernades, A. Pizzinga, R. Riera, The log-periodic-AR(1)-GARCH(1,1) model of financial crashes, European Physics Journal B 61 (2008) 355–362.

[114] R. Barro, E. Fama, D. Fischel, R. R. A.H. Meltzer, L. Telser, Black monday and the future of financial markets, in: J. R.W. Kamphuis, R. Kormendi, J. Watson (Eds.), Mid American Institute for Public Policy Research, Richard D Irwin, 1989.

[115] C. Granger, P. Newbold, Spurious regressions in econometrics, Journal of Econometrics 2 (1974) 111–120.

[116] P. Phillips, Understanding spurious regressions in econometrics, Journal of Econometrics 31 (1986) 311–340.

[117] J. Knight, S. Satchell, Linear Factor Models in Finance, 1st Edition, Butterworth-Heinemann, 2005.

[118] E. F. Fama, R. F. Kenneth, The cross-section of expected stock returns, Journal of Finance 47 (1992) 427–465.

[119] E. F. Fama, R. F. Kenneth, Common risk factors in the returns on stocks and bonds, Journal of Financial Economics 33 (1993) 3–56.

[120] E. F. Fama, R. F. Kenneth, Size and book-to-market factors in earnings and returns, Journal of Finance 50 (1995) 131–155.

[121] E. F. Fama, R. F. Kenneth, Multifactor explanations of asset pricing anomalies, Journal of Finance 51 (1996) 55–84.

[122] M. Carhart, On persistence of mutual fund performance, Journal of Finance 52 (1997) 57–82.

[123] Y. Malevergne, D. Sornette, A two-factor asset pricing model and the fat tail distribution of firm sizes, `http://papers.ssrn.com/sol3/papers.cfm?abstract_id=960002` (2007).

[124] Y. Malevergne, P. Santa-Clara, D. Sornette, Professor Zipf goes to Wall Street, NBER Working Paper No. 15295, `http://ssrn.com/abstract=1458280` (2009).

[125] D. Sornette, A. Johansen, Significance of log-periodic precursors to financial crashes, Quantitative Finance 1 (4) (2001) 452–471.

[126] L. H. Pedersen, When everyone runs for the exit, International Journal of Central Banking 5(4) (2009) 177–199.

[127] S. Nagel, Evaporating liquidity, `http://faculty-gsb.stanford.edu/nagel/documents/LiqSupply_9.pdf` (2011).

[128] J. Y. Campbell, R. J. Shiller, The dividend-price ratio and expectations of future dividends and discount factors, Review of Financial Studies 1(3) (1988) 195–228.

[129] A. Johansen, D. Sornette, Large stock market price drawdowns are outliers, Journal of Risk 4(2) (2001) 69–110.

[130] I. M. Gelfand, S. A. Guberman, V. I. Keilis-Borok, L. Knopoff, F. Press, E. Y. Ranzman, I. M. Rotwain, A. M. Sadovsky, Pattern recognition applied to earthquake epicenters in california, Physics of The Earth and Planetary Interiors 11 (3) (1976) 227–283.

[131] B. Worton, Kernel methods for estimating the utilization distribution in home-range studies, Ecology 70 (1) (1989) 164–168.

[132] I. Chakravarti, R. Laha, J. Roy, Handbook of Methods of Applied Statistics, John Wiley & Sons Ltd, 1967.

[133] G. M. Mochan, Earthquake prediction as a decision making problem, Pure and Applied Geophysics 149 (1997) 233–247.

[134] G. M. Mochan, Y. Y. Kagan, Earthquake prediction and its optimization, Journal of Geophysical Research 97 (1992) 4823–4838.

[135] P. L. Briggs, F. Press, Pattern recognition applied to uranium prospecting, Nature 268 (5616) (1977) 125–127.

[136] V. Keilis-Borok, A. Soloviev, C. Allègre, A. Sobolevskii, M. Intriligator, Patterns of macroeconomic indicators preceding the unemployment rise in western europe and the USA, Pattern Recognition 38 (3) (2005) 423–435.

[137] G. Schwert, Stock volatility and the crash of '87, Review of Financial Studies 3 (1) (1990) 77 –102.

[138] T. Adrian, H.-S. Shin, Liquidity and leverage, Journal of Financial Intermediation 19 (2010) 418–437.

[139] D. Sornette, A. Johansen, J. P. Bouchaud, Stock market crashes, precursors and replicas, Journal de Physique I 6 (1996) 167–175.

[140] D. Sornette, R. Woodard, Financial bubbles, real estate bubbles, derivative bubbles, and the financial and economic crisis, in: M. Takayasu, T. Watanabe, H. Takayasu (Eds.), New Approaches to the Analysis of Large-Scale Business

and Economic Data, Proceedings of APFA7 (Applications of Physics in Financial Analysis), Springer, 2010, `http://arxiv.org/abs/0905.0220`.

[141] A.-L. Barabási, The origin of bursts and heavy tails in human dynamics, Nature 435 (2005) 207–211.

[142] J. Candia, M. C. Conzález, P. Wang, T. Schoenharl, G. Madey, A.-L. Barabási, Uncovering individual and collective human dynamics from mobile phone records, Journal of Physics A: Mathematical and Theoretical 41 (2008) 224015.

[143] W. Hong, X.-P. Han, T. Zhou, B.-H. Wang, Heavy-tailed statistical in short-message communication, Chinese Physics Letters 26 (2009) 028902.

[144] Y. Wu, C.-S. Zhou, J.-H. Xiao, J. Kurths, H. J. Schellnhuber, Evidence for a bimodal distribution in human communication, Proc. Nat. Acad. Sci. USA (2010) 18803–18808.

[145] J. G. Oliveira, A.-L. Barabási, Human dynamics: Darwin and einstein correspondence patterns, Nature 437 (2005) 1251.

[146] Z. Dezsö, E. Almaas, A. Lukács, B. Rácz, I. Szakadát, A.-L. Barabási, Dynamics of information access on the web, Physical Review E 73 (2006) 066132.

[147] A. Chmiel, K. Kowalska, J. A. Holyst, Scaling of human behavior during portal browsing, Physical Review E 80 (2009) 066122.

[148] T. Maillart, D. Sornette, S. Frei, T. Duebendorfer, A. Saichev, Quantification of deviations from rationality with heavy-tails in human dynamics, Physical Review E 83 (2011) 056101.

[149] T. Zhou, H. A. T. Kiet, B. J. Kim, B.-H. Wang, P. Holme, Role of activity in human dynamics, EPL Europhysics Letters 82 (2008) 28002.

[150] H.-B. Hu, D.-Y. Han, Empirical analysis of individual popularity and activity on an online music service system, Physica A 387 (2008) 5916–5921.

[151] A. Grabowski, N. Kruszewska, R. A. Kosiński, Dynamics phenomena and human activity in an artifical society, Physical Review E 78 (2008) 066110.

[152] A. Vázquez, Exact results for the barabási model of human dynamics, Physical Review Letters 95 (2005) 248701.

[153] A. Vázquez, J. G. Oliveira, Z. Dezsö, K. I. Goh, I. Kondor, A.-L. Barabási, Modeling bursts and heavy tails in human dynamics, Physical Review E 73 (2006) 036127.

[154] P. Blanchard, M.-O. Hongler, Modeling human activity in the spirit of barabási's queueing systems, Physical Review E 75 (2007) 026102.

[155] G. Grinstein, R. Linsker, Power-law and exponential tails in a stochastic priority-model queue, Physical Review E 77 (2008) 012101.

[156] B. Min, K.-I. Goh, I.-M. Kim, Waiting time dynamics of priority-queue networks, Physical Review E 79 (2009) 056110.

[157] A. Saichev, D. Sornette, Effects of diversity and procrastination in priority queuing theory: the different power law regimes, Physical Review E 81 (2009) 016108.

[158] X.-P. Han, T. Zhou, B.-H. Wang, Modeling human dynamics with adaptive interest, New Journal of Physics 10 (2008) 073010.

[159] A. Vázquez, Impact of memory on human dynamics, Physica A 373 (2007) 747–752.

[160] A. César, R. Hidalgo, Conditions for the emergence of scaling in the inter-event time of uncorrelated and seasonal systems, Physica A 369 (2006) 877–883.

[161] R. D. Malmgren, D. B. Stouffer, A. E. Motter, L. A. N. Amaral, A poissonian explanation for heavy tails in e-mail communication, Proc. Nat. Acad. Sci. USA 105 (2008) 18153–18158.

[162] H.-H. Jo, M. Karsai, J. Kertesz, K. Kaski, Circadian pattern and burstiness in human communication activity (2011) `http://arxiv.org/abs/1101.0377`.

[163] D. Brockmann, L. Hufnagel, T. Geisel, The scaling laws of human travel, Nature 439 (2006) 462–465.

[164] M. C. González, C. A. Hidalgo, A.-L. Barabási, Understanding individual human mobility patterns, Nature 453 (2008) 779–782.

[165] C.-M. Song, T. Koren, P. Wang, A.-L. Barabási, Modeling the scaling properties of human mobility, Nature Physics 6 (2010) 818–823.

[166] C.-M. Song, Z.-H. Qu, N. Blumm, A.-L. Barabási, Limits of predictability in human mobility, Science 327 (2010) 1018–1021.

[167] D. Brockmann, Statistcal mechanics: The physics of where to go, Nature Physics 6 (2010) 720–721.

[168] X.-P. Han, Q. Hao, B.-H. Wang, T. Zhou, Origin of the scaling law in human mobility: Hierarchical organization of traffic systems (2009) `http://arxiv.org/abs/0908.1221`.

[169] Y.-Q. Hu, J. Zhang, D. Huan, Z.-R. Di, Toward a universal understanding of the scaling laws in human and animal mobility (2010) `http://arxiv.org/abs/1008.4394`.

[170] X.-Y. Yan, X.-P. Han, T. Zhou, B.-H. Wang, Exact solution of gyration radius of individual's trajectory for a simplified human mobility model (2010) `http://arxiv.org/abs/1011.5111`.

[171] Z.-Q. Jiang, Research and application on complexity of financial market and human dynamics, Ph.D. thesis, East China University of Science and Technology (2011).

[172] A. L. Lloyd, R. M. May, How viruses spread among computers and people, Science 292 (2001) 1316–1317.

[173] M. J. Keeling, K. T. D. Eames, Networks and epidemic models, J. R. Soc. Interface 2 (2005) 295–307.

[174] J. Gomez-Gardenes, V. Latora, Y. Moreno, E. Profumo, Spreading of sexually transmitted diseases in heterosexual population, Proc. Nat. Acad. Sci. USA 105 (2008) 1399–1404.

[175] S. Eubank, H. Guclu, V. S. A. Kumar, M. V. Marathe, A. Srinivasan, Z. Toroczkai, N. Wang, Modeling disease outbreaks in realistic urban social networks, Nature 429 (2004) 180–184.

[176] Z. Zhao, J. P. Calderón, C. Xu, G. Zhao, D. Fenn, D. Sornette, R. Crane, P. M. Hui, N. F. Johnson, Effect of social group dynamics on contagion, Physical Review E 81 (2010) 056107.

[177] R. Crane, D. Sornette, Robust dynamic classes revealed by measuring the response function of a social system, Proc. Nat. Acad. Sci. USA 105 (41) (2008) 15649–15653.

[178] A. Saichev, D. Sornette, Hierarchy of temporal responses of multivariate self-excited epidemic processes (2011) `http://arxiv.org/abs/1101.1611`.

[179] A. Saichev, D. Sornette, Generating functions and stability study of multi-variate self-excited epidemic processes (2011) `http://arxiv.org/abs/1101.5564`.

[180] A. Vespignani, Predicting the behavior of techo-social systems, Science 325 (2009) 425–428.

[181] D. Balcan, V. Volizza, B. Goncalves, H. Hu, J. J. Ramasco, A. Vespignani, Multiscale mobility networks and the spatical spreading of infectious diseases, Proc. Nat. Acad. Sci. USA 106 (2009) 21484–21489.

[182] S. Merler, M. Ajelli, The role of population heterogeneity and human mobility in the spread of pandemic influenza, Proc. R. Soc. B 277 (2010) 557–565.

[183] P. Wang, M. C. González, C. A. Hidalgo, A.-L. Barabási, Understanding the spreading patterns of mobile phone viruses, Science 325 (2009) 1071–1076.

[184] E. F. Fama, K. R. French, The cross-section of expected stock returns, Journal of Finance 47 (1992) 427–465.

[185] A. Joulin, A. Lefevre, D. Grunberg, J.-P. Bouchaud, Stock price jumps: news and volume play a minor role (2008) `http://arxiv.org/abs/0803.1769`.

[186] P. C. Tetlock, Giving content to investor sentiment: The role of media in the stock market, Journal of Finance 62 (2007) 1139–1168.

[187] L. Fang, J. Peress, Media coverage and the cross-section of stock returns, Journal of Finance 64 (2009) 2023–2052.

[188] P. C. Tetlock, M. Saar-Tsechansky, S. Macskassy, More than words: Quantifying language to measure firms' fundamentals, Journal of Finance 63 (2008) 1437–1467.

[189] R. Tumarkin, R. Whitelaw, News or noise? internet postings and stock prices, Financial Analysts Journal 57 (2001) 41–51.

[190] W. Antweiler, M. Z. Frank, Is all that talk just noise? the information content of internet stock message boards, Journal of Finance 59 (2004) 1259–1294.

[191] T. Preis, D. Reith, H. E. Stanley, Complex dynamics of our economic life on different scales: insights from search engine query data, Philosophical Transactions of the Royal Society A 368 (2010) 5707–5719.